

**DEUTERIUM NMR STUDIES OF GUEST SOLUBILIZATION IN LIQUID
CRYSTALS / PHOTOCHEMISTRY OF CYCLOPROPENES**

by

BRIAN JAMES FAHIE, B.Sc.

A Thesis

**Submitted to the School of Graduate Studies
in Partial Fulfillment of the Requirements
for the Degree
Doctor of Philosophy**

McMaster University

(c) Copyright by Brian James Fahie, April 1989

**DEUTERIUM NMR STUDIES OF GUEST SOLUBILIZATION IN LIQUID
CRYSTALS / PHOTOCHEMISTRY OF CYCLOPROPENES**

To Joan

**DOCTOR OF PHILOSOPHY (1989)
{CHEMISTRY}**

**McMASTER UNIVERSITY
Hamilton, Ontario**

TITLE: Deuterium NMR Studies of Guest Solubilization in Liquid Crystals /
Photochemistry of Cyclopropenes

AUTHOR: Brian James Fahie, B.Sc. (Dalhousie University)

SUPERVISOR: Dr. William J. Leigh

NUMBER OF PAGES: xviii, 176

Deuterium NMR Studies of Guest Solubilization in Liquid Crystals

ABSTRACT

The solubilization of eight aromatic ketones and C_6D_6 in the liquid crystalline phases of *trans,trans*-4'-butylbicyclohexyl-4-carbonitrile(CCH-4), *trans,trans*-4'-ethylbicyclohexyl-4-carbonitrile(CCH-2) and a binary mixture (1:2) of CCH-4 and CCH-2 (EB) has been investigated by deuterium NMR spectroscopy using quadrupolar splitting ($\Delta\nu_Q$) and T_1 measurements. All of the solutes were found to be homogeneously soluble in the nematic phase of these solvents. However, solubilization of these solutes in the smectic phase of these solvents was found to be dependent on temperature, solute size, and solute structure.

All of the solutes investigated were found to have very low solubilities (*ca.* 0.2 - 2.0 mol%) in the smectic phase of these solvents. In general, the solubility of a given solute in the smectic phase increases with decreasing temperature. When the bulk concentration is above the solubility limit in the smectic phase, the solute order parameters (*via* 2H NMR) appear to decrease with decreasing temperature. This results from formation of a biphasic system which consists of a solute-depleted bulk smectic phase and a solute rich phase separated nematic phase. The solubility limit in the smectic phase also appears to be dependent on the size of the solute, with the solubility increasing with decreasing solute size. The nature of substituents on the solute seems to affect the solubilization in the smectic phase as well.

At lower temperatures (at or near the K \leftrightarrow S phase transition) we have observed, as have others, a solute-induced phase (characterized by isotropic like 2H NMR spectra). We have shown that this solute-induced phase is a viscous isotropic liquid.

Photochemistry of Cyclopropenes

ABSTRACT

The direct solution photochemistry of 1,3,3-trimethylcyclopropene and 1-*t*-butyl-3,3-dimethylcyclopropene has been investigated. Primary photoproducts consisting of alkynes, allenes, and 1,3-dienes are formed from vinylcarbene intermediates, a result of cleavage of the C₁ - C₃ or C₂ - C₃ bond. Cleavage of the more substituted (C₁ - C₃) bond to yield a vinylcarbenes can account for > 80% of observed products. Most of the products are formed *via* 1,2- and 1,4-hydrogen migrations from the intermediate vinylcarbenes.

Photolysis of 1,3,3-trimethylcyclopropene-1-¹³C supports the intermediacy of vinylcarbenes in product formation from singlet excited cyclopropenes. In addition, evidence which strongly suggests the importance of a second pathway for formation of alkyne products from alkylcyclopropenes has been obtained. This pathway involves the intermediacy of vinylidene, formed by 1,2-hydrogen migration/ring opening (sequential or concerted) from the singlet excited-state of cyclopropene.

ACKNOWLEDGEMENTS

I would like to thank the following people for their contribution to this thesis:

My supervisor Dr. Willie Leigh, for his guidance, encouragement, and timely inspirations which helped make this work a success.

The Chemistry faculty at McMaster, especially my committee members, Dr. A. D. Bain, Dr. B. E. McCarry, and Dr. N. H. Werstiuk, who without exception gave freely of their time to assist me when asked.

E. Merck (Darmstadt) for generous gifts of CCH-4 and CCH-2.

Dr. C. Rodger (Bruker Canada) for allowing me the use of the AC200 spectrometer.

Dr. K. H. Jeffrey (University of Guelph) for the use of his NMR spectrometer, and for sharing his time and expertise in its operation.

Mr. Brian Sayer for introducing me to the wonderful world of high-field spectrometers and for always making available the AM500 for that "*final and critical*" experiment.

Dr. Don Hughes who patiently taught me the intricacies of the AM500, and answered my queries every other Saturday morning at 8:00 AM.

All of my labmates with whom I shared room 467, especially Brady Clark and Scott Mitchell.

Dr. Thomas Hemsheit and Dr. M. Mahendran who were always willing to share their abundant synthetic insight.

George Timmins, who understands that there is more to life than chemistry.

To those friends that helped make graduate life that much more rewarding, especially Richard (*a.k.a. Walt*) Perrier and Adrian Schwann.

Mr. Rod Ryan for his lasting inspiration and friendship.

Dr. D. R. Arnold for introducing me to *real* chemistry. I will always be thankful for his advice, encouragement, and friendship.

John Orlando for his friendship, advice and for introducing me to J. L. M.

My three sisters, Brenda, Janice and Wanda who are surely the best sisters a brother could have.

My Parents, for their constant love, support and encouragement in all things, academic and otherwise.

Finally, I thank my wife Joan, for her unwavering love, support and encouragement while graciously accepting years of poverty, lonely evenings, and weekends, so that I could pursue a dream. I will always be grateful! May God enable me to repay her.

TABLE OF CONTENTS

<u>PART A:</u> Deuterium NMR Studies of Guest Solubilization in Liquid Crystals	1
LIST OF TABLES	x
LIST OF FIGURES	xi
CHAPTER	
I Introduction	1
1.1 General	1
1.2 Thermotropic Liquid Crystals	2
1.3 Our Interest	6
1.4 Our Work	9
1.5 Deuterium NMR	17
II The Deuterium NMR Investigation of the Solubilization of Substituted β-Phenylpropiophenones in CCH-4, CCH-2, and EB.	27
A. Introduction	27
B. Results	27
2.1 Preparation of Compounds	27
2.2 Deuterium NMR of Solutes in Liquid Crystalline Solvents	28
2.3 Deuterium NMR of 0.3 mol% 1 in CCH-2	36
2.4 Deuterium T_1 Measurements on 1 in Liquid Crystalline Solvents	38
C. Discussion	40
2.5 The Solubilization of 1 in CCH-4 and EB	40
2.6 The Solubilization of 1 in CCH-2	58
2.7 Summary	59

III	A Deuterium Investigation of the Solubilization of Benzene and Four Aromatic Ketones in CCH-4.	60
	A. Introduction	60
	B. Results	62
	3.1 Preparation of Compounds	62
	3.2 Deuterium NMR of MAP, CAP, and PAP in CCH-4	63
	3.3 Deuterium T_1 Measurements on MAP in CCH-4	66
	3.4 Deuterium NMR of 1 mol% 7 in CCH-4	66
	3.5 Deuterium NMR of 3 mol% Benzene- d_6 in CCH-4	73
	C. Discussion	76
	3.6 The Solubilization of MAP, CAP, and PAP, in the Isotropic and Nematic Phases of CCH-4	76
	3.7 The Solubilization of MAP, CAP, and PAP in the Smectic Phase of CCH-4	78
	3.8 The Solubilization of 7 in CCH-4	90
	3.9 The Solubilization of C_6D_6 in CCH-4	91
	3.10 Summary	93
IV	Summary	95
V	Experimental	100
	APPENDIX A	105
	REFERENCES	107
 <u>PART B:</u> Photochemistry of Cyclopropenes		
	LIST OF TABLES	xvi
	LIST OF FIGURES	xvii
	LIST OF SCHEMES	xviii

CHAPTER		
I	Introduction	113
	1.1 General Background	113
	1.2 Ground-State Reactions	115
	1.3 Excited-State Reactions	117
	1.4 Theoretical	124
	1.5 Objectives	130
II	Results	131
	2.1 Preparation of Compounds	131
	2.2 Ultraviolet Absorption Spectra of 8 and 9	132
	2.3 Description of Light Sources	133
	2.4 Relative Product Yield Determinations	133
	2.5 Quantitative ^{13}C Determinations	133
	2.6 Direct Photolysis of 8 and 9 in Solution	134
III	Discussion	139
IV	Experimental	151
	4.1 General	151
	4.2 Commercial Solvents, Reagents and Chemicals Used	152
	4.3 Photolysis of Cyclopropenes	153
	4.4 Identification of Photoproducts	153
	4.5 Carbene Trapping Experiments	154
	4.6 Preparation and Purification of Cyclopropenes	154
	4.7 Synthesis and/or Identification of Photoproducts	158
	4.8 Quantitative ^{13}C Determinations	162
	APPENDIX	163
	REFERENCES	169

Deuterium NMR Studies of Guest Solubilization in Liquid Crystals

LIST OF TABLES

2.1	Elimination/Cyclization Data for 5b in CCH-4.	54
4.1	Solubility Limits in the Smectic Phase of CCH-4.	96

Deuterium NMR Studies of Guest Solubilization in Liquid Crystals

LIST OF FIGURES

1.1	Schematic of molecular orientation and translational order in a compound which exhibits liquid crystalline behavior. Adapted from reference 2.	2
1.2	Schematic showing possible thermotropic liquid crystalline phases. Note the large number of known smectic phases.	3
1.3	Idealized twisted nematic. n indicates direction of molecular axis.	3
1.4	Schematic of Smectic C phase showing tilt angle between the molecules and the plane of the layer.	5
1.5	Idealized schematic illustrating how the transition state geometries for two different products can differ, even when formed from the same reactants.	7
1.6	Arrhenius plot showing temperature dependence of the triplet lifetime of 1 as 1 a mol% mixture in CCH-4. Reproduced with permission from reference 85.	12
1.7	Energy diagram showing the effect of an external magnetic field on the relative energies of the two spin states from ^1H .	18
1.8	Schematic representation of the effect of the electric quadrupole moment of the nucleus on the Zeeman energy levels of a spin 1 nucleus.	20
1.9	Schematic illustrating the relationship between the principal component of the electric field gradient and the magnetic field.	20

1.10	Schematic illustrating the relationship between the principal component of the electric field gradient (N), the molecular axis (M_z), and the magnetic field (B_0).	22
1.11	Schematic illustrating the relationship between the principal axis of the electric field gradient (n), the long molecular axis (M_z), the principal axis (P_z), and the magnetic field (B_0).	23
1.12	^2H spectrum of hexamethylenetetramine- d_{12} , and example of a powder pattern.	25
1.13	An example of a ^2H NMR spectrum of a dissolved solute (p -dioxane- d_8) in the nematic phase (41°C) of Merck "1565 TNC". Adapted from reference 61.	25
2.1a	Deuterium NMR spectra of 1 mol% 1 in CCH-4 as a function of temperature.	30
2.1b	Deuterium quadrupolar splitting ($\Delta\nu_Q$) versus temperature for 1 mol% mixtures of 1(ϕ) and 2(\square) in CCH-4.	31
2.2	Deuterium quadrupolar splitting ($\Delta\nu_Q$) versus temperature for 1.0(\square), 5.0(+), and 10.0(Δ) mol% CCH-4.	31
2.3	Deuterium NMR spectra of 0.2 mol% 1 in CCH-4 as a function of temperature.	34
2.4	Deuterium quadrupolar splitting ($\Delta\nu_Q$) versus temperature for 3 mol% 3 in CCH-4.	35
2.5	Deuterium quadrupolar splitting ($\Delta\nu_Q$) versus temperature for 3 mol% 4 in CCH-4.	35
2.6	Deuterium quadrupolar splitting ($\Delta\nu_Q$) versus temperature for a 3 mol% mixture of 1 in EB.	37
2.7	Deuterium quadrupolar splitting ($\Delta\nu_Q$) versus temperature for 0.3 mol% 1 in CCH-2.	37

2.8	Arrhenius plot showing the temperature dependence of T_1 -values obtained for 3 mol% mixtures of 1 in (A) CCH-4 and (B) CCH-2/CCH-4(EB) between 25 and 120°C. Errors were calculated as twice the standard deviation for each point; error bars are only shown for those points with errors in excess of 10%.	39
2.9	Block diagram depicting the solubilization of a solute in the nematic phase of CCH-4. A: High temperature. B: Low temperature. The positions of the blocks are not meant to imply that there is empty space between the solute molecules, but rather to simulate the average position of the solvent molecules in a mobile fluid. At higher temperatures the solvent molecules will have more thermal energy and as a result will be more mobile, thereby providing more opportunities for the solute to adopt various conformations.	41
2.10	Plot of Δv_Q values <i>versus</i> $T_{N,I} - T$ for the nematic phase temperatures of the 1.0(\square), 5.0(+) and 10.0(Δ) mol% mixtures of 1 in CCH-4.	45
2.11a	Idealized composition/temperature binary phase diagram (heating) for 1 /CCH-4 constructed from DSC and thermal microscopy data. Reproduced with permission from reference 85.	47
2.11b	Composition/temperature binary phase diagram (cooling) for 1 /CCH-4 constructed from DSC and thermal microscopy data (actual data shown). Reproduced with permission from reference 85.	48
2.12	^{13}C NMR spectra of a 3.4 mol% benzene/CCH-4 mixture. A: 65°C. B: 11°C.	51
2.13	^{13}C NMR spectrum of 3 mol% 1 in CCH-4 at 30°C.	53
3.1a	Deuterium NMR spectra of 0.6 mol% MAP- d_3 in CCH-4 as a function of temperature.	67
3.1b	Deuterium NMR spectra of 3.0 mol% MAP- d_3 in CCH-4 as a function of temperature.	68

3.2a	Deuterium NMR spectra of 0.6 mol% CAP-d ₃ in CCH-4 as a function of temperature.	69
3.2b	Deuterium NMR spectra of 2.0 mol% CAP-d ₃ in CCH-4 as a function of temperature.	70
3.3a	Deuterium NMR spectra of 0.6 mol% PAP-d ₃ in CCH-4 as a function of temperature.	71
3.3b	Deuterium NMR spectra of 2.0 mol% PAP-d ₃ in CCH-4 as a function of temperature.	72
3.4	Deuterium quadrupolar splitting ($\Delta\nu_Q$) <i>versus</i> temperature for 1.0 mol% 7 in CCH-4.	73
3.5	Deuterium NMR spectra of 3.0 mol% C ₆ D ₆ in CCH-4 as a function of temperature. Reproduced with permission from reference 85.	74
3.6	Deuterium quadrupolar splitting ($\Delta\nu_Q$) <i>versus</i> temperature for 3.0 mol% C ₆ D ₆ in CCH-4.	75
3.7	Composite plot for $\Delta\nu_Q$ <i>versus</i> temperature for 0.6 mol% MAP(\square), CAP(\times), and PAP(Δ) in the nematic phase of CCH-4.	77
3.8	Illustration of the long molecular axis of <i>syn</i> - and <i>anti</i> -MAP.	77
3.9	Deuterium quadrupolar splitting ($\Delta\nu_Q$) <i>versu</i> temperature for 3.0 mol% MAP in CCH-4.	80
3.10	Composite plot of $\Delta\nu_Q$ <i>versus</i> temperature for 1.0(Δ), 3.0(\square), and 8.0(\circ) mol% mixtures of MAP and CCH-4. Only the splittings for the innermost (nematic) doublet are shown.	80

3.11	Binary phase diagram for the MAP/CCH-4 system, constructed from DSC and thermal microscopy data. Solid lines represent heating data; dashed lines show supercooled behavior. Phase identities: I, isotropic; N, nematic; S, smectic; K, solid. Reproduced with permission from reference 102.	82
3.12	Deuterium quadrupolar splitting ($\Delta\nu_Q$) versus temperature for 2.0 mol% CAP in CCH-4.	84
3.13	Composite plot of $\Delta\nu_Q$ versus temperature for 0.6(Δ), 2.0(\square), and 8.0(x) mol% mixtures of CAP and CCH-4. Only the splittings for the nematic doublets are shown.	84
3.14	Binary phase diagram for the CAP/CCH-4 system, constructed from DSC and thermal microscopy data. Solid lines represent heating data; dashed lines show supercooled behavior. Phase identities: I, isotropic; N, nematic; S, smectic; K, solid. Reproduced with permission from reference 102.	86
3.15	Deuterium quadrupolar splitting ($\Delta\nu_Q$) versus temperature for 2.0 mol% PAP in CCH-4.	88
3.16	Composite plot of $\Delta\nu_Q$ versus temperature for 0.6(Δ), 2.0(\square), and 8.0(x) mol% mixtures of PAP and CCH-4. Only the splittings for the nematic doublets are shown.	88
3.17	Binary phase diagram for the PAP/CCH-4 system, constructed from DSC and thermal microscopy data. The light solid lines represent transition temperatures obtained from heating data, the dashed lines represent those obtained from cooling data, and the dark solid lines represent those that are identical in heating and cooling. Phase identities: I, isotropic; N, nematic; S, smectic; K, solid; A, binary solid modification. Reproduced with permission from reference 102.	89
A.1	Illustration of angles used in the calculation of $\Delta\nu_Q$ for <i>syn</i> - and <i>anti</i> -methoxyacetophenone.	106

Photochemistry of Cyclopropenes

LIST OF TABLES

2.1	Solution UV Absorption Data	134
2.2	Relative Product Yields For Photolysis and Thermolysis of 8 .	137
2.3	Relative Product Yields For Photolysis and Thermolysis of 9 .	138
2.4	Contribution of Paths "a" - "d" (Scheme 3.1) to the Ground- and Excited-State Chemistry of 8 .	138
2.5	Contribution of Paths "a" - "d" (Scheme 3.1) to the Ground- and Excited-State Chemistry of 9 .	138
A.1	Relative Peak Height Data	168
A.2	¹³ C Enrichment at each Carbon Position of Labelled 11 .	170

Photochemistry of Cyclopropenes

LIST OF FIGURES

1.1	Funnel theory diagram showing preference for formation of least stable vinylcarbene on ring-opening of excited phenylated cyclopropenes.	121
1.2	Electronic structures of ground and excited vinylmethylenes.	125
1.3	Lowest energy reaction path for conversion of cyclopropene to allene and acetylene.	127
1.4	Structure of bisected vinylmethylene.	128
A.1	Relative Peak Height (RPH) <i>versus</i> reciprocal of the concentration of the External Standard (Ethanol) for labelled 11.	169

Photochemistry of Cyclopropenes

LIST OF SCHEMES

1.1	Allowed thermal and photochemical interconversions on the C_3H_4 surface.	114
1.2	Vinylcarbene formation from Cyclopropenes	114
1.3	Illustration of postulated vinylcarbene intermediates formed on thermolysis of 1- <i>t</i> -butyl-3,3-dimethylcyclopropene. Note the allene (as indicated by the dashed lines) can be formed from both possible vinylcarbenes, however it was not observed in the thermolysis.	116
1.4	Thermal isomerization of an alkylcyclopropene.	117
1.5	Description of various theoretically investigated excited-state reaction pathways for cyclopropene.	129
3.1	Possible ring-opening reaction mechanisms for an alkyl-substituted cyclopropene.	140
3.2	Possible carbene intermediates in the formation of 10 and 11 .	142
3.3	Possible intermediates involved in the primary photoproducts of 9 .	147
3.4	Possible thermal and photochemical decomposition pathways for 4 .	149

**DEUTERIUM NMR STUDIES OF GUEST SOLUBILIZATION IN LIQUID
CRYSTALS**

CHAPTER I

Introduction

1.1 General

Liquid crystals are a class of compounds which at certain temperatures exhibit thermodynamic properties between those of an isotropic liquid and a crystal. Isotropic liquids do not possess any orientational or translational order, while crystals possess both types of order. Liquid crystals¹ on the other hand do not contain translational order but do have orientational order. It is the orientational order within a mobile framework that gives this class of compounds their unique chemical and physical properties.

Liquid crystals can be classified into two major categories: thermotropic and lyotropic. Thermotropic liquid crystals obtain their liquid crystalline properties by *melting* an appropriate crystalline material. Lyotropic liquid crystals are not pure compounds based on molecular structure, but rather result by the appropriate mixing of two or more components. More often than not one of these components is water.² This thesis involves the use of thermotropic liquid crystals. Hence, only this class of liquid crystals will be discussed in detail.

Why Liquid Crystals?

While interest in the chemistry of liquid crystals has not always been as pronounced as it currently is, there has been a continuous, if not consistent, attraction to them since their first detailed description given by Reinitzer in 1888. A non-enthusiast may wonder what all the fuss is about, but with a brief scan of the literature it quickly becomes evident why there is so much curiosity about the

properties of these unique phases. Many problems encountered daily by the experimental chemist could be better solved if he had the order and rigidity present in crystals, coupled with the fluidity of liquids at his disposal. Liquid crystals present a compromise between these two extremes. How the chemist is able to make use of this compromise has yet to be fully detailed, but certainly the ground work has been laid for many future and exciting discoveries.

1.2 Thermotropic Liquid Crystals

The most common characteristic of thermotropic liquid crystals is that most of them possess a rod-like shape (*i.e.* the length of the molecule is much longer than the width).³ Within the class of thermotropic liquid crystals there are a number of liquid crystalline phases that differ both in the nature and degree of order that they possess. Some of these mesogens form only *one* type of liquid crystalline phase while others can form more than one. For a mesogen which can form more than one liquid crystalline phase the order in the phases decreases as the temperature is raised from the crystalline phase (K) to the isotropic phase (I).

The transition from an ordered crystal through possible liquid crystalline phases to an isotropic liquid is depicted below.

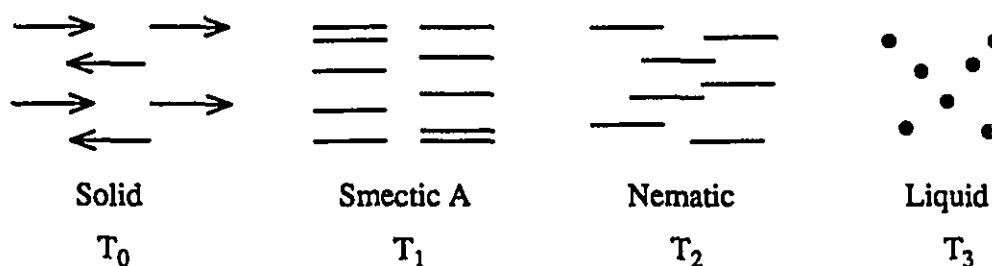


Figure 1.1. Schematic of molecular orientation and translational order in a compound which exhibits liquid crystalline behaviour. Adapted from reference 2

As indicated in Figure 1.1 there is more than one type of liquid crystalline

phase possible as a compound goes from the solid to the liquid phase. These phases have been divided into two main categories: Nematic and Smectic. Both nematic and smectic phases can be further subdivided (Figure 1.2).

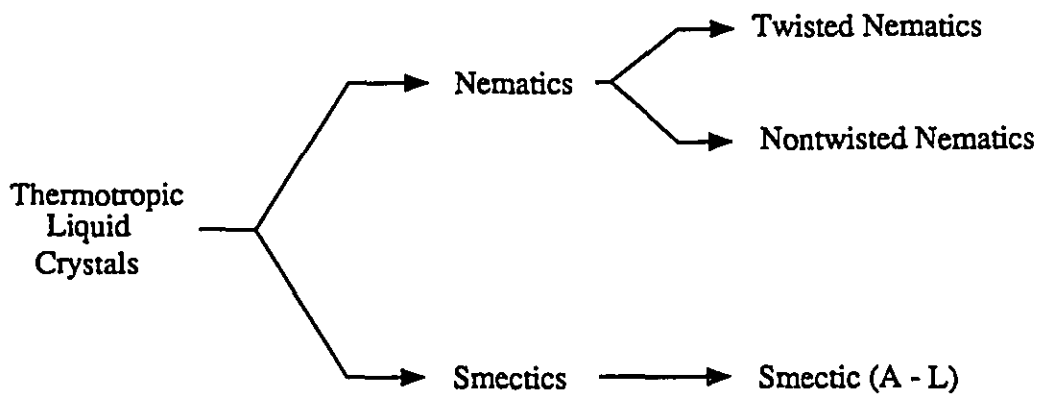


Figure 1.2. Schematic showing possible thermotropic liquid crystalline phases. Note the large number of known smectic phases.

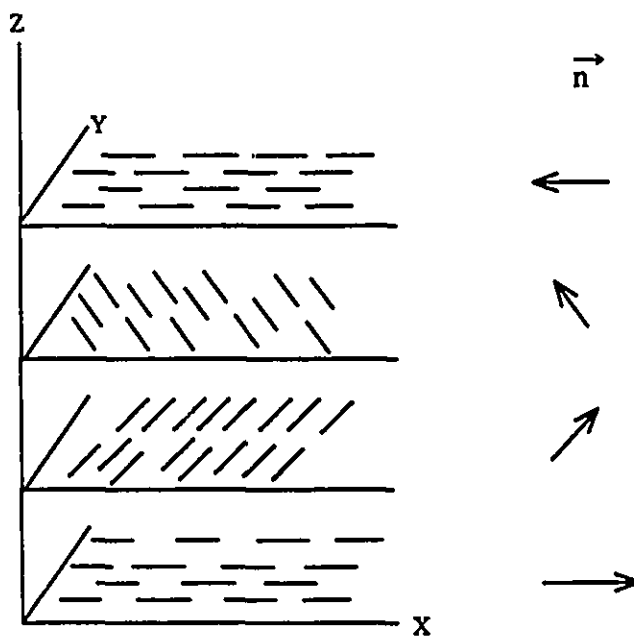


Figure 1.3. Idealized twisted nematic. \vec{n} indicates direction of molecular axis.

Nematics

The nematic phases are the least ordered of all the liquid crystalline phases. In compounds that exhibit both nematic and smectic phases the nematic phases will always occur at higher temperatures than the smectic phases.

Nontwisted nematic phases (commonly referred to as simply *nematic*) contain only one element of order, which is the alignment of the long axis of the neighbouring molecules such that they are parallel (or approximately) parallel to each other (see Figure 1.1).

Twisted nematics (or cholesteric phases as they are commonly referred to) are formed by optically active mesogens or simple nematics containing an optically active solute. The molecular optical activity results in a macroscopic twist in the alignment producing a helical array (see Figure 1.3).

Smectics

The different smectic phases are designated A, B, C *etc.* and have been assigned in the order in which they have been identified. Unlike nematic phases, smectic phases are arranged in layers (with the possible exception of smectic D^a). A description of the more common smectic phases is presented below. Since there is no chemical basis for the labelling scheme used in the identification of the phases, they will be discussed in terms of increasing order.

Smectic A

This phase was the first smectic phase to be identified and is the least ordered of all the smectic phases. The smectic A phase is arranged in layers with

^aThe smectic D phase has been assigned a cubic phase structure³ and it has been suggested that the cubic structure is comprised of spherical units each consisting of several molecules.⁴ However, this model has been challenged and it has even been suggested that the smectic D phase may not be a smectic phase at all.⁵

the long axis of the molecules perpendicular to the plane defined by the layer (see Figure 1.1). Individual molecules are randomly situated within each layer, allowing the molecules considerable translational freedom within the layers. In addition, rotation about the long axis of the molecules is relatively unhindered.

Smectic C

This phase is very similar to smectic A. The distinguishing feature that differentiates this phase from smectic A is that the molecules in the layers are tilted with respect to the plane of the layer (see Figure 1.4). As a result of this tilt, smectic

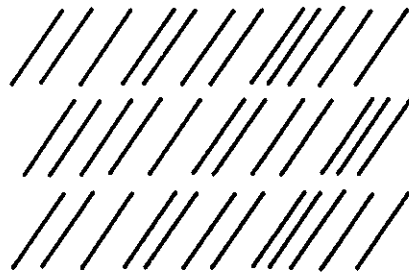


Figure 1.4. Schematic of Smectic C phase showing tilt angle between the molecules and the plane of the layer.

C phases are optically biaxial whereas smectic A phases are optically uniaxial. It has been suggested that there are two types of smectic C phases: one in which the tilt angle is not temperature dependent, and one where the tilt angle is temperature dependent.^{6,7}

Smectic B and H

These phases represent a significant increase in the order present as compared to smectic A and C. For both smectic B and H the molecules are ordered within the individual layers; however the molecules are still able to rotate about their long molecular axis. The cylindrical nature of the molecules causes them to pack with hexagonal or hexatic close packing.⁸⁻¹⁰ The major difference between B

and H is that in B the molecules are aligned perpendicular to the plane of the molecules, while in H the molecules are tilted with respect to the plane (*i.e.* analogous to the difference between A and C).

1.3 Our Interest

Our interest in liquid crystals was spawned by the possibility of manipulating these ordered fluids in such a fashion so as to be able to control chemical reactivity. For example, if reactants A and B react in an isotropic medium to form C and D in equal amounts, would it be possible to selectively enhance the yield of either C or D by carrying out the reaction in the appropriate liquid crystal? In principle this should work if the transition state geometries for the products C and D were significantly different. Figure 1.5 illustrates an idealized situation where the transition state leading to product C requires A and B to be parallel to one another, whereas the transition state leading to product D requires A and B to be perpendicular to one another. If the reaction energetics leading to products C and D are similar, then they should be formed in approximately equal quantities if the reaction is carried out in an isotropic solvent. In contrast to isotropic solutions, liquid crystal solutions have their long axes aligned parallel to one another. Therefore, if reactants A and B are dissolved in an appropriate liquid crystalline phase, then they too may be preferentially held in a geometry such that they are parallel to one another. If this can in fact be accomplished, it seems plausible that A and B could react in a liquid crystalline solvent to form product C preferentially over product D. This idea was not unique to our group, but previous attempts at controlling chemical reactivity with liquid crystalline solvents have been met with limited success.¹¹⁻²⁰

If the above model is to be successful, the choice of both solute and solvent

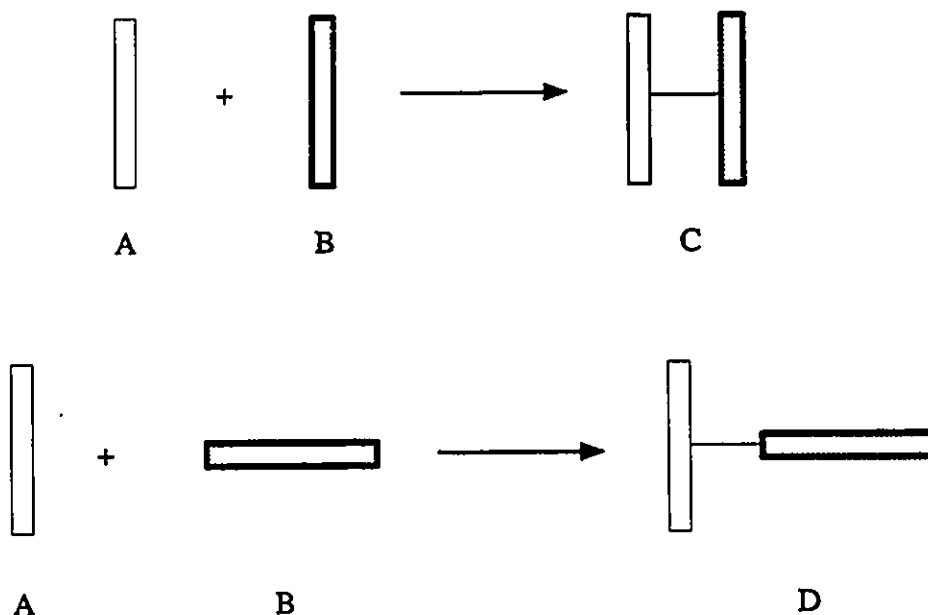


Figure 1.5. Idealized schematic illustrating how the transition state geometries for two different products can differ, even when formed from the same reactants

is critical. It has been well established that the degree to which a dissolved solute disrupts the solvent matrix of a liquid crystal depends almost exclusively on the compatibility of the solute's and solvent's molecular structure.^{14,15,18,21-23} In many instances where both the solute and the solvent appear to be compatible, little or no phase dependent behavior is observed.¹¹⁻²⁰

After some initial, early disappointments^{24,33} it became obvious to us that if we were to fully exploit the potential of liquid crystals as a medium in which to control chemical reactivity, we must first better understand the interactions between the dissolved solute and the liquid crystal. Clearly the details of guest solubilization in liquid crystals are more complex than both we and others have anticipated.

There is a large array of techniques from which the experimental chemist can choose from for use in monitoring the interactions between a dissolved solute and a liquid crystal. These include product analysis of both thermally^{11,12,16,17,20,24,26,33-37}

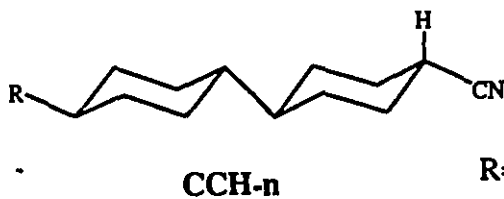
and photochemically^{13-15,18,19,38} activated reactions (unimolecular and/or bimolecular). In addition spectroscopic techniques such as nanosecond laser flash photolysis,^{14,25,26} UV absorption,³⁹⁻⁴⁵ fluorescence,⁴⁶⁻⁵³ infrared,⁵⁴ electron spin resonance,⁵⁵⁻⁶⁰ and nuclear magnetic resonance^{54,61-69} have also been successfully employed. As well, thermal microscopy,^{34,54} DSC^{34,54} and X-ray diffraction³⁴ studies have been extensively used in the investigations of binary mixtures involving liquid crystals. Often it is necessary to use a number of different techniques before a complete understanding of the interactions occurring in a particular system can be fully understood.

There are many factors which need to be considered when choosing a liquid crystal on which to base a research project. This results primarily because it is often necessary (as previously mentioned) to use more than one technique to probe the complex interactions that can arise in a binary (solute/liquid crystal) liquid crystalline environment. Obviously the experimenter should attempt to choose a liquid crystal that will be compatible with the techniques that he is most likely to use in his investigations. Considerations such as the phase(s) present in the liquid crystal (i.e. is the order present likely to achieve the desired effect), the temperature(s) (ranges) at which the phase(s) occur (i.e. are they appropriate for thermally activated reactions) are critical to ensure success. Other considerations such as the UV absorption of the liquid crystal may be important if optical experiments such as nanosecond laser flash photolysis and photochemically initiated reactions are to be employed. The commercial availability of the liquid crystal and its cost are also important considerations, which may seriously effect the types of experiments that can be explored.

1.4 Our Work

Liquid Crystal of Interest

The liquid crystals that we chose to investigate were the commercially available CCH- n ($n = 2,4$) homologues, as well as a binary mixture (1:2) of CCH-4 and CCH-2 which we have called EB. These particular liquid crystals are very well



R= ethyl: $n=2$

R= n-butyl: $n=4$

suited to investigations of solute/solvent interactions. Both CCH-4 and CCH-2 are commercially available in spectroscopic grade purity, are optically transparent above *ca.* 210 nm, and exhibit isotropic, nematic and highly ordered smectic phases at convenient temperatures: K→S, 28°C; S→N, 54°C; N→I, 79°C and K→S, 28°C; S→N, 44°C; N→I, 48°C for CCH-4⁷⁰ and CCH-2²⁶ respectively. EB is a particularly useful solvent as it provides a low temperature nematic phase in a temperature region that compliments the nematic phases of CCH-4 and CCH-2: K→S, 10°C; S→N, 25°C; N→I, 57°C.³⁸

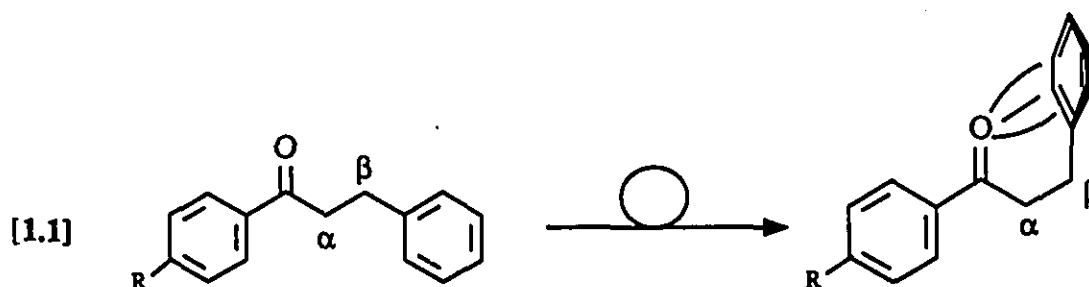
The morphology of the smectic phase of CCH-4 has been well established by X-ray diffraction and has been determined to be a bilayer crystal-B phase,⁷¹ similar to the smectic phase present in the 4'-propyl homologue (CCH-3).⁷² This phase is characterized by molecules arranged in correlated bilayers of thickness just slightly shorter than twice their molecular length. Within the bilayers the molecules are hexagonally close-packed, and oriented parallel to one another and perpendicular to the layered plane.⁷¹⁻⁷⁵ The crystal-B phase is distinct from the earlier described smectic B phase in that it contains a degree of three dimensional order.⁷² Throughout the rest of this thesis, the *crystal-B* phase of CCH-4 will simply be

referred to as the *smectic* phase.

The exact characteristics of the smectic phase of CCH-2 are not as well defined as those for CCH-4, but it has been assigned a structure of slightly higher order than that found for CCH-4, consisting of rhombohedral packing.^{38,76} The smectic phase of EB appears to have the same general structure as that of CCH-2.³⁸

Although the morphologies of the liquid crystalline phases of pure CCH-4 and CCH-2 are apparently well-established, the solubilization of guest molecules in the different liquid crystalline phases of both CCH-4 and CCH-2 remains unclear and is a topic of considerable current debate.^{14,22,25,26,38,49}

Our group's first efforts were directed towards investigating the effects of smectic and nematic liquid crystalline order on the conformational mobilities of dissolved solutes, using CCH-4 and CCH-2. This involved the study of solvent order present in these liquid crystals on the intramolecular quenching of substituted β -phenylpropiophenones (Equation [1.1]).^{25,26}



It had been previously well established that β -phenylpropiophenone triplets undergo efficient intramolecular quenching *via* exciplex interactions between the carbonyl group and the β -phenyl ring (see Equation [1.1]).⁷⁷⁻⁷⁹ The similarity in the shapes of the ketones and the solvent should increase the likelihood that the ketones would be easily solubilized in the liquid crystalline phases of CCH-4 and CCH-2 without

disrupting the solvent order present. Once the ketone was solubilized in a liquid crystalline phase the efficiency of β -phenyl quenching, which could be monitored by nanosecond laser flash photolysis, should be reduced.

This work resulted in the observation of one of the largest solvent order effects (to date) on the energetics of an unimolecular reaction.^{25,26} Shown below (Figure 1.6) is an Arrhenius plot for the temperature dependence of the triplet lifetime of 4-methoxy- β -phenylpropiophenone (**1**) in CCH-4. The large change in the slope (at the bulk N \rightarrow S phase transition) was interpreted as being a result of the significant increase in solvent order that arises as the sample undergoes a N \rightarrow S phase transition. While this result was very encouraging, a number of questions remained unanswered. For example, the triplet lifetime of **1** displayed phase-independent behavior in CCH-2. This was rather surprising, and was interpreted as indicating that the length of the solute relative to the length of the mesogen, was critical if phase dependent behavior was to be observed. Using space filling models **1** was determined to be slightly longer than CCH-2, while it was slightly shorter than CCH-4. Indeed, other substituted β -phenylpropiophenones showed no phase-dependent behavior in either CCH-4 or CCH-2.^{25,26} While preliminary results indicated that the length of the solute drastically affected "the fit" of the solute in the smectic phase, the exact cause of this phenomena was not well understood.

Paramount to the success of investigations pertaining to the effects of solvent order on a dissolved solute's mobility (both translational and conformational motions), is the identification of the phase(s) in which the solute resides. Early studies (see above) assumed⁸⁰ homogeneous (or nearly homogeneous) solubilization of guest solutes in the smectic phase of CCH-4 and CCH-2. Recent studies however, have indicated that the solubilization of guest molecules in the smectic

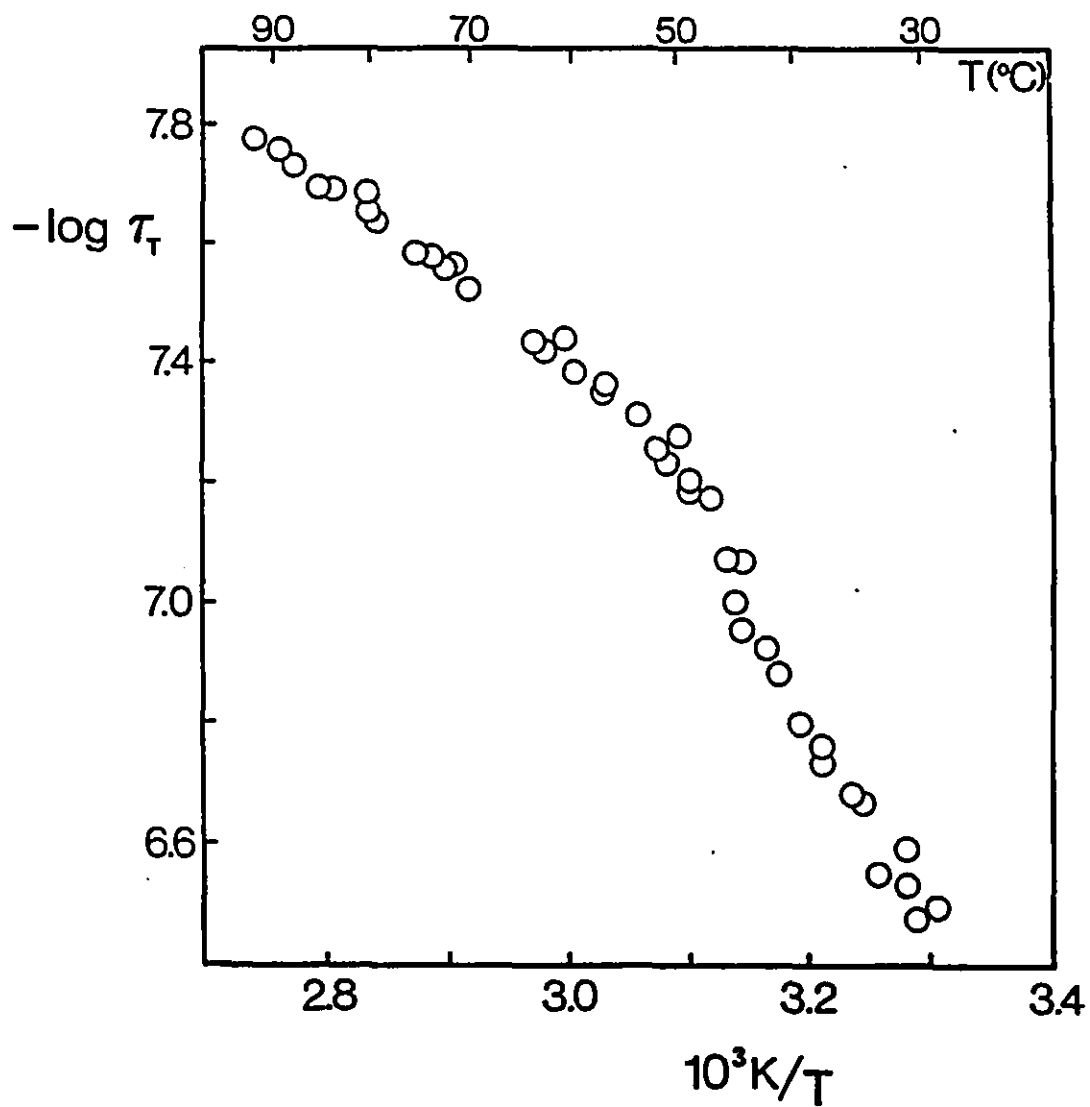


Figure 1.6. Arrhenius plot showing temperature dependence of the triplet lifetime of 1 as a 1 mol% mixture in CCH-4. Reproduced with permission from reference 85.

phase of CCH-4 may be much more complex than previously thought,^{22,81-86} and it may be incorrect to assume homogeneous solubilization. For example, Fung and Gangoda have reported that mixtures containing 3 - 5 mol% benzene in CCH-4 exhibits partially isotropic ¹³C NMR behavior at temperatures below 10°C.⁸¹ They assigned this as being due to the formation of a solute-induced plastic- or cubic-phase formed on slow cooling from the nematic phase.

Similar isotropic-like NMR spectra were observed in ²H NMR investigations of aromatic ketones in CCH-4 by Weiss and co-workers.⁸³ They concurred with Fung and Gangoda that this was the result of a solute-induced plastic- or cubic-phase. Although the ²H NMR spectra of these aromatic ketones throughout the smectic phase temperature range of pure CCH-4 showed a somewhat unusual behavior, no mention was made of this. At temperatures above the onset of the plastic- or cubic-phase, Weiss and co-workers assumed that the ketones were homogeneously solubilized in the smectic phase of CCH-4.

Perhaps a more significant result pertaining to the solubilization of guest solutes in the smectic phase of CCH-4 was reported by Leigh and Jakobs³⁸ in their study of intramolecular quenching by hydrogen abstraction in elongated aromatic ketones. These workers reported that some aromatic ketones induced *phase separation* when solubilized in the bulk smectic phase of CCH-4; suggesting that the solute was solubilized in a ketone-rich nematic phase within the bulk smectic framework.

Clearly, there remains much confusion regarding the solubilization of solutes in the liquid crystalline (particularly smectic) phases of CCH-4 and CCH-2, and the effects that these phases can have on the conformational motions of dissolved solutes. Our work was initiated as part of a broader program to better characterize the nature of the solubilization of these ketones in these liquid crystals, to enable an

accurate interpretation of photochemical results.

We wish to report the results of an extensive investigation pertaining to the solubilization of aromatic ketones and benzene in the liquid crystalline phases of CCH-4, and to a lesser extent CCH-2 and EB. This work represents the most comprehensive study and description of guest solute solubilization in the liquid crystalline phases of these solvents to date. In addition, the exploitation of ^2H NMR as an analytical tool for identifying and quantifying the phase and/or phases in which the solute is solubilized is presented.

Finally, the results reported herein allow for a better understanding of the results from previous studies (both photochemical and NMR) pertaining to the solubilization of the solutes presented here, and as well other work involving similar solutes not investigated here.

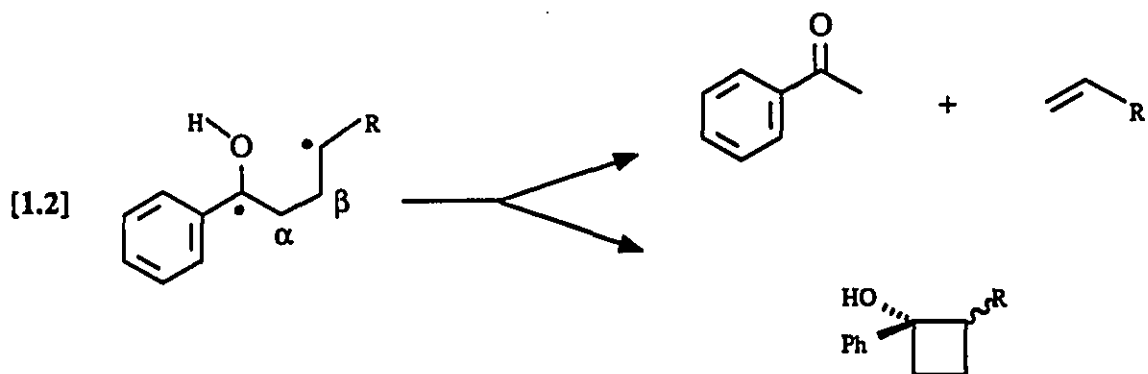
Techniques Used

In the absence of ionic interactions between solute and solvent, there are two ways in which a solvent can influence the freedom of motions that are available to a solute molecule; solvent viscosity and/or solvent order. As previously outlined, there are numerous techniques from which one can choose to monitor solute/solvent interactions. The success of a project may depend a great deal on the choice of technique used.

It is important, for example, that the techniques used be able to distinguish between solvent viscosity and solvent order. Solvent viscosity (without solvent order), or microviscosity as it pertains to a dissolved solute, will inhibit the conformational motions of a dissolved solute without affecting the relative population of the allowed solute conformations. In contrast, solvent order should directly influence the relative population of obtainable conformations for a dissolved solute, as well as inhibiting conformational mobility.

Methods for monitoring such solute/solvent interactions such as triplet lifetime studies^{25,26} and/or investigations pertaining to the photoreactivity of dissolved solutes^{13-15,18,19,38} for example, may not be able to distinguish between the effects of solvent viscosity and solvent order. For example, triplet lifetime studies on substituted β -phenylpropiophenones^{25,26} monitor the ease of rotation about the $\alpha\beta$ bond (Equation 1.1) which can conceivably be impeded as much by solvent viscosity changes as changes in the solvent order, regardless of the initial geometry of the solute. At the very least, it would be extremely difficult to discern between solvent viscosity and solvent order effects in a system where an increase in solvent order is accompanied by an increase in solvent viscosity.

Likewise, the use of the Norrish II reaction (Equation [1.2]) to monitor solvent order effects can also give misleading results. These experiments rely on the subsequent product forming reactions of the 1,4-biradical to gain information regarding solvent order effects^{21-23,84} (*i.e.* how is the solvent disrupting or enhancing rotation about the $\alpha\beta$ bond in the biradical).



However, since little is known about what the effects of solvent viscosity are on the product distribution in the Norrish II reaction, these results must be viewed with caution unless they are supported with data obtained by other methods. In contrast, ^2H NMR (see later) experiments can (in most instances) easily distinguish between

molecular motions which are restricted or slowed because of solvent ordering from those which are restricted or slowed because of an increase in solvent viscosity.

In view of the above, the main technique that will be exploited throughout this investigation is ^2H NMR. Both CCH-4 and CCH-2 are particularly well suited for NMR investigations as they have negative diamagnetic anisotropy, causing the nematic and smectic phases to be aligned perpendicular to the applied field direction.^{63,87-91} This has the advantage of allowing the sample to be spun (in superconducting magnets), if desired, without disruption of the liquid crystalline order present.

An important advantage of ^2H NMR over other techniques is that the labelling of the liquid crystal or dissolved solute with a deuterium atom does not alter any of the physical properties of the molecule such as length or width; in essence providing an *invisible spy*. As well, ^2H NMR makes it possible to probe the mobility of the liquid crystalline molecule (or dissolved solute) at more than one site by incorporating more than one label on the molecule (*i.e.* for each motionally non-equivalent deuterated site in the molecule there will be a distinct quadrupolar doublet). This has tremendous advantages over other techniques which cannot isolate distinct regions of the liquid crystalline molecule or dissolved solutes.

The major disadvantage of ^2H NMR is that it is not always a trivial matter to label the molecule of interest at the site of interest. Often this obstacle will discourage experimenters from further exploiting ^2H NMR as a probe of ordered media.

The goal of this work was to provide more information (*via* ^2H NMR studies) on the solubilization of β -phenylpropiophenones in CCH-4 and CCH-2 than was obtainable from calorimetry and thermal microscopy studies. Before our work there were relatively few examples of deuterium NMR spectra of dissolved solutes

in the liquid crystalline phases of CCH-4 and CCH-2. As a result, it was necessary to establish enough examples of ^2H NMR spectra of dissolved solutes in the liquid crystalline phases of CCH-4 and CCH-2 to ensure the credibility to our interpretation.

To this end, the results obtained from detailed ^2H NMR investigations of substituted α -deuterated- β -phenylpropiophenones solubilized in CCH-4 and/or CCH-2 are presented and discussed in Chapter II. Similarly, results obtained from *para*-substituted α -deuterated-acetophenones, α -deuterated-methoxyvalerophenone, and deuterated benzene are presented and discussed in Chapter III. Chapter V provides a description of the experimental procedures used to obtain the data presented in this thesis.

Finally, it should be noted that with the better understanding that we now have (a result of the work presented in this thesis and other work in our laboratory) regarding the solubilization of guest molecules in liquid crystalline solvents, other members of our group have been able to successfully control the product distribution of a bimolecular reaction.²⁷

The remainder of this chapter provides a detailed description of the necessary background for successful utilization of ^2H NMR in the investigation of ordered fluids.

1.5 Deuterium NMR

Traditional spectroscopic techniques such as UV/Visible and IR deal with the study of transitions between energy levels in the molecule which are characteristic of the electronic structure and atomic makeup of the molecule.⁹² Nuclear magnetic resonance (NMR) spectroscopy⁹³ is different from these forms of spectroscopy in that the spacing between the energy levels that is probed is directly dependent on the strength of the magnetic field that is applied to the sample.

The particles which make up a nucleus, the proton and the neutron, each have intrinsic angular momenta which combine in the nucleus to give a net nuclear spin (I). The spinning of the nucleus circulates the nuclear charge which generates a magnetic dipole or electric quadrupole along the axis of rotation (the nuclear axis). The magnetic pole associated with a nucleus can be thought of as a tiny magnet. Depending on the nucleus, I can be zero as is the case for ^{12}C and ^{16}O , while for others it can be integral or half integral values. For example, I for ^1H and ^{13}C is $1/2$ while I for ^2H is 1. The spin number I determines the number of orientations a nucleus may assume. In the absence of a magnetic field, all of these orientations are degenerate, but in the presence of a homogeneous external magnetic field, each of these orientations (spin states) will have a different energy depending on how they line up with the external field. The number of possible spin states can be calculated using the formulation $2I + 1$. As a result, we can observe transitions from one spin state to another for those nuclei with I not equal to zero (see Figure 1.7).

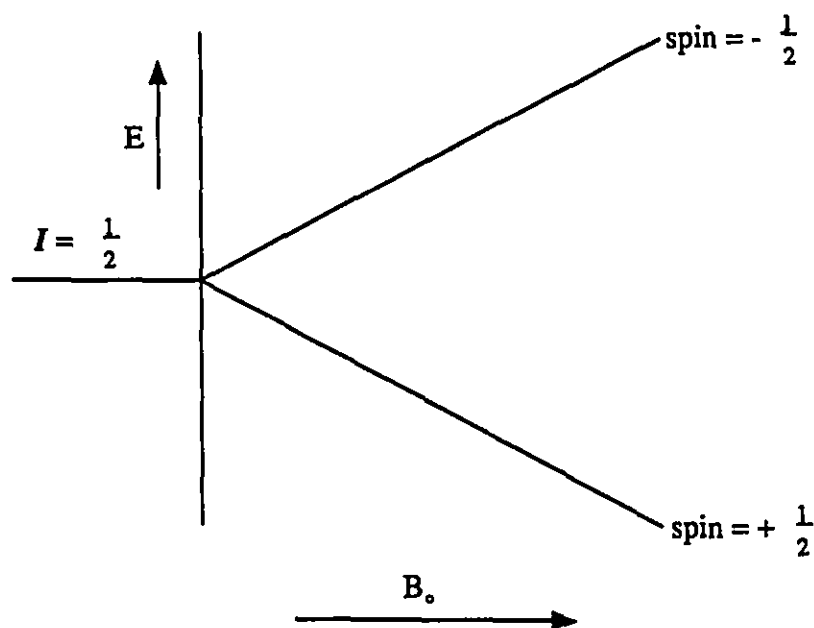


Figure 1.7. Energy diagram showing the effect of an external magnetic field on the relative energies of the two spin states from ^1H .

NMR spectroscopy is the study of the transitions between the possible nuclear spin states of a given nucleus. Fortunately, the strength of the magnetic field is not the only factor which influences the energy difference between the spin states. In reality, there are at least 5 contributing factors which can alter the energy splitting between two spin states. A general Hamiltonian for the interactions which may influence the energy difference between spin states is shown in Equation [1.3] where H_Z is the Zeeman interaction, H_D is the dipolar coupling, H_{CS} is the chemical shift contribution, H_{SC} is the scalar coupling, and H_Q is the quadrupolar interaction.

$$[1.3] \quad H = H_Z + H_D + H_{CS} + H_{SC} + H_Q$$

In many cases however, one or two of these factors usually dominates a given system.⁹⁴ In solution NMR, H_D and H_Q are usually very small contributors. For solid state NMR however, nuclei with $I > 1/2$, usually have their spectra dominated by the quadrupolar interaction and the Hamiltonian is simplified to [1.4].⁹⁴

$$[1.4] \quad H = H_Z + H_Q$$

The remainder of this discussion will be concerned with the quadrupolar interaction and how it applies to the deuterium nucleus.

The quadrupole interaction arises from the interaction of nuclear charge with a non-spherically symmetric electric field gradient (Figure 1.8). It is important to note that the quadrupolar interaction affects the spin states with $m = \pm 1$ equally and in the same direction, while the $m = 0$ state is affected in the opposite direction.⁹⁴ The quadrupolar splitting $\Delta\nu_Q$ (in Hz) is equal to 2α (see Figure 1.8) and can be determined for *solids* (single crystals) using Equation [1.5] where θ is the angle between the principle component of the electric field gradient (N) and the magnetic field (B_0), η is a measure of the asymmetry in fluctuations of the electric field about N , and ψ defines the orientation of the electric field about B_0 (see Figure 1.9).

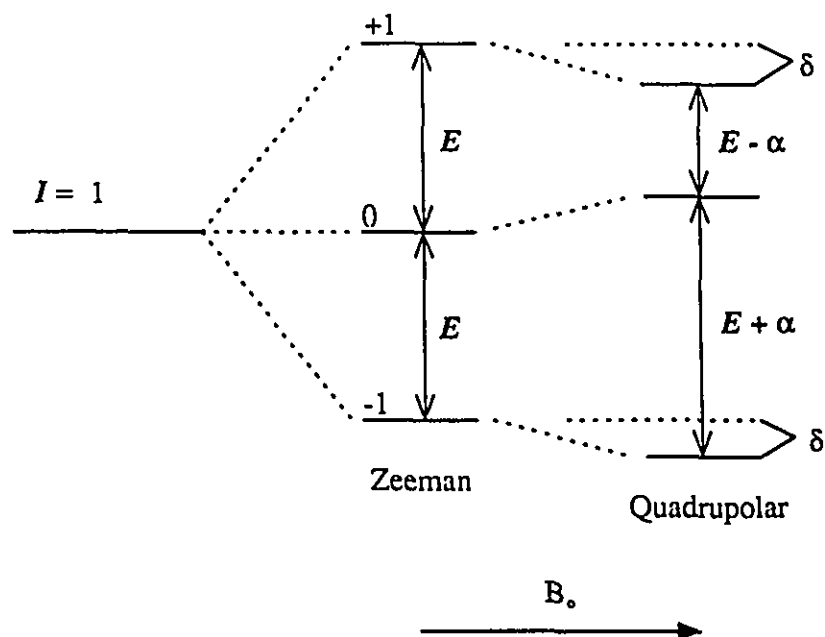


Figure 1.8. Schematic representation of the effect of the quadrupole moment of the nucleus on the Zeeman energy levels of a spin 1 nucleus.

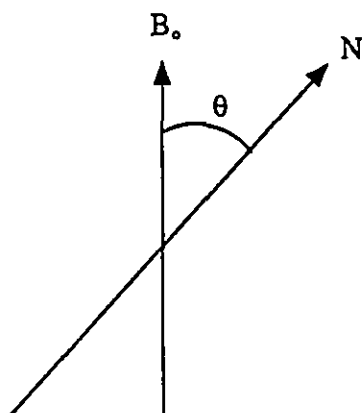


Figure 1.9. Schematic illustrating the relationship between the principal component of the electric field gradient and the magnetic field.

$$[1.5] \quad \Delta\nu = \frac{3}{4} \left[\frac{e^2qQ}{h} \right] \left((3 \cos^2\theta - 1) + \eta \cos 2\psi \sin^2\theta \right)$$

Since deuterium can only form sigma bonds, it is convenient to choose the C - D bond as the principle axis, as sigma bonds are generally considered to be symmetric about their central axis. As a result, η can be assumed to be zero or very small.⁹⁴ This greatly simplifies the expression for the quadrupolar splitting, allowing Equation [1.5] to be reduced to [1.6].

$$[1.6] \quad \Delta\nu = \frac{3}{4} \left[\frac{e^2qQ}{h} \right] (3 \cos^2\theta - 1)$$

The constant (e^2qQ/h) is the quadrupole coupling constant.

In the case of liquid crystals, Equation [1.6] no longer adequately describes the quadrupolar splitting. This result occurs because liquid crystals are *fluid* ordered media in which some molecular motions are fast on the NMR time scale. Consequently the value of θ (*i.e.* the direction of N with respect to B_0) is constantly changing with time. In this situation it is necessary to determine a *time averaged* value of θ .⁹⁵ This is indicated by the $\langle \rangle$ brackets in Equation [1.7].

$$[1.7] \quad \Delta\nu = \frac{3}{4} \left[\frac{e^2qQ}{h} \right] \langle 3\cos^2\theta - 1 \rangle$$

In isotropic solutions, where molecular motions are fast on an NMR time scale and all values of θ are equally probable, the value of $\langle 3\cos^2\theta - 1 \rangle$ will be zero and as a result no quadrupolar splitting will be observed (*i.e.* $\Delta\nu_Q$ will be zero).

Often when working with liquid crystals, it is difficult to predict a time averaged value of θ for a particular system. In these situations, it is advantageous to separate the various molecular motions that will contribute to the overall time averaged value of θ . For example, nematic phases often have uniaxial order present which allows the liquid crystal to rotate freely about its long axis. In this situation θ can be separated into two values; θ_0 and β (see Equation [1.8]) where θ_0 is the angle

$$[1.8] \quad \Delta v = \frac{3}{4} \left[\frac{e^2 q Q}{h} \right] \langle 3 \cos^2 \theta_0 - 1 \rangle \langle 3 \cos^2 \beta - 1 \rangle$$

between the long molecular axis of the liquid crystal (M_z) and the magnetic field, and β is the angle between N and the long molecular axis of the liquid crystal (see Figure 1.10). There is still a need to time average $\langle 3 \cos^2 \theta_0 - 1 \rangle$ because the angle

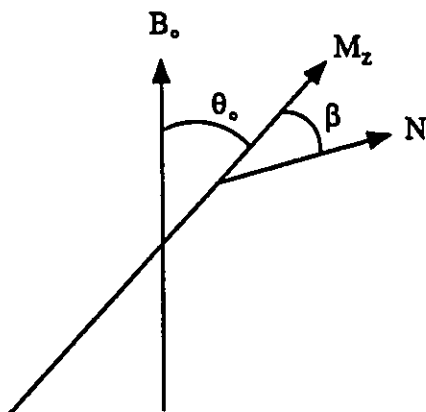


Figure 1.10. Schematic illustrating the relationship between the principal component of the electric field gradient (N), the molecular axis (M_z), and the magnetic field (B_0).

that the long molecular axis of the liquid crystal molecule makes with the magnetic field will change with time. In addition, $\langle 3 \cos^2 \beta - 1 \rangle$ must also be time averaged as

the molecule adopts different allowed conformations. To simplify this description further, $\langle 3\cos^2\theta_0 - 1 \rangle$ can be separated into two terms (see Figure 1.11). In this

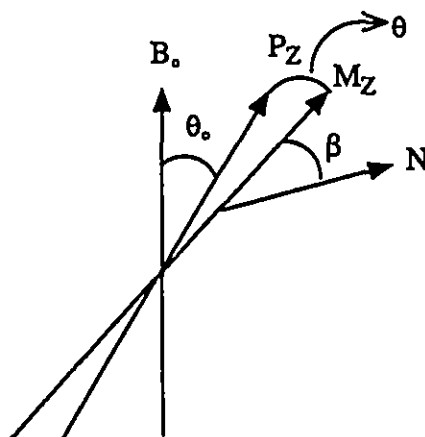


Figure 1.11. Schematic illustrating the relationship between the principal axis of the electric field gradient (n), the long molecular axis (M_z), the principle axis (P_z), and the magnetic field (B_0).

description θ_0 is redefined as the angle between the principle axis P_z (P_z is fixed in the frame of the liquid crystal and as such is not time dependent) and the magnetic field. A new angle, θ , is introduced; this is the angle that the molecular axis (M_z), has at any given instant, with P_z . Of course since the liquid crystal molecules are continuously moving, this angle is time dependent and must also be time averaged (Equation [1.9]). The term $(3\cos^2\theta - 1)$ in Equation [1.9] is defined as the

$$[1.9] \quad \Delta v = \frac{3}{4} \left[\frac{e^2 q Q}{h} \right] (3\cos^2\theta_0 - 1) \langle 3\cos^2\theta - 1 \rangle \langle 3\cos^2\beta - 1 \rangle$$

order parameter, S_{ZZ} , which allows Equation [1.9] to be rewritten as Equation [1.10].

$$[1.10] \quad \Delta\nu = \frac{3}{4} \left[\frac{e^2qQ}{h} \right] (3\cos^2\theta_0 - 1) S_{ZZ} \langle 3\cos^2\beta - 1 \rangle$$

Clearly, ^2H NMR provides an excellent means for probing selected motions in ordered environments such as liquid crystals.

Qualitative Features of ^2H NMR Spectra

Fortunately, the qualitative features of non-isotropic ^2H NMR spectra can reveal a significant amount of information about the nature of a particular system. For example, it is relatively easy to distinguish between ^2H NMR spectra which are the result of powders, from those which arise from ordered environments such as those found in liquid crystals.

In simple terms, a powdered sample (of molecules containing a single C - D bond) can be thought of as one in which all the C - D bonds are oriented with respect to the magnetic field (*i.e.* the molecules reorientate themselves slowly on the NMR time scale). However, there is no correlation between how one molecule (C - D bond) is oriented with respect to the rest of the molecules (C - D bonds) in the sample. In this situation the spectrum that is observed is the result of a *statistical distribution* of all possible orientations of the C - D bond with respect to the magnetic field. An example of such a spectrum is shown below in Figure 1.12.

In contrast, an oriented sample like those found in nematic phase liquid crystals can be thought of as one in which *all* of the C - D bonds are on average (over time) oriented in a given direction with respect to the magnetic field (*i.e.* the time-averaged components of Equation [1.9] are the same for all molecules in the sample which results in a well defined doublet). Therefore, the spectra which is observed is *not* the result of a statistical distribution and as a result has a much different appearance. A typical example of an *oriented* spectrum is shown below in

Figure 1.13.

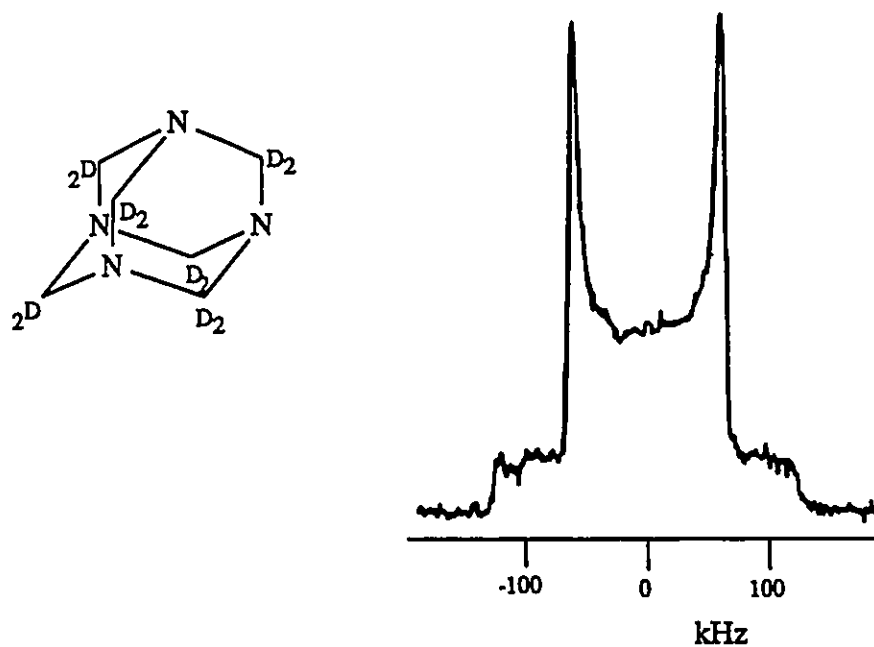


Figure 1.12. ^2H spectrum of hexamethylenetetramine- d_{12} , an example of a powder pattern. Adapted from reference 94.

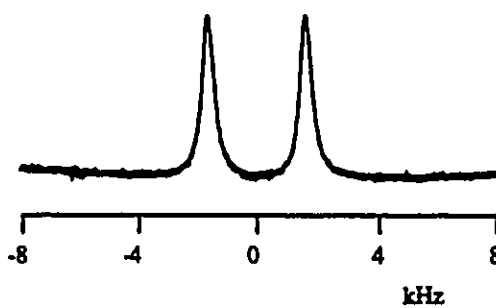


Figure 1.13. An example of a ^2H NMR spectrum of dissolved solute (p -dioxane- d_8) in the nematic phase (41 °C) of Merck "1565 TNC". Adapted from reference 61.

The degree of order within a given liquid crystalline sample can dramatically alter the appearance of the ^2H NMR spectrum that is observed for a particular sample. For example, the spectrum shown in Figure 1.13 is the result of a sample in which there is still a large degree of freedom in the motions for the molecule containing the C - D bond. In this example, the motions are occurring fast on the NMR time scale, and the observed spectrum is time-averaged. If however, the order within the sample was sufficient to slow the reorientation motions of the molecule containing the C - D bond, such that they were now slow on the NMR time scale, then the observed spectra would broaden considerably. This is the result of the fact that the C - D bond can now be observed in more than one orientation with respect to the magnetic field.

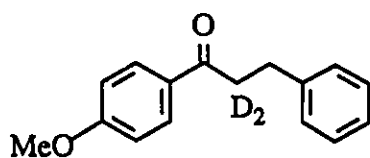
In thermotropic liquid crystals, where the order in the system is temperature dependent, changes in temperature may also result in significant changes to the appearance of the observed spectrum. In certain cases, the whole range of spectra discussed above may be observed from a single sample, simply by changing the temperature.

CHAPTER II

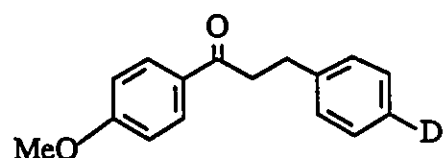
The Deuterium NMR Investigation of the Solubilization of Substituted β -Phenylpropiophenones in CCH-4, CCH-2, and EB.

A. Introduction

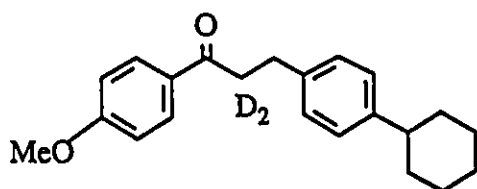
This chapter describes the results obtained from the ^2H NMR investigation of the solubility of substituted α -deuterated- β -phenylpropiophenones (1 - 4) in the liquid crystalline phases of CCH-4. These results have allowed for the development



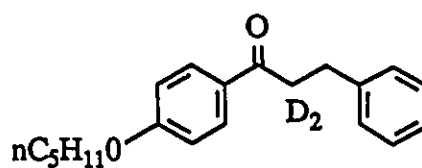
1



2



3



4

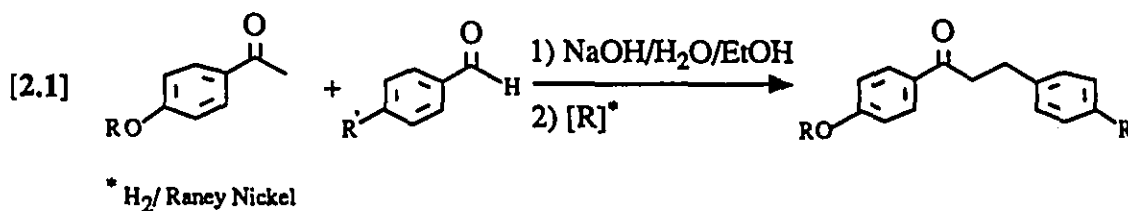
of a new model describing the solubilization of large aromatic ketones in the liquid crystalline phases of CCH-4.

B. Results

2.1 Preparation of Compounds

The substituted β -Phenylpropiophenones were prepared (using a previously

described method^{25,26}) by condensation of the appropriate alkoxyacetophenone with the appropriately substituted benzaldehyde, followed by hydrogenation of the resulting α,β -unsaturated ketone over Raney nickel (Equation 2.1).



The α -deuterated ketones (1 - 4) employed in this study were prepared from their protio-analogs by exchange deuteration in alkaline deuterium oxide/dioxane, and were estimated to be $\geq 90\%$ isotopically pure in the α -position by ^1H NMR spectroscopy.

β -(4-Deuteriophenyl)-4-methoxypropiophenone (2) was synthesized from 4-deuteriobenzaldehyde by a similar procedure to that used for 1.^{25,26} 4-deuteriobenzaldehyde was prepared by $\text{D}_2\text{O}/\text{THF}$ quenching of the aryllithium prepared from 4-bromo-(2-(1,3-dioxacyclopentyl)benzene with subsequent hydrolysis of the acetal.

2.2 Deuterium NMR of Solutes in Liquid Crystalline Solvents

Sample Preparation for Deuterium NMR Studies

The deuterated ketone/Liquid Crystal samples were prepared in 5 mm NMR tubes by adding the appropriate amounts of the solute and liquid crystal and heating to the isotropic phase to ensure complete and uniform mixing of the solute.

General Deuterium NMR Methods Used

Deuterium NMR spectra of all deuterated ketones in CCH-4 were recorded on stationary samples at 76.8 MHz (unless otherwise indicated) with temperatures

ranging between 20°C and 80°C, using the quadrupolar echo pulse sequence.^{96,97} Sample temperatures in the spectrometer were controlled to $\pm 1^\circ\text{C}$. The sample and probe temperatures were allowed to equilibrate at each temperature for as long as was necessary to obtain reproducible spectra. Each sample was heated within the spectrometer to 80°C and allowed to equilibrate before being cooled to the desired temperature. At no time was the sample and/or probe temperature lowered in increments exceeding 5°C. Both the probe and the sample were allowed to equilibrate at each temperature (5°C interval) regardless of whether or not a spectrum was recorded.

Deuterium T_1 measurements were made at 76.8 or 30.7 MHz, and employed a π - τ -quadecho or $\pi/2$ - τ -quadecho (for T_1 values less than 20 ms) non-selective inversion-recovery pulse sequence.

Deuterium NMR of 1 and 2 in CCH-4

The isotropic ^2H NMR spectra (above *ca.* 78°C) of 1 mol% mixtures of both 1 and 2 in CCH-4 were characterized by a single, narrow resonance. Below the bulk nematic→isotropic phase transition, the spectra consist of a single well defined quadrupolar doublet ($\Delta\nu_Q$) characteristic of a uniformly oriented sample^{98,99} that increases in magnitude as the temperature is lowered (see Figure 2.1). The spectra recorded below the bulk N → S phase transition (*ca.* 52°C) are very similar to those observed for the bulk nematic phase. However, for the temperature region defined by the bulk smectic phase, the magnitude of $\Delta\nu_Q$ *decreases* with decreasing temperature. Prior to the onset of the S → K phase transition (35°C), the quadrupolar doublet coalesces to a singlet of similar linewidth to that observed in the isotropic phase. With careful control of the sample temperature it is possible to simultaneously observe both the singlet and quadrupolar doublet (*ca.* 78 and 35°C) as the sample undergoes a phase transition.

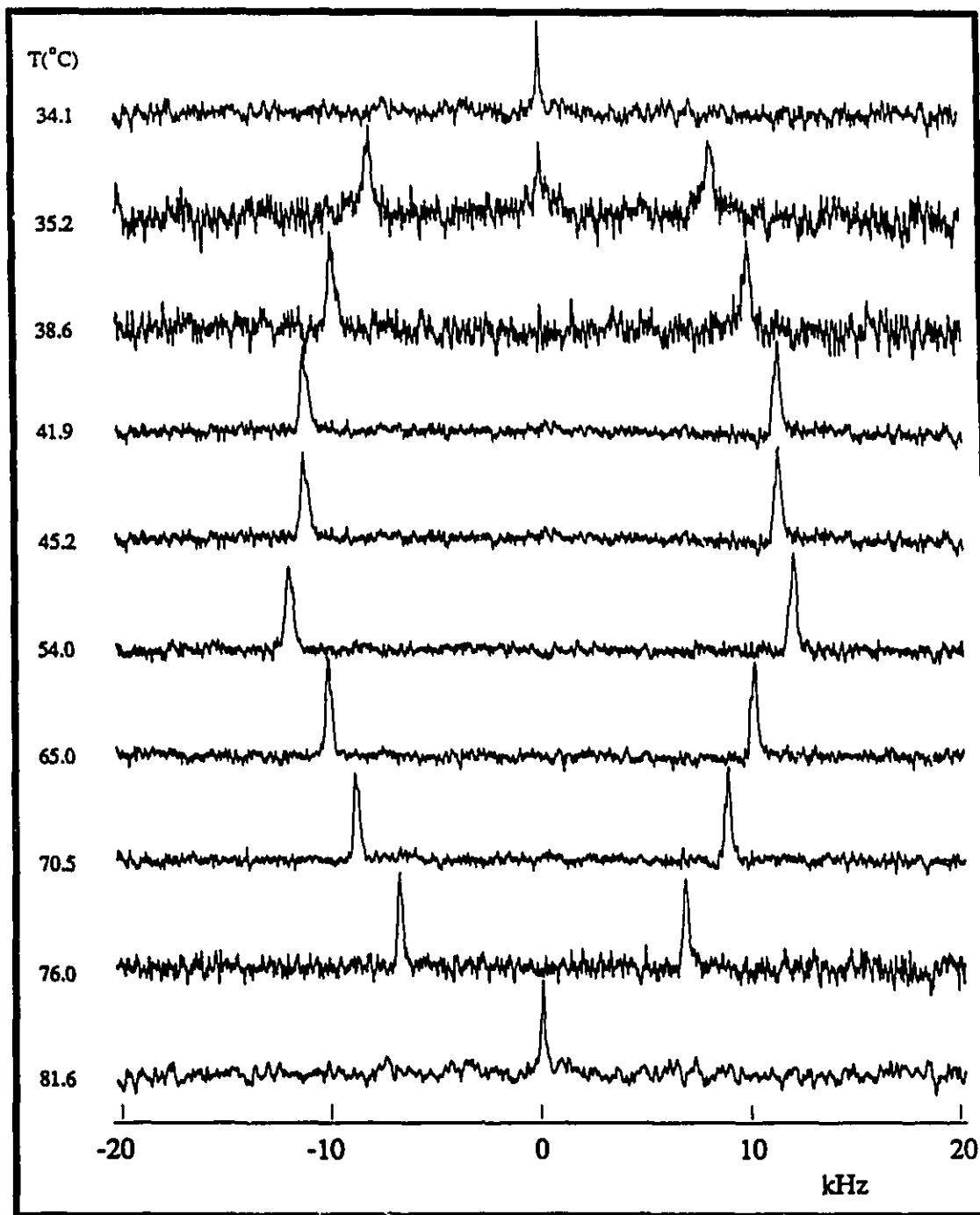


Figure 2.1a. Deuterium NMR spectra of 1.0 mol% 1 in CCH-4 as a function of temperature.

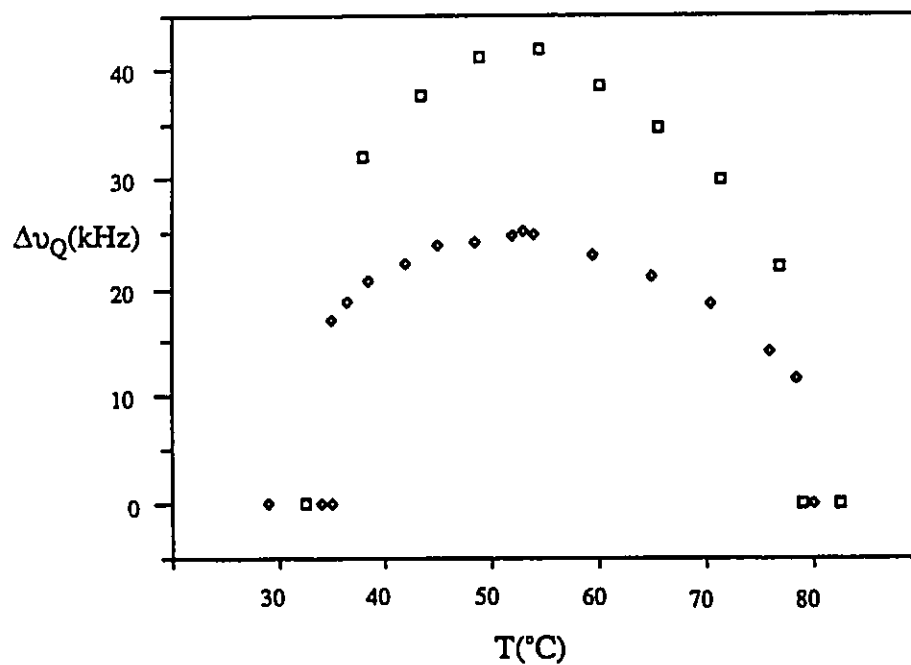


Figure 2.1b. Deuterium quadrupolar splitting ($\Delta\nu_Q$) versus temperature for 1 mol% mixtures of 1(◇) and 2(□) in CCH-4.

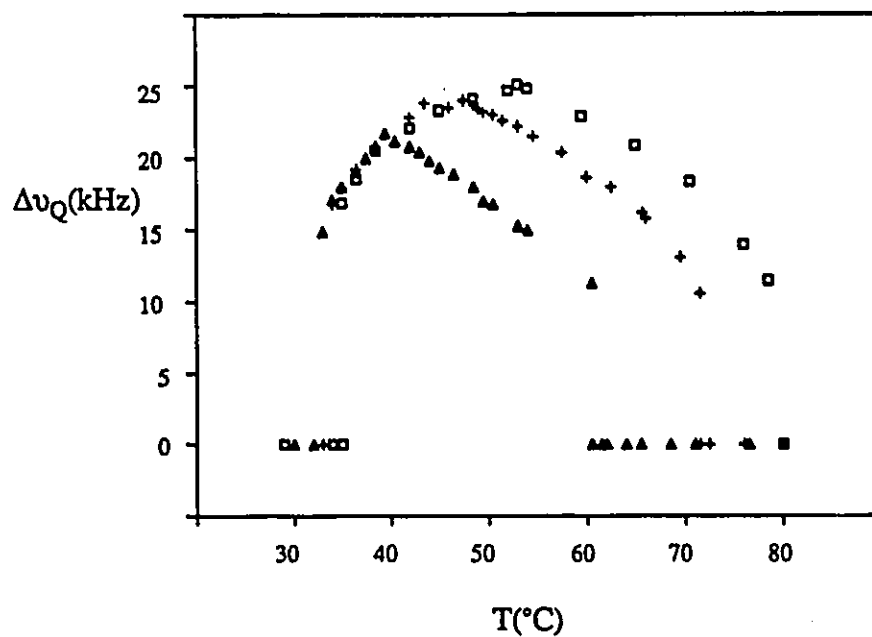


Figure 2.2. Deuterium Quadrupolar splitting ($\Delta\nu_Q$) versus temperature for 1.0(□), 5.0(+), and 10.0(Δ) mol% mixtures of 1 in CCH-4.

Similar experiments were also performed on 3, 5, and 10 mol% mixtures of **1** in CCH-4, and those for the 5 and 10 mol% samples are shown in Figure 2.2. All of the samples investigated were allowed to equilibrate at each temperature before spectra were recorded (*ca.* 10 - 45 minutes for those samples of composition <5 mol% ketone, and as long as 2 hours for samples containing greater than 5% ketone). Particular care had to be taken for the higher concentration samples for temperatures throughout the bulk smectic phase as equilibration is slowed greatly by the decreased ease of diffusion. For both the 5 and 10 mol% samples, if sufficient time for equilibration was not allowed, the apices in the Δv_Q vs. T plots could be supercooled by as much as 5°C. As the bulk concentration of **1** and **2** is increased, the temperature ranges which define the I \rightarrow N and 35°C phase transition were observed to broaden.

We have carefully verified the reversibility of the ^2H NMR behavior of the 3 mol% **1**/CCH-4 sample. The spectra which are observed on cooling of the sample from the isotropic phase are mirrored exactly as long as sufficient time for equilibration is allowed. The only limit to this is that the sample cannot be cooled below 20°C for extended periods of time. In such cases where the sample has been cooled below 20°C for too long, the sample appears to crystallize. We have been unsuccessful in our attempts to observe the ^2H NMR spectrum of this crystallized sample. If the crystallized sample is slowly reheated, we are once again able to observe the ^2H NMR spectrum of the sample at temperatures above 43°C. The spectra which result are identical in every respect to those that were observed for temperatures above 43°C when the sample was cooled from 80°C.

Solubility Limits of **1 in the Smectic Phase of CCH-4**

In an attempt to define the solubility limit of **1** in the smectic phase of CCH-4, experiments were carried out with 0.2 and 0.5 mol% **1** in CCH-4. The 0.5

mol% sample exhibited behaviour similar to that of the 1.0 mol% sample, although the signal-to-noise ratio deteriorated dramatically (much more than was evident with the 1 mol% sample) as the temperature was lowered throughout the 52 - 35°C range. In the case of the 0.2 mol% sample, no deuterium signals could be observed at any temperatures between 10° and 50°C. However, the isotropic singlet characteristic of what was observed for the higher concentration samples (≥ 0.5 mol%, below 35°C) was present in spectra recorded below 8°C for the 0.2 mol% sample (Figure 2.3). The absence of a deuterium signal for the 10 - 50°C temperature region may indicate that the ketone is totally soluble in the smectic phase of CCH-4 at this concentration (0.2 mol%), and that the spectrum in this phase is either too broad or the components too widely separated to be observed with our spectrometer.

Deuterium NMR of 3 mol% 3 in CCH-4

The ^2H NMR of 3 mol% 3 in CCH-4 was similar in all respects to that observed for 3 mol% 1 and 2 in CCH-4, except that $\Delta\nu_Q$ is slightly larger for 3 (see Figure 2.4) than was observed for 1 and 2 at comparable temperatures. The splitting varies between 12.9 and 27.7 kHz in the nematic phase, and decreases to a value of 19.8 kHz as the temperature is lowered below 50°C before collapsing to a singlet at *ca.* 30°C.

Deuterium NMR of 3 mol% 4 in CCH-4

The ^2H NMR of 3 mol% 4 in CCH-4 was similar to that observed for 3% 3 in CCH-4, with $\Delta\nu_Q$ varying between 10.8 and 24.7 kHz in the nematic phase and decreasing to 18.1 kHz as the temperature is lowered below 50°C, before collapsing to a singlet at *ca.* 33°C (see Figure 2.5).

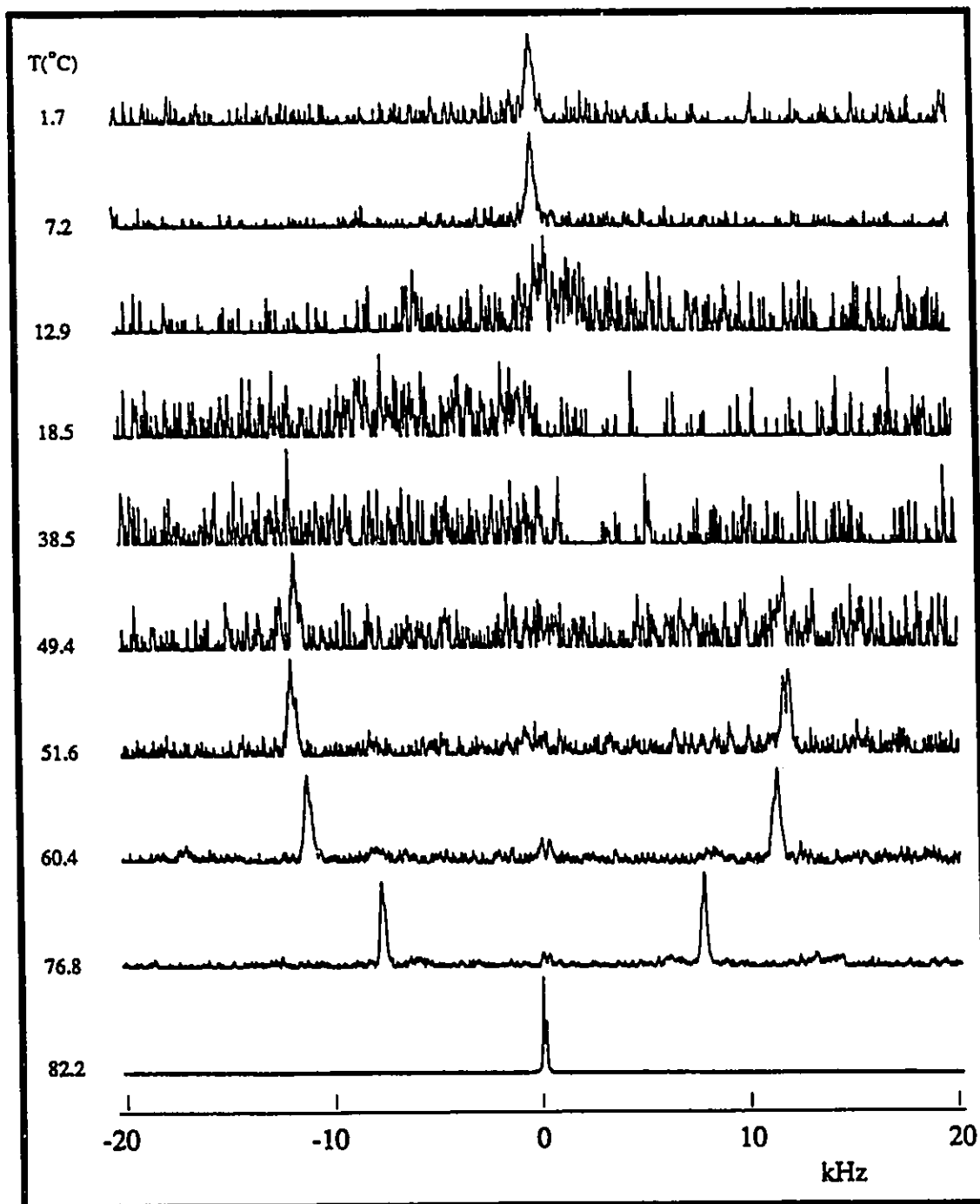


Figure 2.3. Deuterium NMR spectra of 0.2 mol% 1 in CCH-4 as a function of temperature.

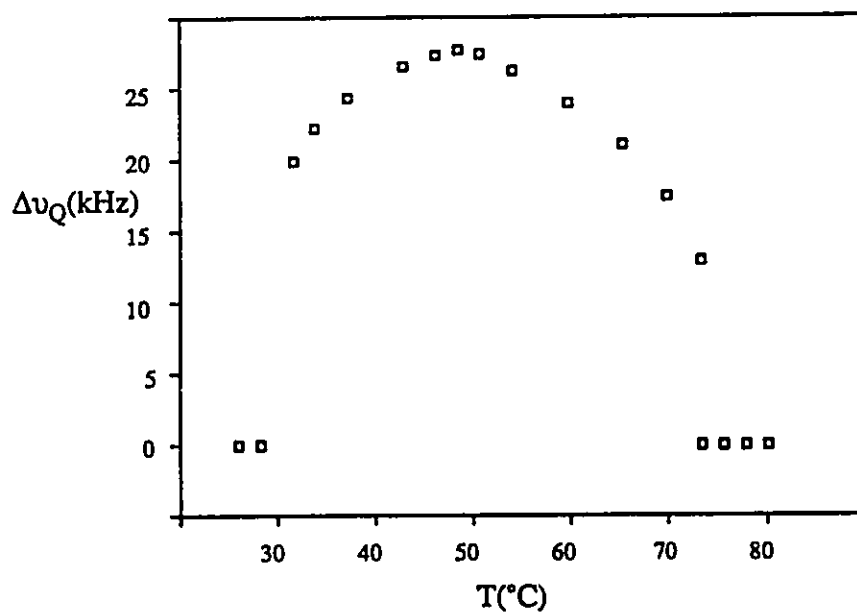


Figure 2.4. Deuterium quadrupolar splitting ($\Delta\nu_Q$) versus temperature for 3 mol% 3 in CCH-4.

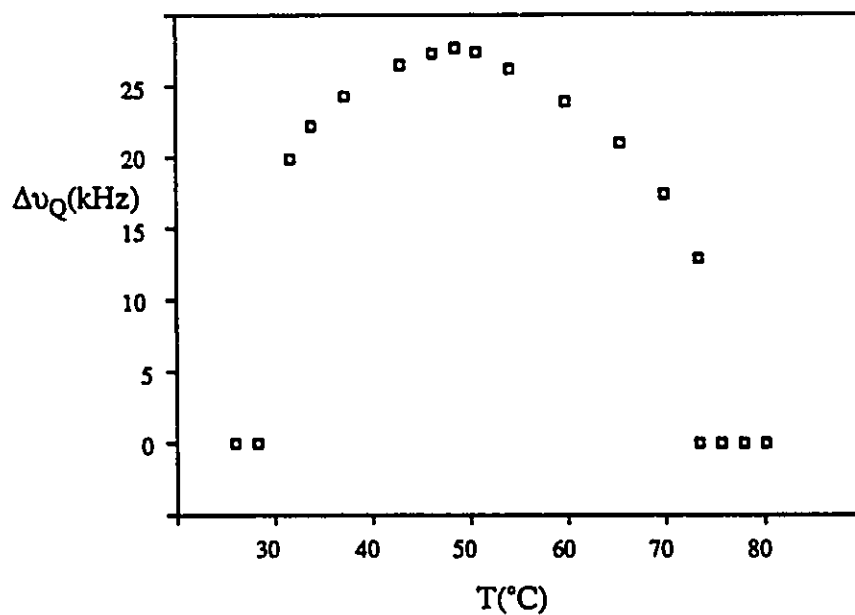


Figure 2.5. Deuterium quadrupolar splitting ($\Delta\nu_Q$) versus temperature for 3 mol% 4 in CCH-4.

Control Experiments

In an attempt to define the observable spectral width of our spectrometer (76.8 MHz), a number of control experiments were performed. This was necessary to ensure that we were not missing any signals (for temperatures below the bulk N \rightarrow S phase transition) that were outside the spectral width of our spectrometer. This was accomplished by varying the offset frequency of the spectrometer in *ca.* 30 kHz steps, to a maximum offset of 65 kHz, from the carrier frequency. In all cases we were still able to observe the characteristic quadrupolar doublet, but did not observe any additional signals. We further explored this possibility by repeating our experiments on a spectrometer that is better equipped to handle larger spectral widths (see Experimental Section). These experiments also showed no other signals.

Deuterium NMR of 3 mol% **1** in EB

The ^2H NMR behaviour of 3 mol% **1** in EB was qualitatively very similar to that observed for **1** in CCH-4. Since the N \rightarrow I and S \rightarrow N phase transitions for EB occur at lower temperatures, the plot of $\Delta\nu_Q$ vs T is shifted to lower temperatures (See Figure 2.6). The splitting varies between 12.0 and 25.0 kHz in the nematic phase. $\Delta\nu_Q$ values were not measured for the smectic phase of EB, although preliminary evidence indicates that the quadrupolar splitting will be zero once the temperature is lowered below the bulk N \rightarrow S transition temperature.

2.3 Deuterium NMR of 0.3 mol% **1** in CCH-2

The ^2H NMR behaviour of 0.3 mol% **1** in CCH-2 was significantly different from that observed for both higher and lower concentrations of **1** in CCH-4 (Figure 2.7). The nematic phase region was qualitatively very similar to that observed for the 0.2 mol% sample in CCH-4, with quadrupolar splittings ranging from 12.2 to

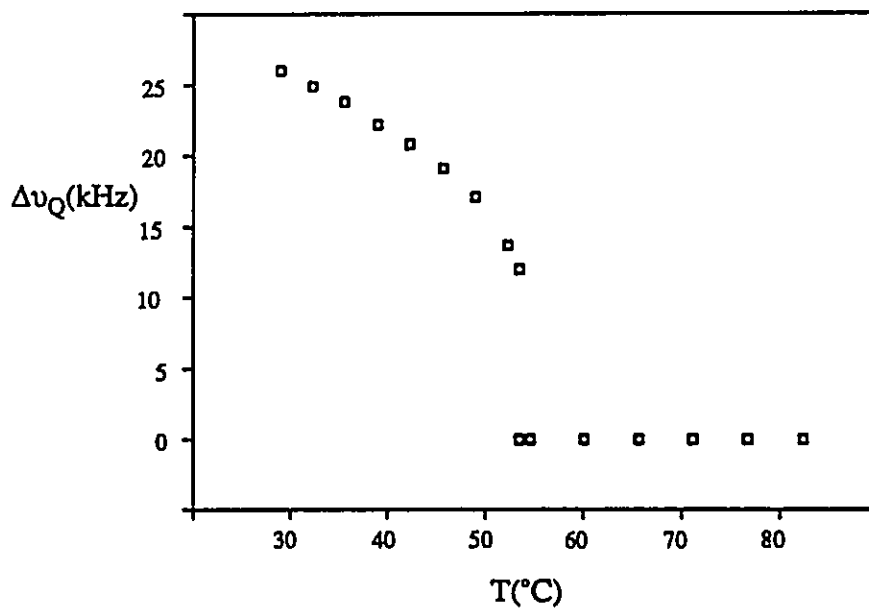


Figure 2.6. Deuterium quadrupolar splitting ($\Delta\nu_Q$) versus temperature for a 3 mol% mixture of 1 in EB.

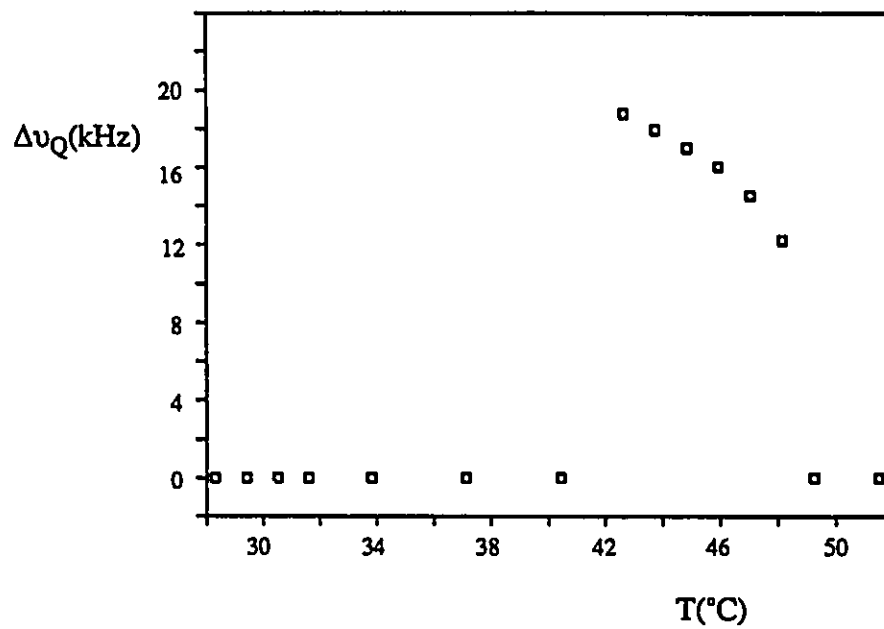


Figure 2.7. Deuterium quadrupolar splitting ($\Delta\nu_Q$) versus temperature for 0.3 mol% 1 in CCH-2.

18.8 kHz. However, below the bulk N \rightarrow S phase transition (43°C) the quadrupolar doublet collapses to a singlet. This singlet persists to temperatures as low as 28°C.

2.4 Deuterium T_1 Measurements on **1** in Liquid Crystalline Solvents.

Deuterium T_1 measurements were recorded on 3 mol% samples of **1** in CCH-4 and EB over temperature ranges of 23 - 110°C and 23 - 90°C, respectively. These experiments were carried out using a consecutive inversion-recovery/quadrupolar echo pulse sequence, and the results are plotted as $-\ln(T_1)$ vs. $1/T$ in Figure 2.8. T_1 -values recorded for the **1**/CCH-4 sample at representative temperatures throughout the same temperature range on a 33 MHz spectrometer were consistently shorter than those measured at 76.8 MHz, but showed similar temperature dependence.

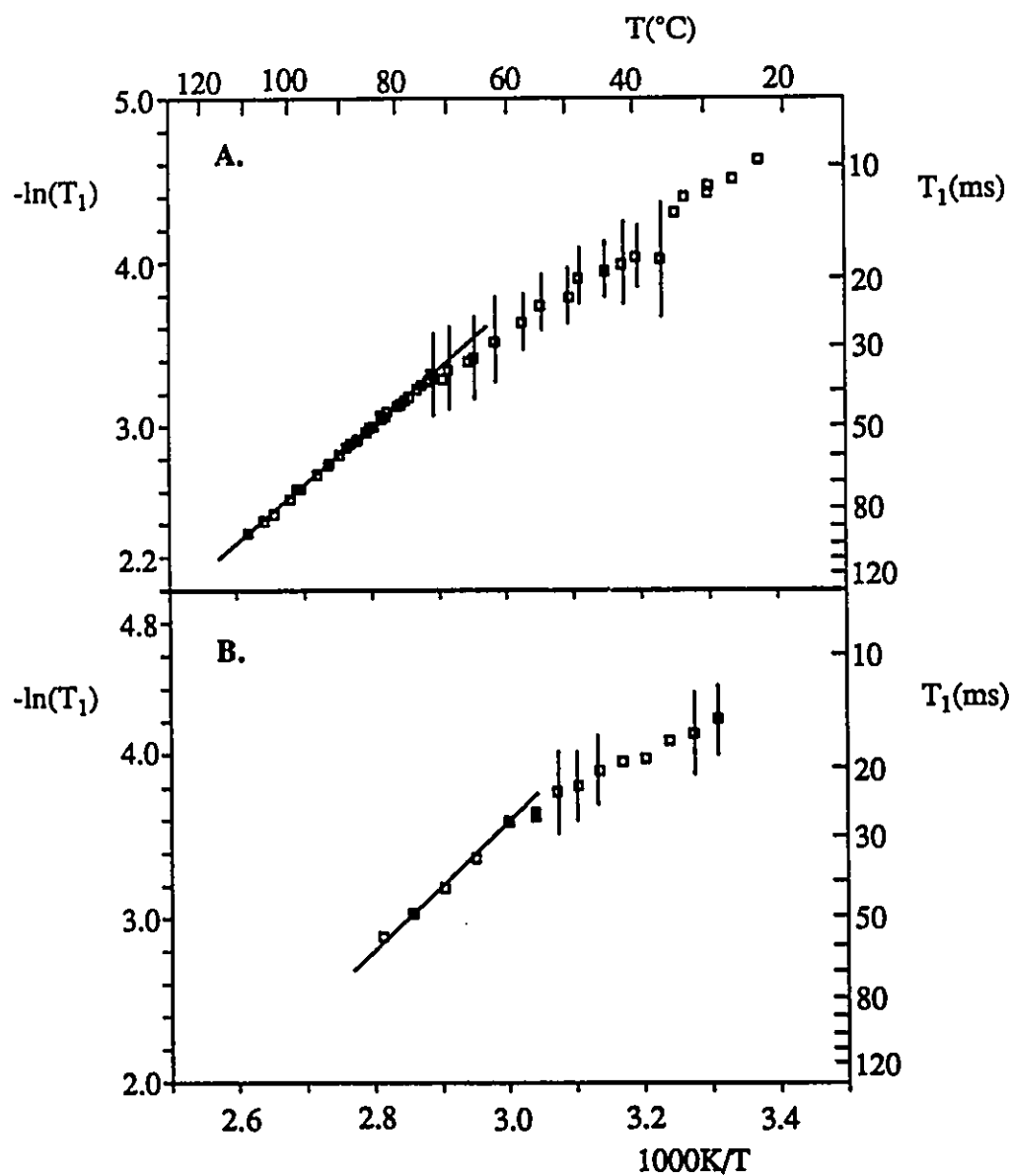
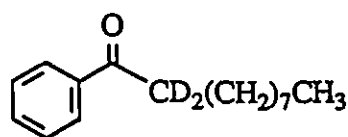


Figure 2.8. Arrhenius plot showing the temperature dependence of T_1 -values obtained for 3 mol% mixtures of **1** in (A) CCH-4 and (B) CCH-2/CCH-4(EB) between 25 and 120°C. Errors were calculated as twice the standard deviation for each point. Error bars are only shown for those points with errors in excess of 10%.

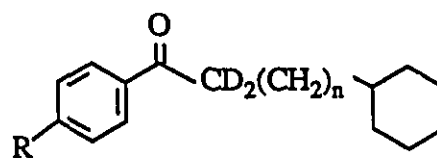
C. Discussion

2.5 The Solubilization of 1 in CCH-4 and EB

The variation in Δv_Q with temperature between 30°C and 80°C that is shown in Figure 2.1 for the 1 mol% 1/CCH-4 mixture is qualitatively very similar to those reported previously for 5 and 6.⁸³



5



6

a: $n = 0$; $R = \text{CH}_2\text{CH}_3$

b: $n = 2$; $R = \text{H}$

c: $n = 3$; $R = \text{H}$

The Nematic Phase

The increase in Δv_Q with decreasing temperature throughout the nematic phase is typical for these kinds of systems, and indicates an increase in the order parameter of the solute as the rigidity of the nematic phase increases.^{61-69,98,99} Once the temperature is lowered below that of the bulk I→N phase transition, a general ordering of the solvent takes place as was described in the introduction. CCH-4 has negative diamagnetic anisotropy,^{63,92} and the sample will thus be aligned in a magnetic field such that the long molecular axes are oriented perpendicular to the field. As the temperature is lowered, the mobility within the nematic phase decreases as there is less thermal energy available to the solvent molecules. This in turn causes the mobility of the solute molecules to be reduced and the observed Δv_Q

to increase (Figure 2.9).

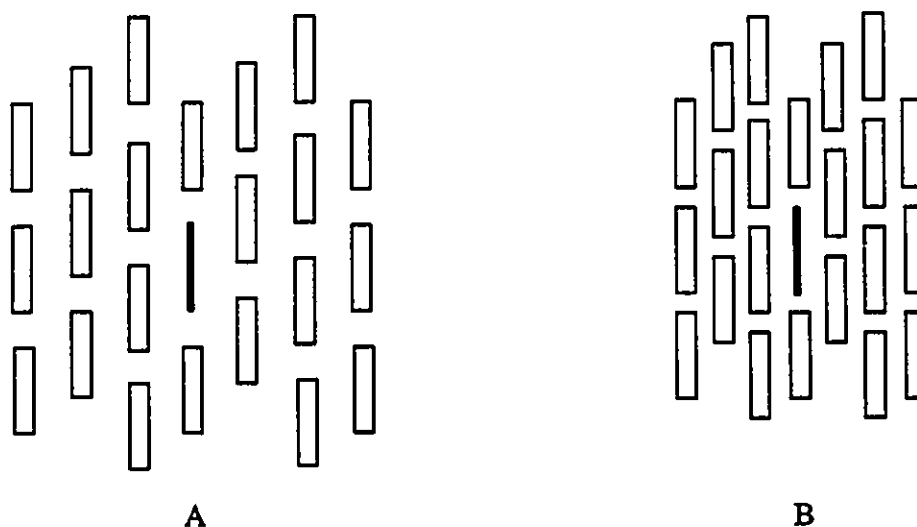


Figure 2.9. Block diagram depicting the solubilization of a solute in the nematic phase of CCH-4. **A:** High temperature. **B:** Low temperature. The positions of the blocks are not meant to imply that there is empty space between the solute molecules, but rather to simulate the average position of the solvent molecules in a mobile fluid. At higher temperatures the solvent molecules will have more thermal energy and as a result will be more mobile, thereby providing more opportunities for the solute to adopt various conformations.

The Smectic Phase

The continuous decrease in Δv_Q that accompanies decreasing temperature within the smectic phase of the bulk mixture seems to be a fairly general observation for solubilized deuterated aromatic ketones in CCH-4.⁸³ Although this behavior has been observed by others⁸³ and is not a typical observation for deuterated guest molecules in ordered media, there has been no previous attempt to explain the origin of this behavior. An abrupt change in a Δv_Q vs T plot of this type near the vicinity of a solvent phase transition, is however, quite typical,⁶¹⁻⁶⁹ and the nature of the change often reveals important information regarding the changes in solvent order and/or solute solubilization. The cause of the discontinuity results primarily from

the difference between the microscopic structures of the two phases (*i.e.* the microscopic environment experienced by the C - D bond), rather than differences in macroscopic order that are reflected in the thermodynamics of the phase transition.^{24,26,33,61-69} As a result, there are three possibilities for how $\Delta\nu_Q$ may be affected by a transition from one phase to a thermodynamically more-ordered phase; an abrupt decrease or increase in the magnitude of $\Delta\nu_Q$, or merely a change in the slope of the plot.

In the case of 1 mol% **1** in CCH-4 (Figure 2.1), the smooth and continuous decrease in the magnitude of $\Delta\nu_Q$ as the temperature is lowered throughout the 35 - 53°C range indicates that either the order parameter of the solute decreases as the temperature is lowered, or that the time-averaged orientation (*i.e.* perpendicular or parallel to the applied field) of **1** changes as the temperature is lowered through this region. The $\Delta\nu_Q$ vs T results for **2** (Figure 2.1) rule out the possibility that solute reorientation effects are responsible for the observed behavior of $\Delta\nu_Q$ vs. T in the temperature region of 35 - 53°C for **1** in CCH-4. If alteration of the time-averaged orientation of the solute was responsible for the decrease in $\Delta\nu_Q$ that accompanies decreasing temperature in the 35 - 53°C range, $\Delta\nu_Q$ should respond differently to temperature in the case of **2** than it does in the case of **1**. This results from the fact that the orientations of the C - D bonds in **1** and **2** with respect to the long molecular axes are roughly perpendicular. In fact, the similarity of the $\Delta\nu_Q$ vs T plots exhibited by **1** and **2** indicates that the favoured orientation of the solute remains the same throughout both the 53 - 78°C and 35 - 53°C temperature ranges. If this were not the case, we should have observed some kind of dissimilarity between the two plots.

The difference in the magnitudes of $\Delta\nu_Q$ observed for **1** and **2** at a given

temperature can be attributed to differences in the motionally averaged orientations of the C - D bonds in the two molecules with respect to the applied field. The consistently smaller value for $\Delta\nu_Q$ for **1** vs. **2** at a given temperature, indicates that the C - D bond in **1** is sampling a much larger range of angles with respect to the applied field than is the C - D bond in **2** (the difference in the quadrupolar coupling constants¹⁰⁰ for aromatic (*ca.* 173 - 197 kHz) and aliphatic (*ca.* 165 -170 kHz) deuterons is much too small to account for the factor of *ca.* 2 difference between $\Delta\nu_Q$ for **1** and **2**). This would be the case if rotation about the long molecular axis was the predominant motion that is sampled by the quadrupolar interaction.

The inescapable conclusion which follows is that the observed behavior of $\Delta\nu_Q$ below 53°C results from a decrease in the order parameter of the solute with decreasing temperature. This type of behavior is not without precedence,⁵⁶ and can be caused by one of several unique solvation phenomena. For example, a change in the solubilization site of **1** from a relatively highly ordered environment at high temperature, to a less ordered environment at low temperature, could account for the observed behavior of $\Delta\nu_Q$ vs. T.⁵⁶ A related possibility is that the solvation site adopts a cavity-like structure as the sample is cooled. This allows for the possibility that the solvation site of the solute may respond differently than that of the pure solvent as the temperature is lowered throughout the region which corresponds to that assigned to the bulk smectic phase of CCH-4.¹⁰¹ With this model, the solvent would become less able to control solute orientation if the order within the cavity decreases with decreasing temperature and as the structure of the cavity becomes better defined. A third possibility results if the solubility of the ketone in the smectic phase of CCH-4 decreases with decreasing temperature, and is lower than the bulk solute concentration. This would result in a continuous leaching of the ketone from the smectic phase (phase separation) at temperatures below 53°C,

causing the ketone to reside in a *nematic* phase between 35°C and 53°C. In this situation the concentration of the ketone in the nematic phase is continually changing. These possibilities are discussed in detail below.

A composite Δv_Q vs. T. plot was constructed of the 1.0, 5.0 and 10.0 mol% mixtures of **1** in CCH-4 (Figure 2.2). As the concentration of **1** in CCH-4 is increased, the onset of the I→N and the N→S phase transitions is depressed to lower temperatures resulting in a series of approximately parallel curves. This is consistent with what would be expected for a series of homogeneous solutions of increasing concentration of **1** in the nematic phase of CCH-4.

Further evidence supporting this description is provided by a composite plot of Δv_Q vs. reduced temperature ($T_{N\rightarrow I} - T$, where $T_{N\rightarrow I}$ is the nematic→isotropic phase transition temperature for the sample of interest) for the data above the S→N phase transition (Figure 2.10). This plot yields a single line that encompasses all of the data for all concentrations.

The plot of the Δv_Q data (Figure 2.2) for the temperatures below the bulk S→N phase transition (as indicated by the apex of the Δv_Q vs T plot for each concentration) fall on a single curve that is independent of the bulk sample concentration. This very strongly suggests that at temperatures below the onset of the S→N transition, the ketone is in a medium whose composition depends only on the temperature, and not on the *bulk* solute concentration.

DSC thermograms have been reported for a wide range of concentrations of **1** in CCH-4.⁸⁵ This study reports a lowering and broadening of the N→I and S→N phase transitions that is in complete agreement with what we observed by ²H NMR. Thermal microscopy(TM) studies of the same samples which were used to record the DSC traces have also been reported.⁸⁵ These results revealed that for **1**/CCH-4

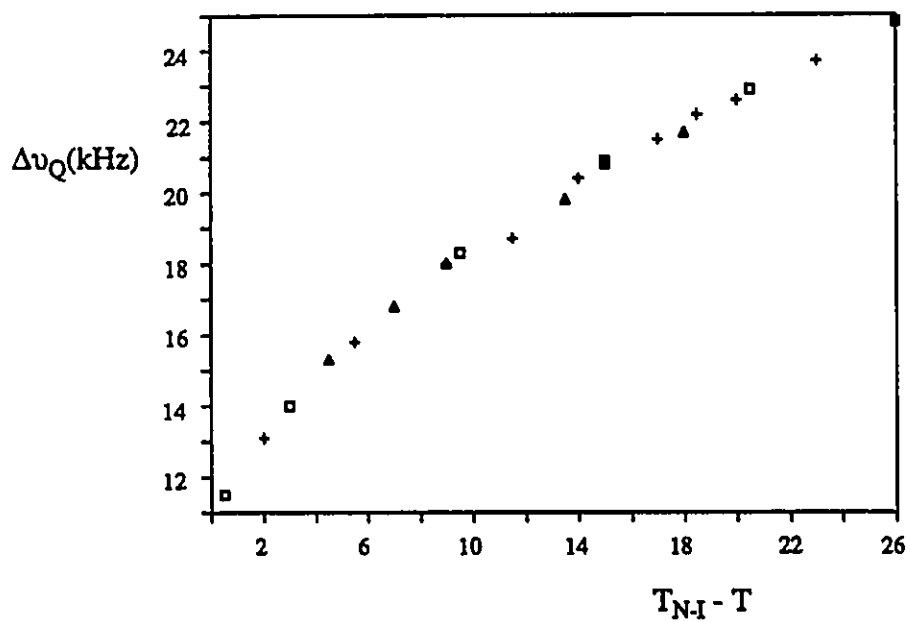


Figure 2.10. Plot of $\Delta\nu_Q$ values versus $T_{N-I} - T$ for the nematic phase temperatures of the 1.0(\square), 5.0($+$) and 10.0(Δ) mol% mixtures of 1 in CCH-4.

samples ranging in concentration from 0.5 - 15 mol%, slow cooling from the nematic phase resulted in phase separation (smectic + residual nematic) at temperatures below the bulk S→N phase transition. Again, this is consistent with what was observed by ^2H NMR and further supports the conclusion that the composition of this *phase separated nematic phase* is temperature dependent only, and not dependent on the bulk solute concentration.

The DSC and TM cooling and heating experiments described above were reported as the complete binary phase diagram for the 1/CCH-4 binary system (Figure 2.11).⁸⁵ The phase diagram clearly shows that for concentrations as low as 0.5 mol%, phase separation occurs below the bulk N→S transition temperature. This is completely consistent with what we observed by ^2H NMR for the 0.5 mol% sample of 1 in CCH-4.

Figure 2.3 shows a stacked-plot of the ^2H NMR spectra as a function of temperature for 0.2 mol% 1 in CCH-4 at various temperatures ranging from 82°C down to 2°C. Notice the absence of deuterium signals for the temperature region 10 - 50°C. Clearly 1 (at this concentration and temperature range) is not in the same environment as it was for samples of higher concentration. A reasonable conclusion is that the ketone is totally soluble in the smectic phase of CCH-4, throughout the 28 - 50°C temperature range, at a concentration of 0.2 mol%. The absence of deuterium signals indicates that for the 0.2 mol% 1/CCH-4 mixture the deuterium signals are either too broad, or the components too widely separated to be observed with our spectrometer. However, these experiments allow an upper (0.5 mol%) and lower (0.2 mol%) limit to be assigned to the solubility limit of 1 in the smectic phase of CCH-4 for the 28 - 50°C temperature range.

Since T_1 measurements probe molecular motions which occur during a much

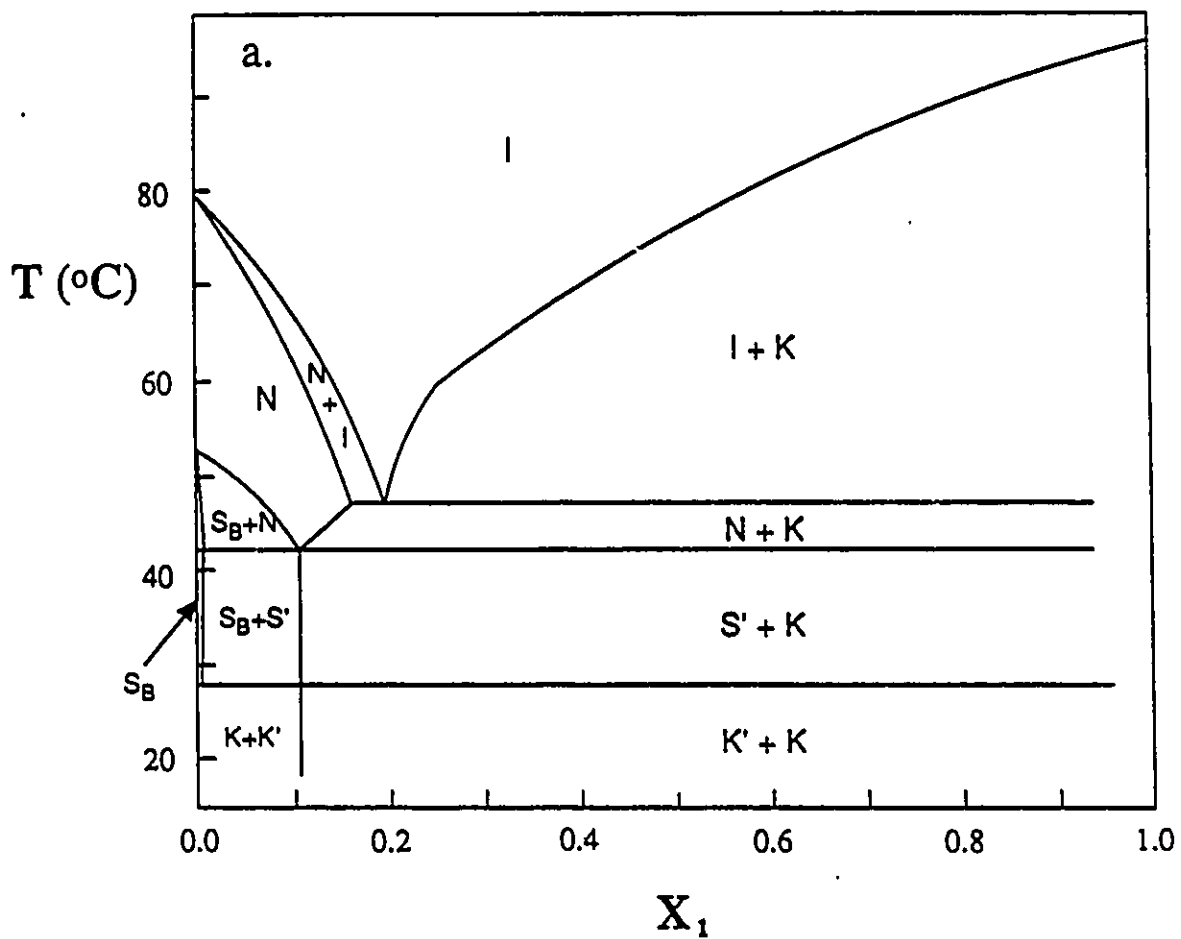


Figure 2.11a. Idealized composition/temperature binary phase diagram (heating) for I/CCH-4 constructed from DSC and thermal microscopy data. Reproduced with permission from reference 85.

shorter time period than do Δv_Q measurements (as short as 10 ps^{98,99}), it was our hope that additional information pertaining to the mobility (and hence solubilization) of **1** in the bulk smectic phase of CCH-4 could be gained *via* deuterium T_1 measurements on the 3 mol% **1**/CCH-4 sample (see Figure 2.8). While there is a clear change in the slope of the plot at the bulk N→I transition temperature, it was impossible within the error limits of our data to identify any substantial change in the mobility of **1** at the bulk N→S transition temperature. Although the error in the data for the 35 - 45°C temperature region is rather large, the lack of a change in the slope of the plot at the bulk N→S transition temperature is consistent with both the Δv_Q and the DSC/TM data. Since the solubility of **1** is < 0.5 mol% in the smectic phase of CCH-4 (as determined by ²H NMR), this requires that the majority of **1** in the 3 mol% **1**/CCH-4 mixture will reside in the phase separated nematic phase. It is therefore reasonable, since the majority of **1** is still in the nematic phase of CCH-4, that there would be little noticeable affect on the deuterium T_1 -value caused by the bulk of the sample undergoing a N→S phase transition. Clearly, the motions which are responsible for the relaxation of the deuterium are unaffected by any small changes in solvent order or viscosity that may be taking place in the phase separated nematic phase relative to the nematic phase of CCH-4. This is further supported by the observation that there is only a small change in the slope of the plot (a factor of < 1.5) when the sample undergoes the I→N transition.

In an effort to ensure that our interpretation of the T_1 data for the **1**/CCH-4 mixture was indeed correct, and the observation that the change in the slope of the Arrhenius plot at the I→N phase transition was real, we carried out a similar investigation using EB(S→N, 25°C; N→I, 54°C) on the spin-lattice relaxation rate of **1** (Figure 2.8). As was the case for the **1**/CCH-4 solution, an Arrhenius plot of T_1

data for the 1/EB mixture also exhibits a change in the slope of the plot at the N→I phase transition. However, the change in the slope is slightly more pronounced for the 1/EB mixture than it is for the 1/CCH-4 mixture. It is unlikely that the more pronounced change in the slope for the 1/EB mixture is due to tighter solvation of 1 in the nematic phase of EB, as the Δv_Q vs T plot (Figure 2.6) exhibits a range of Δv_Q values that are very similar to those observed for 1 in the bulk nematic phase of CCH-4. This is consistent with previous descriptions which report the nematic phases of CCH-4 and EB as being similar.^{38,76}

Our ^2H NMR/ T_1 results as well as the DSC/TM data⁸⁵ very strongly suggest that the solubilization of 1 in the smectic phase of CCH-4 is substantially different than has been previously suggested to explain the flash photolysis data obtained for 1.²⁵ Between *ca.* 52 - 35°C, the sample consists of a biphasic system in which < 0.5 mol% of 1 resides in the smectic phase of CCH-4. The remainder of 1 remains in a solute-enriched (relative to the initial bulk concentration) nematic phase which is similar in characteristics to that of pure CCH-4. The relative proportions of the two phases present (smectic and solute-enriched nematic) and their compositions continuously changes with temperature. It is very likely that this description is applicable for a large number of solute/CCH-4 mixtures, including compounds 5 and 6, and may lead to a re-interpretation of previous photoreactivity data obtained in this solvent.^{22,25,27,38,49,83}

The "P-Phase"

The collapse of the quadrupolar doublet at *ca.* 35°C to a sharp singlet (see Figure 2.1) indicates that the ketone, as observed by the NMR spectrometer, is experiencing isotropic tumbling. As was mentioned in the Introduction Chapter, this type of solute induced phase which results in isotropic NMR spectra, was first

reported by Fung and Gangoda.^{81,82} They observed the ^{13}C NMR spectra of benzene and dioxane in the solute induced phase of CCH-4 (*i.e.* below 30°C). The ^{13}C spectra were qualitatively similar (*i.e.* narrow linewidths uncharacteristic of spectra recorded in a crystal or smectic phase) to those which they observed above the N→I phase transition temperature (Figure 2.12).

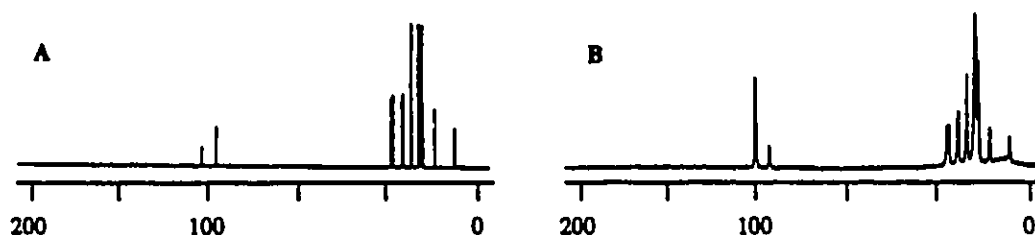


Figure 2.12. ^{13}C NMR spectra of a 3.4 mol% benzene/CCH-4 mixture. A: 65°C . B: 11°C . Adapted from reference 81.

They assigned this solute induced phase as a cubic- or plastic-crystalline structure.^{81,82}

A cubic phase is best defined as a phase in which the molecules remain at unique lattice site, as is the case for solid crystals. Unlike crystalline materials the individual molecules have significant rotational freedom to rotate about any one of a number of axis. This causes cubic phases to appear less ordered than crystalline compounds when observed by NMR and, in the extreme limit, can give rise to spectra that are indistinguishable from those obtained in isotropic solution.⁹⁴ Plastic crystals are somewhat similar to liquid crystals in that they usually consist of elongated or globular molecules. However, whereas liquid crystals have local orientational order but lack positional order, plastic crystals have positional order but lack orientational order. At low temperatures plastic crystals have a normal ordered lattice, similar to those found in ordinary crystals. However, when heated plastic crystals usually give rise to a *pseudo*-cubic phase⁹⁴ which causes them to

lose their orientational order.

Weiss and co-workers have also observed this behavior (by both ^2H and ^{13}C NMR) for substituted aromatic ketones (**5** and **6**) in CCH-4, and they labelled the phase responsible for this behavior the "p-phase".⁸³ Formation of the "p-phase" seems to be quite general for a wide variety of solutes, as is evident by the similarity (*i.e.* the isotropic-like appearance) of the ^2H and/or ^{13}C NMR spectra for dioxane, **5**, **6**, benzene (Figure 2.12), and **1** (see Figure 2.13 for a ^{13}C spectrum of **1** in CCH-4 at 30°C).

The appearance of the isotropic-like singlet in the ^2H NMR spectra may be caused by several possible solvation phenomena. The simplest and least complicated possibility is that the ketone actually resides in a solute-induced isotropic environment. This could be caused if the ketone reached a critical concentration in the phase separated nematic phase such that the CCH-4 could no longer maintain orientational order. A second possibility would result if the preferred orientation of the ketone in the phase separated nematic phase, or a new solute-induced liquid crystalline phase, was coincidentally at the magic angle with respect to the magnetic field.⁹⁴ The similarity of the $\Delta\nu_Q$ vs T data for both the **1**/CCH-4 and **2**/CCH-4 mixtures, particularly the observation that the collapse of the quadrupolar doublet to a singlet occurs at the same temperature in both instances, can rule out this possibility because the C - D bond angles in **1** and **2** are approximately perpendicular. A third possibility, which may explain the nature of the "p-phase" in CCH-4 that exists below $20 - 35^\circ\text{C}$ (the temperature depends on the solute), has been proposed by Weiss and co-workers. Their explanation, which is based on the results of ^2H and ^{13}C NMR experiments, as well as photoreactivity studies of **5** and **6**,⁸³ proposes that the "p-phase" consists of dispersed,

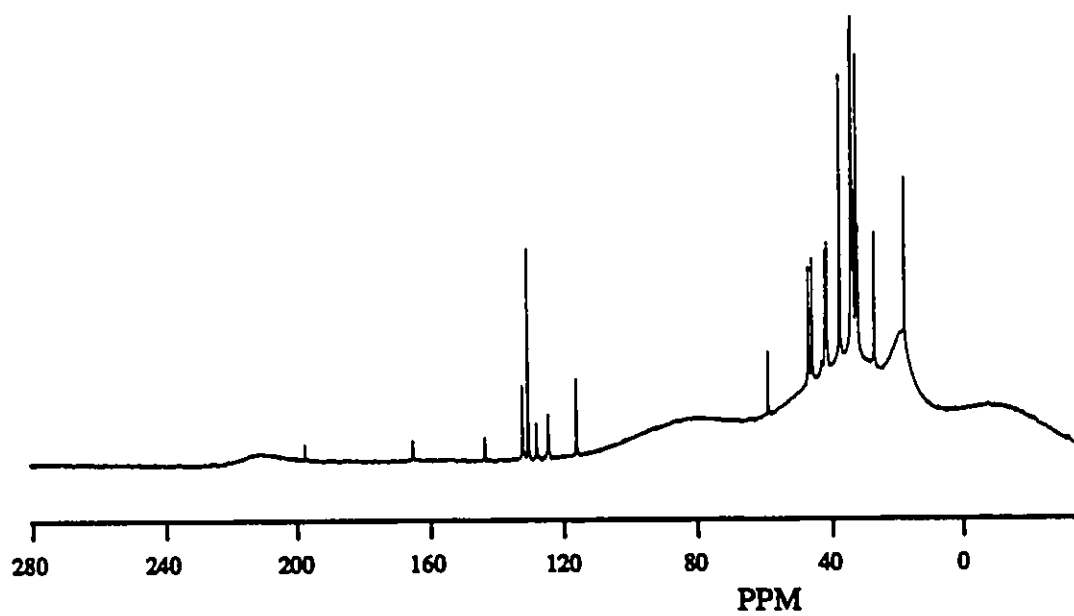


Figure 2.13. ^{13}C NMR spectrum of 3 mol% 1 in CCH-4 at 30°C.

solute-included molecular "pools" which appear to be macroscopically disordered (as observed by NMR) but which are microscopically ordered (as shown by the photoreactivity data).

Weiss and co-workers supported their conclusion on the basis of the isotropic-like nature of both the ^2H and ^{13}C NMR spectra coupled with the observation that there was a significant change in the elimination/cyclization (E/C) ratio (a result of the Norrish II reaction) at both the S \rightarrow N and K \rightarrow S phase transition temperatures (see Table 2.1). It has been well established that E/C ratios provide for

Table 2.1.
Elimination/Cyclization Data^a for 5b in CCH-4.

Temperature	E/C Ratio	Bulk Phase
82	2.5	Isotropic
69	4.0	Nematic
64	4.8	Nematic
56	5.5	Nematic
50	31	Smectic
45	20	Smectic
36	18.5	Smectic
34	19	Smectic
28	22.5	Smectic
24	9	Crystalline
19	9.5	Crystalline
11	10	Crystalline

^aThis data was adapted from reference 83.

a direct measure of the microscopic environment (order and mobility) experienced by a reacting ketone^{12,21,22} if the photochemistry is carried out in an ordered medium. The observed changes in the E/C ratios which occurred at the bulk phase transition temperatures for ketones 5 and 6, were interpreted as evidence that the conformational mobility of 5 and 6 was being retarded by *solvent order* (See

Introduction Chapter). For this interpretation to be compatible with the NMR data for ketones 5 and 6, Weiss concluded that ketones 5 and 6 must be experiencing solvent order on a microscopic level while being part of a larger, isotropically tumbling, ketone/CCH-4 cluster.

Although our ^2H NMR data for both 1 and 2 in CCH-4 have significantly added to the body of data pertaining to the "p-phase", in addition to enabling a more complete understanding of the nature of the "p-phase" (see above), we were unable to determine precisely the composition and/or structural characteristics of this phase. However, DSC thermograms and TM data recently reported for mixtures of 1/CCH-4⁸⁵ in concert with spectroscopic data pertaining to the "p-phase" reported by us⁸⁵ and others,^{22,81-83} have enabled a complete description of the "p-phase".

The DSC (cooling) traces display a transition at 32 - 35°C that was not present in the pure CCH-4. This corresponds exactly to the observed isotropic-like behavior of 1 in CCH-4, and confirms that the isotropic-like nature of 1 in CCH-4 below 35°C is indeed solute induced. The transition at 32 - 35°C was found to be reversible providing that the sample was not cooled below 5°C. However, the authors of this study found that when the sample temperature was cooled to below -10°C, the heating cycle did not mirror the cooling cycle. The transition at 32 - 35°C is not observed, and a new transition appears at 43 - 44°C. This is consistent with what we observed by ^2H NMR when the 1/CCH-4 sample was cooled below 20°C, rapidly cooled from above 50°C, or allowed to sit at room temperature for a few days.

Thermal microscopy studies reveal that the residual phase separated nematic phase for 1/CCH-4 mixtures was transformed to a non-birefringent phase at *ca.* 35°C. The non-birefringent phase was identified as the same "p-phase" that has been reported for solute/CCH-4 mixtures by us⁸⁵ and others.^{22,81-83} The "p-phase"

was observed (at concentrations ≥ 5 mol%) to be a fairly viscous, *isotropic fluid* with no liquid crystalline properties. Storage of samples containing < 10 mol% **1** for short periods of time at room temperature was observed to cause the contraction of the "p-phase" to form what has been described as crystallites dispersed throughout the monodomains of the bulk smectic phase. On heating, the crystallites were found to undergo a distinct phase transition at $43 - 44^\circ\text{C}$ to yield a nematic phase. These same workers have also observed this crystallization by DSC and have identified the phase as a homogenous, solid binary mixture. We have assigned this phase as that responsible for the crystallization which we observed in the NMR studies when the sample was cooled below 20°C (see Results section). Clearly this phase is different than that of pure CCH-4 and of the phase separated nematic phase. Indeed it may have important ramifications on photochemical studies (Norrish Type II, etc.) if careful attention is not paid to the details surrounding sample preparation.

The appearance of the isotropic-like singlet for the 0.2 mol% **1**/CCH-4 mixture (ca. 10°C , Figure 2.3) indicates that depending on the bulk sample concentration, "p-phase" formation can arise from either the smectic or nematic solutions of **1** in CCH-4.

We are unable to identify any significant changes in the T_1 data for 3 mol% **1** in CCH-4 at the "N \rightarrow p" transition (ca. 35°C) (see Figure 2.8). However, as was the case for the higher temperature data, the uncertainty in this data is quite large, thereby making it impossible to notice any subtle differences in the data that may be present. The results are sufficiently good however, to at least determine that any change that may show up with better data would certainly be small (a factor of < 2), indicating that the motions sampled by the T_1 measurements are rather insignificantly affected by the phase change. Since the "p-phase" has been

identified as an isotropic liquid, it may be reasonable to expect that the slope of the Arrhenius plot for the "p-phase" temperatures will be similar to that found for the isotropic phase. Unfortunately, the data was insufficiently good to determine if this was the case.

Again, our ^2H NMR/ T_1 results as well as the DSC/TM⁸⁵ data for temperatures below 35°C indicate that the solubilization of **1** (and most likely other solutes) in CCH-4 in this temperature region is substantially different than previously thought.⁸¹⁻⁸³ Below 35°C, the biphasic system can be best described as a solute-depleted smectic phase (of similar composition to that above 35°C) in equilibrium with a solute-enriched isotropic liquid.

It should be noted that in their study of the "p-phase", Gangoda and Fung dismissed the possibility that the "p-phase" was an isotropic solution on the basis that there were no known examples of isotropic phases which exist at *lower* temperatures than the corresponding nematic phase^{81,82} (see Introduction Chapter). However, this requires that there is only two interconverting phases involved in the transition. It is possible that cooling the nematic phase gives rise to *both* a smectic (and/or crystalline) and a nematic phase. While we have no direct evidence that such a transition is occurring in this case, it seems plausible in light of the convincing data pertaining to the nature of the "p-phase".

Substituent Effects on the Mobility of **1 in CCH-4.**

In an attempt to better define how **1** was solubilized in the nematic and phase separated nematic phases of CCH-4, the affect of substituents at both ends of **1** was investigated by ^2H NMR. Compound **3** which contains a *para* cyclohexyl ring on the β carbon of **1** gave $\Delta\nu_Q$ values similar to **1** except that they were slightly larger (*ca.* 1 - 3 kHz) depending on the temperature. Replacement of the methoxy substituent in **1** with a pentoxy substituent (compound **4**) also gave $\Delta\nu_Q$ vs T values

similar to **1**, except that in this case they were consistently smaller for each temperature. Since both compounds are deuterated α to the ketone, these results imply that substituents on the β phenyl ring enable the ketone to be better solubilized in CCH-4, while lengthening the alkoxy substituent results in the ketone being more poorly solubilized by CCH-4. This is consistent with previously reported laser flash photolysis work.^{25,26} One possibility is that the ketone is somehow coordinating with the cyano function on CCH-4. This notion is further supported by the fact that the UV spectra of **1** in CCH-4 is very similar to that observed in acetonitrile.^{25,26}

2.6 The Solubilization of **1** in CCH-2

Once we had developed a good understanding of the solubilization of **1** in CCH-4, we were interested as to how **1** might be solubilized in the CCH-2 homologue.

The Nematic Phase

The solubilization of **1** in the nematic phases of CCH-2 and CCH-4 were very similar (see Figure 2.1 and 2.7). This is not unexpected because the nematic phases of these two solutes are very similar.

The Smectic Phase

We had good reason to suspect that **1** was not solubilized in the smectic phase of CCH-2 in the same way as it was solubilized in the smectic phase of CCH-4, based on laser flash photolysis experiments which were recorded for these two systems in our laboratory. Recall that there was a definite break (at the $N \rightarrow S$ phase transition; see Figure 1.6) in the Arrhenius plot for **1** in CCH-4.^{25,26} However, no apparent phase dependence was observed for a similar Arrhenius plot for **1** in

CCH-2.^{25,26} Indeed, comparison of the smectic phase regions of Figures 2.1 and 2.7 supports this hypothesis. Rather than undergo phase separation to give a solute rich nematic phase, Figure 2.7 indicates that below the bulk N→S phase transition, solutions of **1** in CCH-2 undergo phase separation to give a phase which is probably of similar composition to the "p-phase" identified for solutions of **1** in CCH-4.

Given that the smectic phase of CCH-2 is of higher order than the smectic phase of CCH-4,^{38,76} it is not surprising that solutions of solutes in their respective smectic phases behave differently. Based on the previously reported laser flash photolysis data, the viscosity of the solute induced "p-phase" in CCH-2 must be similar to that of the nematic phase of the pure mesogen.

2.7 Summary

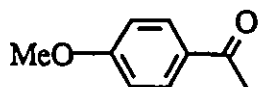
The solubilization of ketones **1** - **4** in the liquid crystalline phases of CCH-4 as well as the solubilization of **1** in EB and CCH-2 has been discussed. While the solubilization of these solutes in the nematic phases of these solvents is reasonably straightforward, all of the above mentioned solutes have extremely low solubilities (*ca.* 0.5 mol%) in the smectic phases of either CCH-4, EB, or CCH-2. Instead phase separation occurs with the solute being solubilized in either a solute-rich nematic or "p-phase" which is surrounded by a solute poor bulk smectic phase.

CHAPTER III

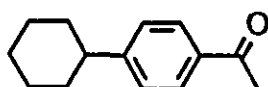
A Deuterium NMR Investigation of the Solubilization of Benzene and 4 Aromatic Ketones in CCH-4.

A. Introduction

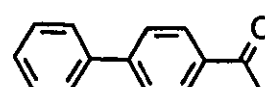
Following our investigations of substituted β -phenylpropiophenones in CCH-4 (Chapter II), we continued to investigate the nature of solute/liquid crystal interactions with the hope of being better able to define the factors that influence the solubility of solutes in the liquid crystalline phases of CCH-4. In addition we hoped to observe discrete examples of smectic phase spectra which would allow us to more completely develop our understanding of the solubilization of 1 in CCH-4 and CCH-2. In this chapter we report the results of a ^2H NMR investigation of the behaviour of binary mixtures of three α -deuterated acetophenone derivatives, 4-methoxy-(MAP), 4-cyclohexyl-(CAP), and 4-phenylacetophenone-(PAP), methoxyvalerophenone(7), and deuterated benzene (C_6D_6).



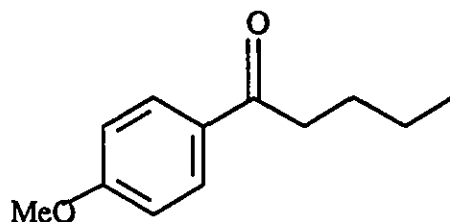
MAP



CAP



PAP



7

The decision to investigate substituted acetophenones was a natural extension of our previous efforts. In the initial studies involving lifetime measurements of substituted β -phenylpropiophenones,^{25,26} the lifetime of MAP was measured under the same conditions (both concentration and temperature) as those used for the β -phenylpropiophenones. This was necessary in order to determine if the liquid crystalline phases of CCH-4 would affect the triplet lifetime of a ketone whose decay mechanism was *not* dependent on its ability to undergo certain conformational motions. Indeed, there was an order of magnitude difference (longer) in the measured lifetimes of MAP in the smectic phase of CCH-4 relative to that observed in the nematic and isotropic phases. It was suggested^{25,26} that this difference was likely the result of more efficient impurity quenching in the more mobile nematic and isotropic phases. It is important to keep in mind that in order to compare lifetime measurements for MAP, to those for the β -phenylpropiophenones, the two solutes *must* be solubilized similarly in the smectic phase of CCH-4. However, it is unlikely that this is the case in view of the model that we have proposed for the solubilization of the β -phenylpropiophenones in the smectic phase of CCH-4 (*i.e.* the majority of the ketone resides in a phase separated nematic phase, see Chapter II). Our model, and indeed all of our ²H NMR data, indicates that the mobility of the β -phenylpropiophenones in the phase separated nematic phase is similar to that found in the nematic phase. If this is indeed the case, there should be little difference in the diffusion rates of impurities in the solvent, and as a result there should *not* be a phase dependence on the observed triplet lifetime of MAP if it is solubilized in the same phase separated nematic phase. This led us to the current work which was to try and determine more precisely how MAP, and other acetophenone derivatives, were solubilized in the liquid crystalline phases of CCH-4.

The investigation of the CAP/CCH-4 binary system which will be discussed in this thesis represents a much more detailed study of the solubilization of this compound in CCH-4 than has been previously reported in the literature.⁸³ We have been able to correlate our results (for the substituted acetophenones) with DSC and thermal microscopy results which have been reported by other workers.¹⁰²

Similarly, our investigation of the solubilization of **7** was a direct extension of a previous Norrish II photochemical study³⁸ in our group, which measured the effects of the liquid crystalline phases of CCH-4 on the fragmentation/cyclization(F/C) ratio of **7**. This study determined that the smectic phase of CCH-4 alters the F/C product ratio from photolysis of **7** relative to its value in model isotropic solvents. By doing a complete ²H NMR study of the solubility of **7** in the liquid crystalline phase of CCH-4, we hoped to further clarify our photochemical results by determining to what extent **7** was indeed solubilized in the smectic phase of CCH-4.

Our investigation of C₆D₆ is related to work presented in Chapter II as well as this Chapter. Recall that Fung and Gangoda first reported evidence of the solute-induced "p-phase" with a C₆H₆/CCH-4 solution.⁸¹ Our intention was to be able to further add to the body of data regarding the "p-phase" by monitoring the solubilization of C₆D₆ in the liquid crystalline phases of CCH-4 with ²H NMR. In addition this study would allow us to more completely define the effects of solute size on the degree to which a solute can be solubilized in the smectic phase of CCH-4.

B. Results

3.1 Preparation of Compounds.

The α -deuterated ketones employed in this study were prepared from the commercially available all-protonated analogs in the same manner as those in

Chapter II. Benzene- d_6 was obtained from MSD Isotopes.

3.2 Deuterium NMR of MAP, CAP, and PAP in CCH-4.

Deuterium NMR spectra of 0.6, 2.0 or 3.0, and 8.0 mol% mixtures of MAP, CAP, and PAP (as the α -deuterated derivatives) in CCH-4 were recorded (in a manner similar to that employed for the ketones studied in Chapter II) at 76.8 MHz, at various temperatures between 10°C and 82°C, using the quadrupolar echo pulse sequence.^{96,97} Selected portions of these data are shown for each ketone/CCH-4 system in Figures 3.1, 3.2, and 3.3.

The ^2H NMR behaviour of each of the ketone/CCH-4 mixtures in the isotropic and nematic phases is similar to that observed for 1 - 4 (Chapter II). The isotropic spectrum ($> 80^\circ\text{C}$) for each consists of a single deuterium resonance which splits into a single, well-defined quadrupolar doublet with splitting $\Delta\nu_Q$ as the temperature of the sample is lowered below the nematic \rightarrow isotropic(N \rightarrow I) phase transition of the mixture. The magnitude of $\Delta\nu_Q$ increases as the temperature is lowered throughout the nematic phase region of the sample. The splitting reaches a maximum at the temperature which corresponds to the smectic \rightarrow nematic(S \rightarrow N) phase transition or its onset.

At a given temperature in the nematic phase, the observed values of $\Delta\nu_Q$ for each of the three ketone/CCH-4 mixtures decreases in the order MAP > CAP > PAP.

The behaviour of the three ketone/CCH-4 mixtures below the bulk S \rightarrow N phase transition (*ca.* 53°C) depends on the ketone of interest and its bulk concentration in the mixture. All of the ketones looked at in this study exhibited complex and unique spectral patterns below the S \rightarrow N phase transition, in contrast to what was observed for 1 - 4 (Chapter II). As a result, it is impossible to describe their spectra below the S \rightarrow N phase transition as a group. Each ketone/CCH-4

system will be discussed individually.

The MAP/CCH-4 Binary System.

The spectral pattern observed for the 0.6 mol% mixture of MAP/CCH-4 becomes much more complex below 53°C, with the fairly sharp nematic phase doublet ($\Delta\nu_Q = 4.9$ kHz) being replaced by two broad doublets with a much larger quadrupolar splitting (see Figure 3.1a). The splitting associated with the inner doublet (*ca.* 11.8 kHz) is more or less independent of temperature, while that of the outer one increases significantly with decreasing temperature (*ca.* 14kHz at 50°C and *ca.* 18 kHz at 33°C). This is the same spectral pattern that is observed as a minor component of the total spectrum for the 3.0 mol% MAP/CCH-4 sample in the 23 - 50°C temperature range (Figure 3.1b; *vide infra*). The entire spectrum collapses to an isotropic singlet at *ca.* 23°C for the 0.6 mol% sample.

The spectra of mixtures containing more than 1 mol% MAP exhibit a more complex spectral pattern for the temperature range of 23 - 50°C (see Figure 3.1b) consisting of a prominent doublet ($\Delta\nu_Q = 2.6 - 4.8$ kHz) and a less intense, broader doublet of splitting *ca.* 11.8 kHz. As the bulk concentration of MAP is increased, the intensity of the inner doublet is much more pronounced, making it increasingly more difficult to observe the outer doublet.

The CAP/CCH-4 Binary System.

The ^2H NMR spectra of the CAP/CCH-4 binary system is similar in many respects to the MAP/CCH-4 binary system. The ^2H NMR data recorded for the 0.6 and 2.0 mol% CCH-4/CCH-4 mixtures are shown in Figure 3.2.

As was the case for MAP, the nematic phase doublet present in the 0.6 mol% CAP/CCH-4 mixture is replaced by two different spectral patterns as the temperature of the sample is lowered through the bulk S→N transition. Figure 3.2a

contains spectra (51.5 and 49.2°C) obtained as the sample was going through the bulk S→N transition. These spectra show the sharp nematic phase doublet superimposed on a considerably broader pattern which consists of two doublets of *ca.* 1.1 and 5.5 kHz. These spectral changes are consistent with CAP leaving the nematic phase, and entering a *new* phase which is markedly different from that of the nematic phase. The nematic phase doublet has completely disappeared when the sample is equilibrated at 46°C. The two remaining doublets respond differently to decreasing temperature; the inner pattern narrows to a very broad single (perhaps a powder pattern), while $\Delta\nu_Q$ for the outer doublet increases in magnitude as the temperature is lowered (5.5 kHz at 49°C and 7.3 kHz at 27°C). The relative intensities of the two spectral patterns is independent of the rate at which the sample is cooled from the nematic phase. The entire spectrum collapses to a narrow, isotropic singlet between 28 and 23°C.

The ^2H NMR spectrum of the 2.0 mol% CAP/CCH-4 mixture consists of a prominent, sharp doublet in the 35 - 50°C temperature range. However, there is additional broad absorption in the spectral region between the sharp doublet components (see Figure 3.2b).

The PAP/CCH-4 Binary System.

The PAP/CCH-4 binary mixture gives rise to a significantly different spectral pattern than was found for MAP/CCH-4 and CAP/CCH-4 (see Figure 3.3). As PAP enters a phase different from the nematic phase, the nematic phase doublet of the 0.6 mol% sample is replaced by a broad central peak and a broad doublet (as the sample temperature is lowered below the bulk S→N phase transition). The broad central peak gradually assumes the appearance of a powder pattern as the temperature is lowered to *ca.* 32°C. The entire spectrum broadens dramatically below 26°C, such that it can no longer be described as containing separate distinct

regions. The appearance is similar to that observed for polycrystalline solids.⁹⁴

The 2.0 mol% sample (see Figure 3.3b) is best described as a combination of the nematic phase doublet of the PAP/CCH-4 mixture superimposed on a spectral pattern similar to that observed for the 0.6 mol% sample.

3.3 Deuterium T_1 Measurements on MAP in CCH-4.

T_1 measurements (performed in a similar manner as those reported in Chapter II) were carried out for the two broad doublets observed between 49 and 23°C for the 0.6 mol% MAP/CCH-4 solution. The two doublets are characterized by *different* T_1 relaxation times. Measurements recorded at 43°C gave T_1 values of 184 ± 40 ms and 99 ± 32 ms for the doublets, with $\Delta\nu_Q$ values of 11.8 and 14 kHz respectively.

3.4 Deuterium NMR of 1 mol% 7 in CCH-4

Deuterium NMR spectra of 1 mol% 7 in CCH-4 were recorded between 84 - 30°C, in a similar manner to that employed for all of the substituted acetophenones. The ^2H NMR behaviour of 7 (see Figure 3.4) in the isotropic and nematic phase of CCH-4 is qualitatively very similar to that observed for both the substituted β -phenylpropiophenones studied in Chapter II and to the substituted acetophenones presented in this Chapter. The quadrupolar splitting increased with decreasing temperature with values ranging from 13 - 24 kHz.

No ^2H NMR signals could be observed for 7 throughout the entire bulk smectic phase region. This was similar to what was observed for the 0.2 mol% sample of 1 in CCH-4 (see Figure 2.3). We were unable to detect the formation of the "p-phase", as indicated by an isotropic singlet, but this result must be interpreted with caution as we did not do a complete temperature study of this sample below 30°C.

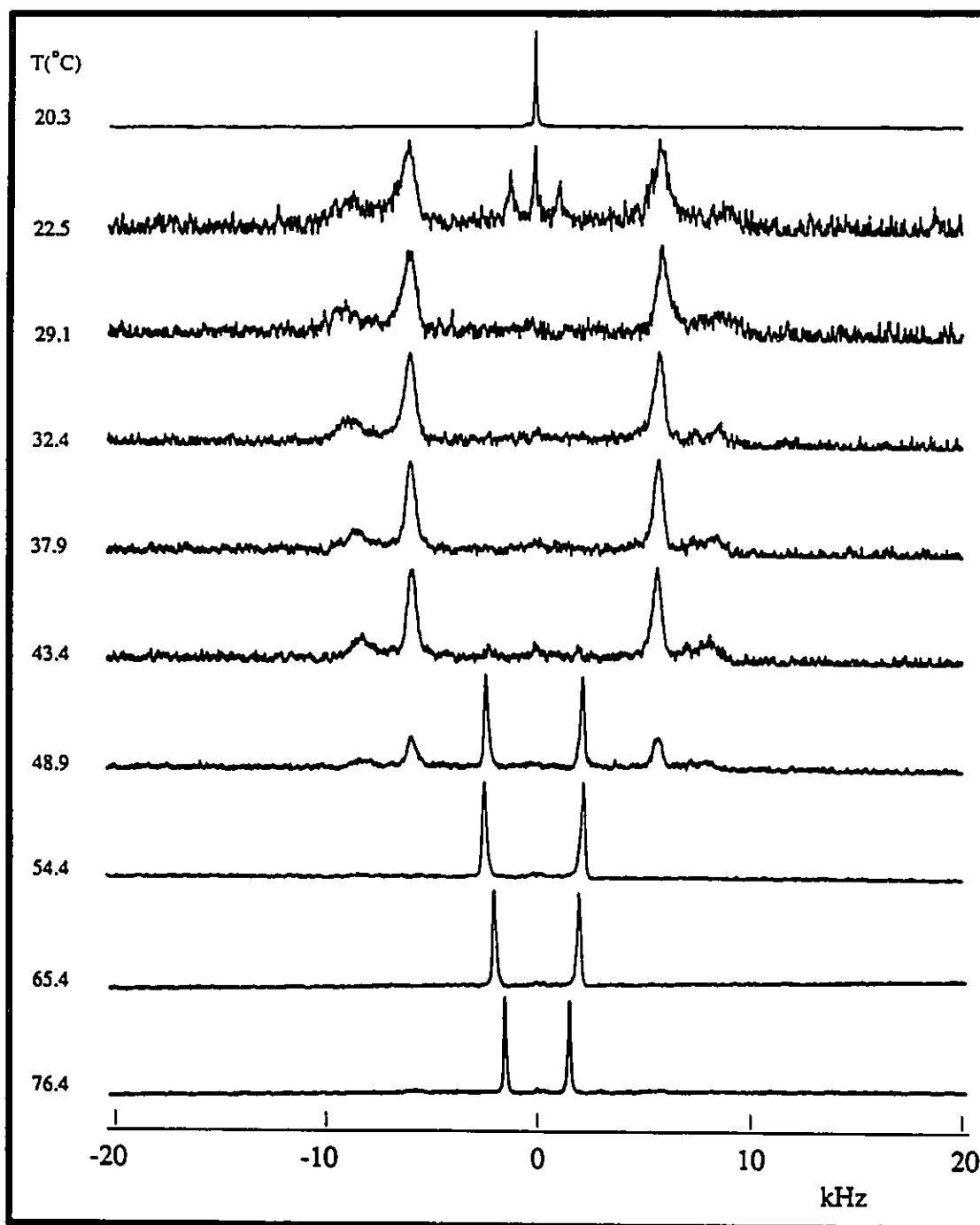


Figure 3.1a. Deuterium NMR spectra of 0.6 mol% MAP-d₃ in CCH-4 as a function of temperature.

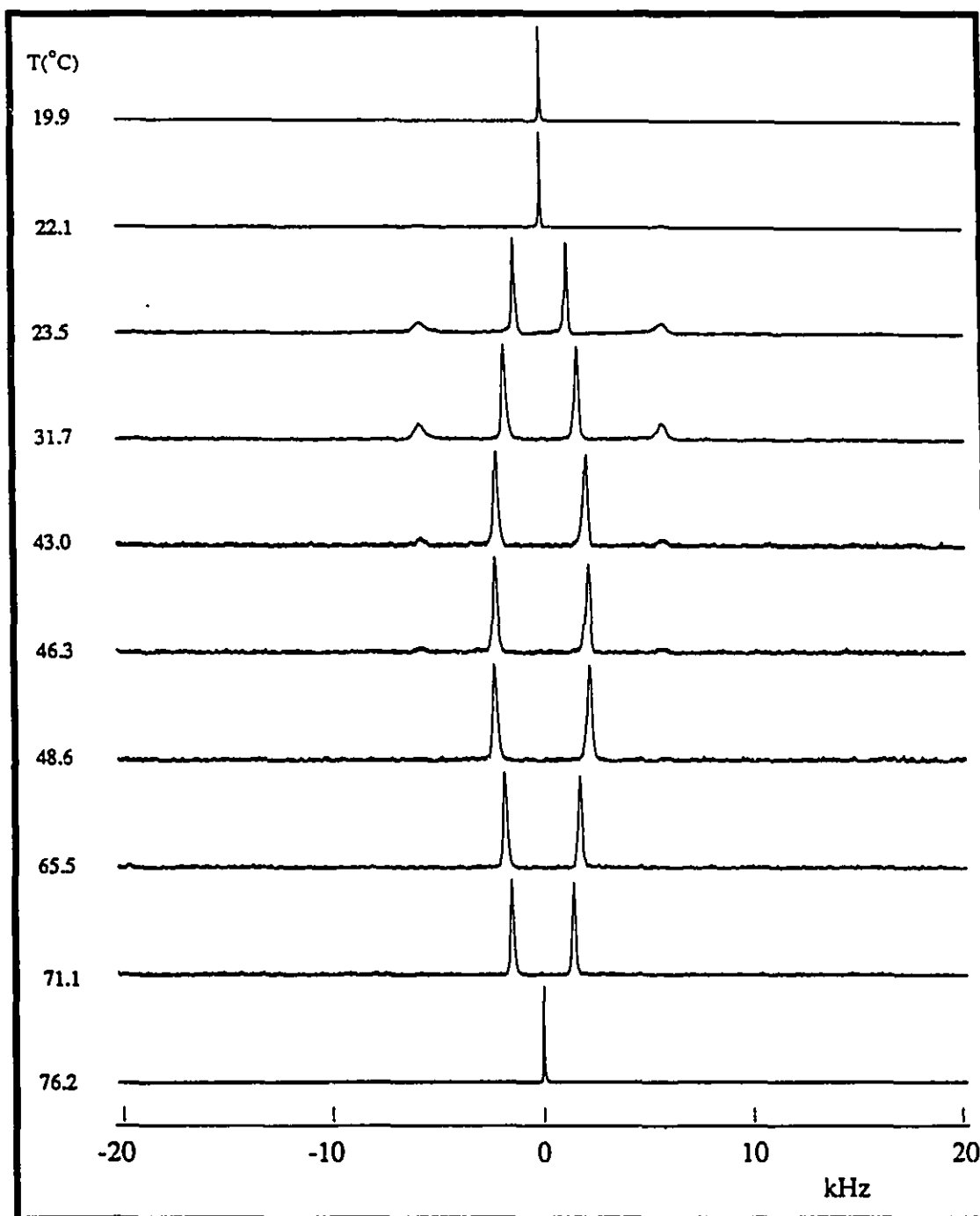


Figure 3.1b. Deuterium NMR spectra of 3.0 mol% MAP-d₃ in CCH-4 as a function of temperature.

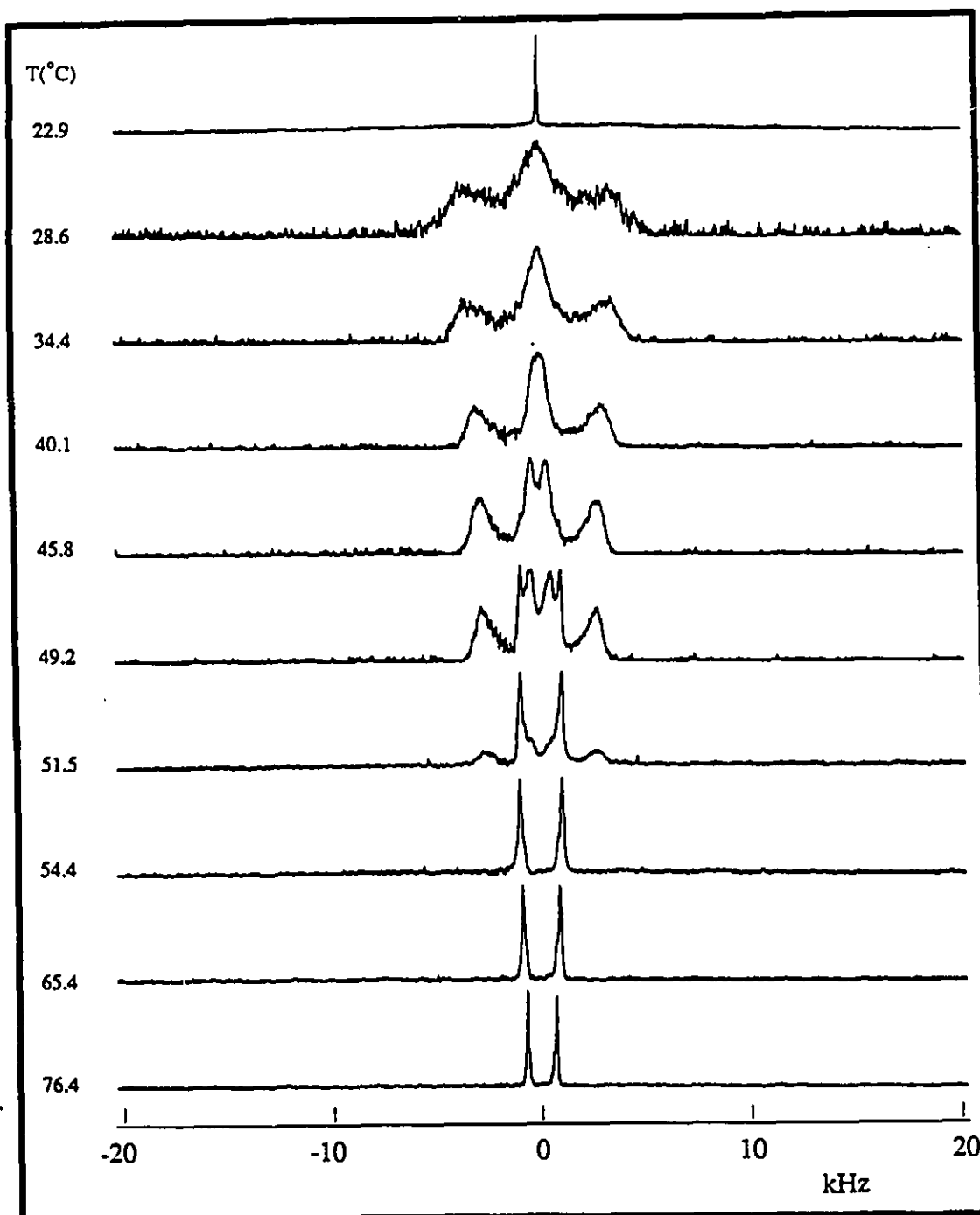


Figure 3.2a. Deuterium NMR spectra of 0.6 mol% CAP-d₃ in CCH-4 as a function of temperature.

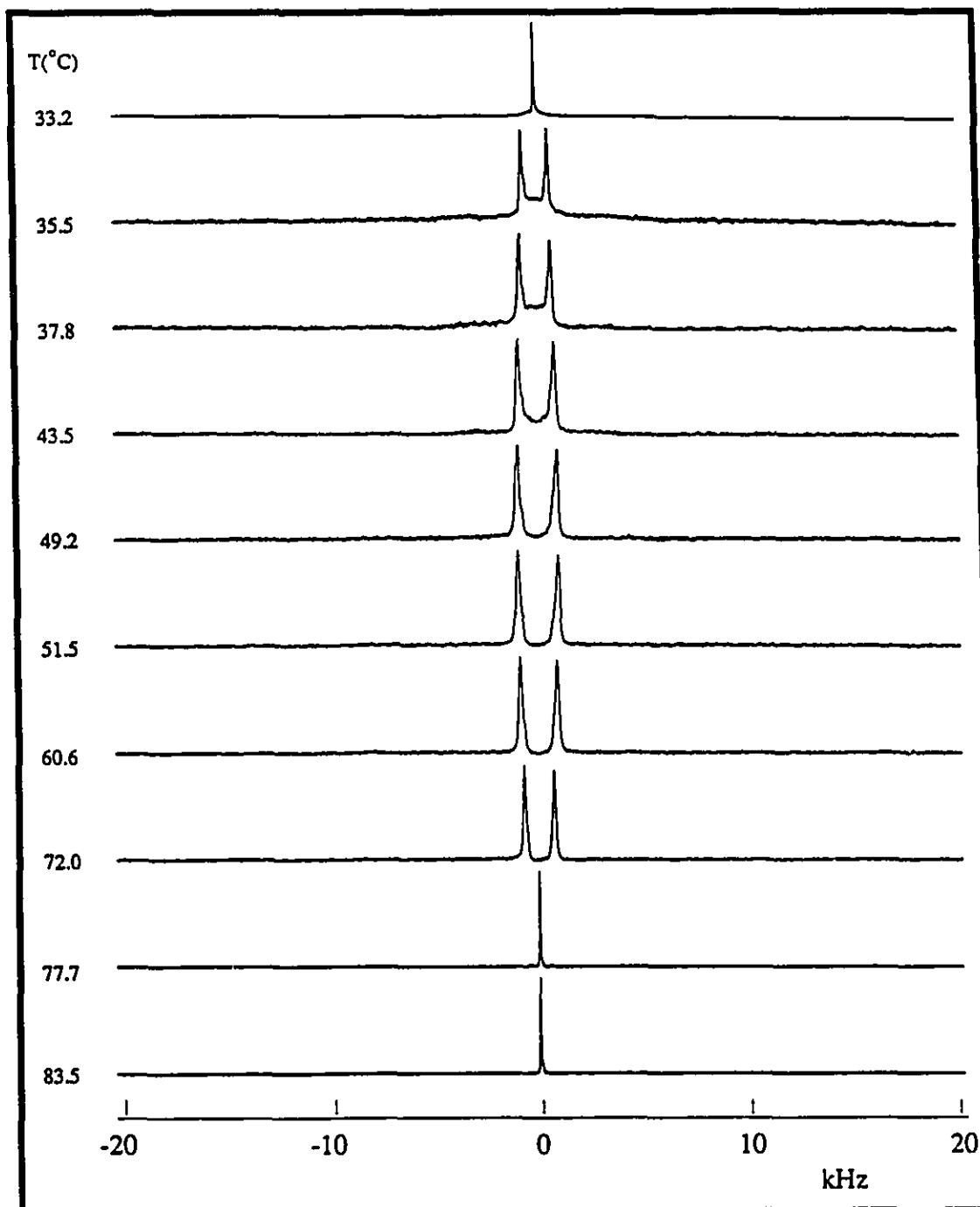


Figure 3.2b. Deuterium NMR spectra of 2.0 mol% CAP-d₃ in CCH-4 as a function of temperature.

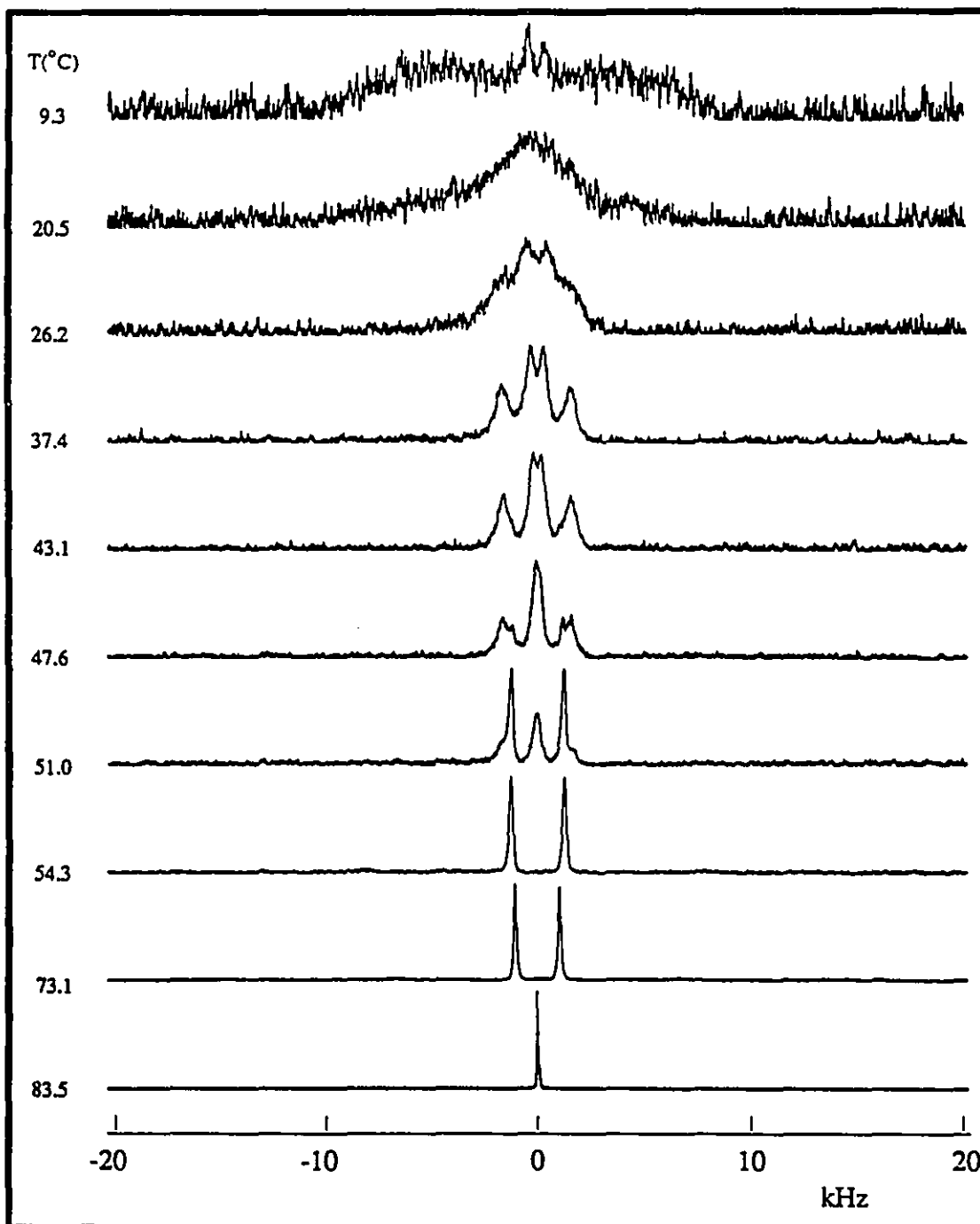


Figure 3.3a. Deuterium NMR spectra of 0.6 mol% PAP-d₃ in CCH-4 as a function of temperature.

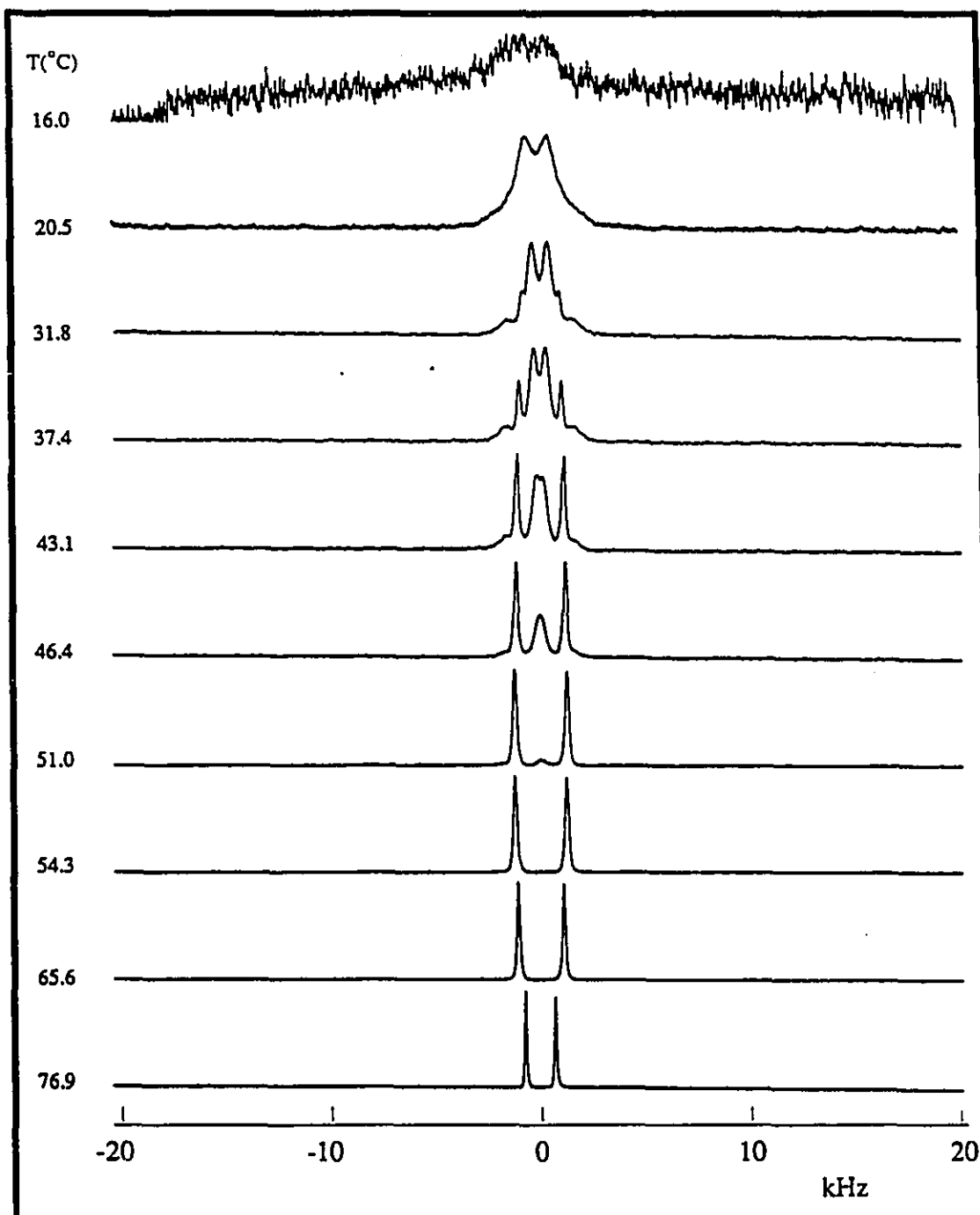


Figure 3.3b. Deuterium NMR spectra of 2.0 mol% PAP-d₃ in CCH-4 as a function of temperature.

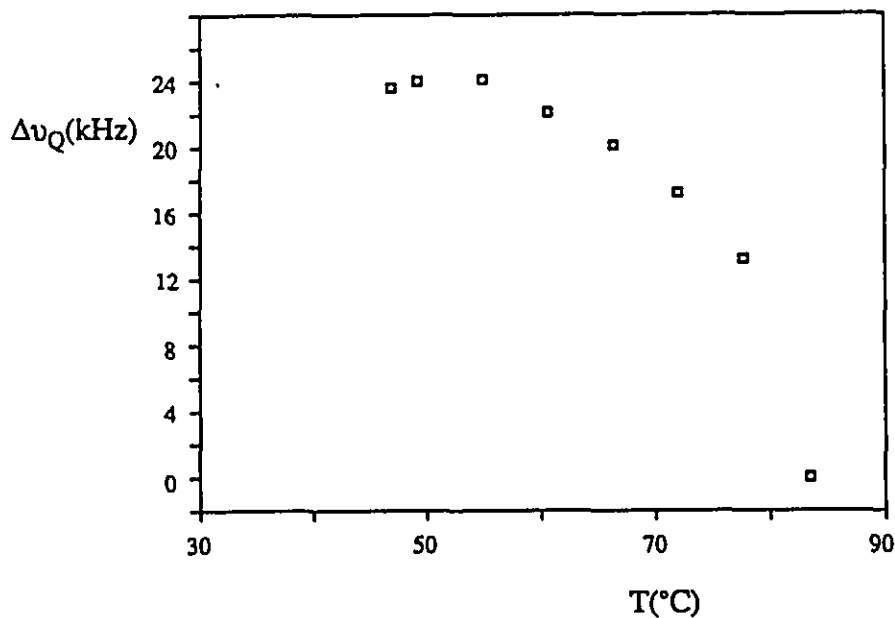


Figure 3.4. Deuterium quadrupolar splitting ($\Delta\nu_Q$) versus temperature for 1.0 mol% 7 in CCH-4.

3.5 Deuterium NMR of 3 mol% Benzene-d₆ in CCH-4

Deuterium NMR spectra of 3 mol% C₆D₆ in CCH-4 were recorded in a similar manner to that employed for the previous ketones. The behaviour (as monitored by ²H NMR) of C₆D₆ was somewhat different than that observed for the ketones (Figures 3.5 and 3.6). In particular, the spectra obtained for temperatures corresponding to the bulk nematic phase did not consist of a single doublet, but rather, consisted of two doublets (*i.e.* 11.3 and 11.9 kHz at 71°C; Figures 3.5 and 3.6). The splitting of both of these doublets increases with decreasing temperature. The difference between the magnitudes of the doublet splittings throughout the nematic phase remains approximately constant *i.e.* 0.3 - 0.7 kHz. The two doublets coalesce to a single quadrupolar doublet at 52°C (the bulk N → S phase transition temperature). Further cooling below 52°C results in the appearance of a second

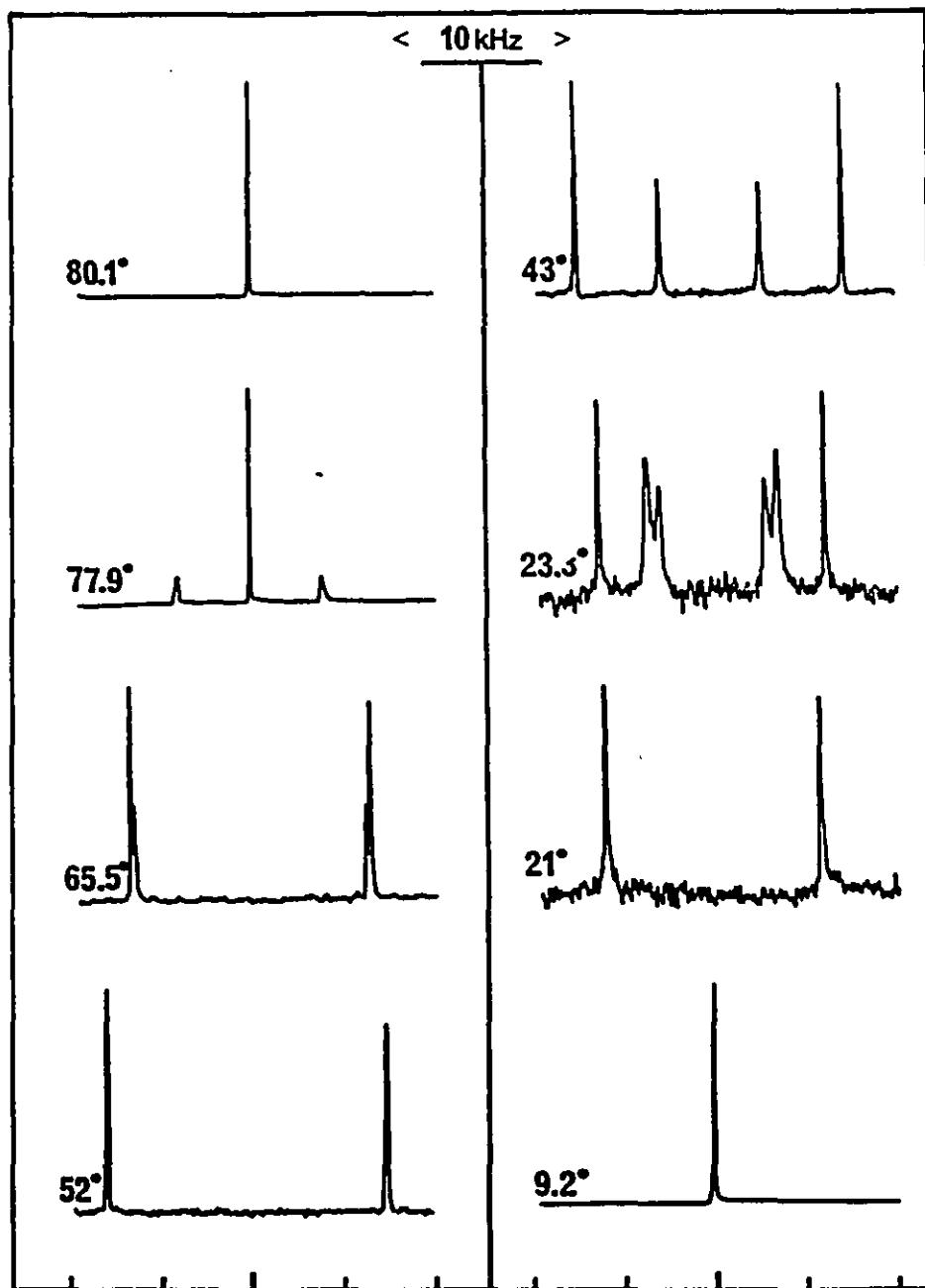


Figure 3.5. Deuterium NMR spectra of 3.0 mol% C_6D_6 in CCH-4 as a function of temperature. Reproduced with permission from reference 85.

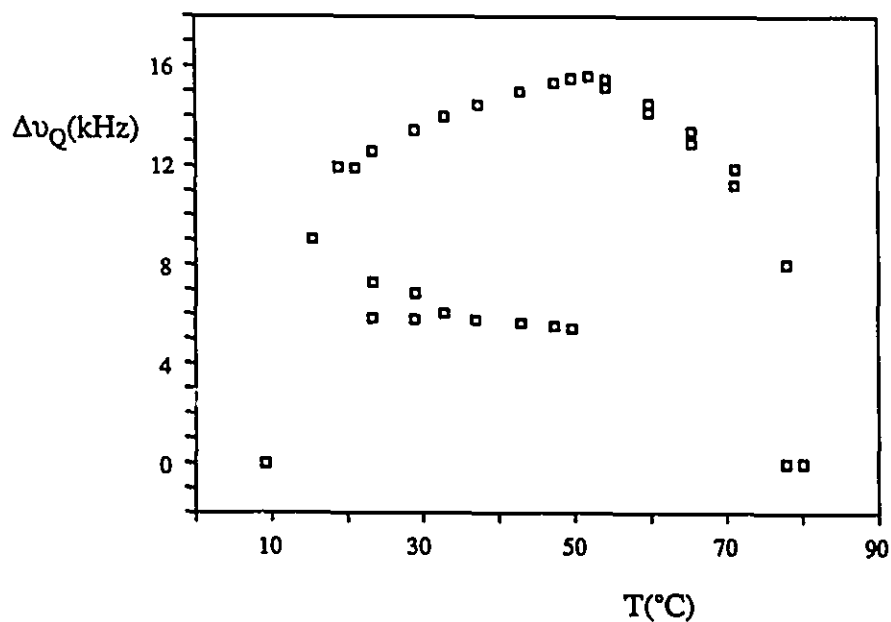


Figure 3.6. Deuterium quadrupolar splitting ($\Delta\nu_Q$) versus temperature for 3.0 mol% C_6D_6 in CCH-4.

doublet with a smaller quadrupolar splitting (5.6 kHz, 43°C) than those observed in the nematic phase temperature region. At approximately the temperature which corresponds to the bulk S \rightarrow K phase transition, a second inner doublet appears (12.6, 7.3, and 5.9 kHz; 23°C). Further cooling results in the complete disappearance of both inner doublets, with only the outer doublet remaining (11.9 kHz, 21°C). This remaining doublet collapses to a singlet at 9°C, behaviour similar to those observed for the ketones which were solubilized in the "p-phase".

C. Discussion

3.6 The Solubilization of MAP, CAP, and PAP, in the Isotropic and Nematic Phases of CCH-4.

The behaviour of MAP, CAP, and PAP in the isotropic and nematic phases of CCH-4 is qualitatively very similar to what was observed for 1 - 4 in CCH-4 (see Chapter II). The isotropic phase is characterized by a single narrow singlet typical of a mono-deuterated solute in an isotropic medium. The singlet is replaced by a narrow, well defined doublet in the nematic phase characteristic of a well-oriented solute that is experiencing restricted reorientational motions, with fast exchange of the three C - D bonds on the time scale of the NMR experiment.^{2,98,99,103-109}

The temperature dependence of these solutes in the nematic phase of CCH-4 is similar to that observed for the substituted β -phenylpropiophenones investigated in Chapter II. As the temperature is lowered throughout the nematic phase the observed $\Delta\nu_Q$ increases. This is a result of increasing restrictions to molecular reorientation (*i.e.* increasing solute order parameter, see Chapter I) as the order in the phase increases.

The differences in the $\Delta\nu_Q$ values for CAP and PAP (for a given temperature) should mirror their individual solute order parameters in the nematic phase of CCH-4 since their molecular shapes are nearly identical. The larger splitting observed for PAP relative to CAP is somewhat surprising in view of the inherent similarities of CCH-4 and CAP, *i.e.* both containing cyclohexyl groups. One possibility is that CAP is less able to adopt a conformation as suitable to the solvent surroundings because the acetophenone fragment in CAP is almost certainly locked in the equatorial position, with the cyclohexyl group in chair conformation.

The observed $\Delta\nu_Q$ for MAP (see Figure 3.7) in the nematic phase cannot be compared to CAP and PAP, as the conformational behaviour of MAP causes it to

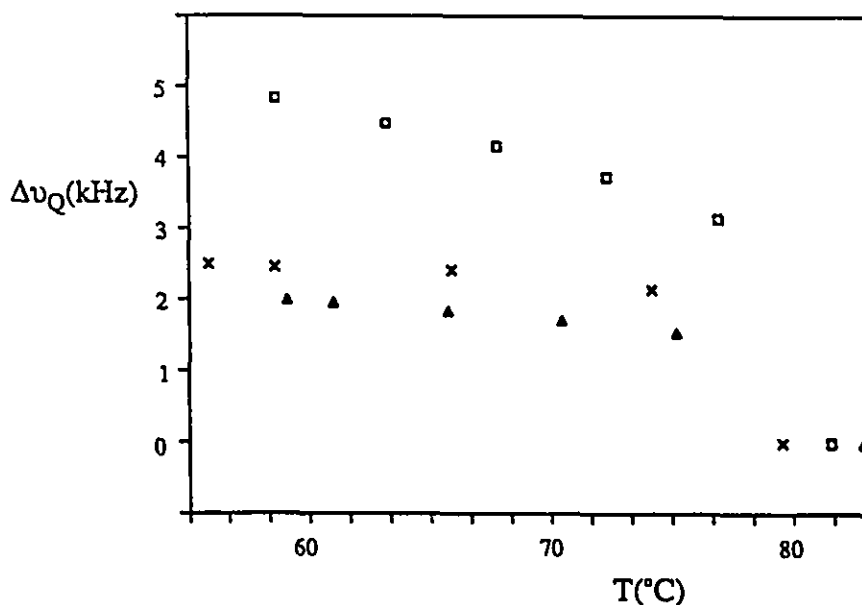


Figure 3.7. Composite plot for $\Delta\nu_Q$ versus temperature for 0.6 mol% MAP(□), CAP(Δ), and PAP(x) in the nematic phase of CCH-4.

behave significantly different than CAP and PAP.^{104,110} MAP has two discrete conformations (*i.e.* *syn* or *anti*) for the methoxy and acetyl groups (see Figure 3.8). It is likely that they are equally populated in solution,¹¹¹ and are undergoing fast exchange in the nematic phase of CCH-4.¹¹²

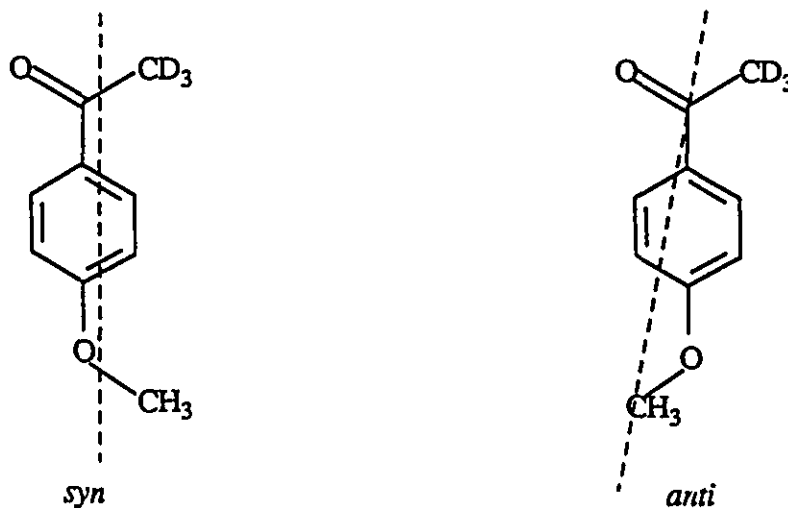


Figure 3.8. Illustration of the long molecular axis of *syn*- and *anti*-MAP

Assuming that the long molecular axis of **MAP**, **CAP**, and **PAP** are aligned parallel with the long molecular axis of **CCH-4**, then it is also probable that these solutes are aligned perpendicular to the applied field direction. We have assumed that the long molecular axis of the *anti*-conformer of **MAP** is taken as the one that bisects the acetyl and methoxy-methyl carbons, and the long molecular axis of the *syn*-conformer is parallel to the 1,4-axis of the benzene ring. If these assumptions are accurate, then it can be shown^{2,109} (see Appendix A) that the *anti*-conformer should exhibit a somewhat larger quadrupolar splitting than *syn*-**MAP**, **CAP**, and **PAP**. This occurs because the C - D bonds of *anti*-**MAP** are at different angles with respect to the long molecular axis of **CCH-4** (and hence the applied field) than are the C - D bonds of *syn*-**MAP**, **CAP**,¹¹³ and **PAP**.¹¹³ Fast equilibrium between *syn*- and *anti*-conformers would account for the larger quadrupolar splitting observed for **MAP** as compared to the **CAP** and **PAP**.

As was indicated in the Results section, the behaviour of **MAP**, **CAP**, and **PAP** (as observed by ²H NMR) below the onset of the bulk N→S transition temperature is dependent on both the solute and its bulk concentration. The ramifications of these spectra are discussed separately below.

3.7 The Solubilization of **MAP**, **CAP**, and **PAP** in the Smectic Phase of **CCH-4**. The **MAP/CCH-4** Binary System

The 3.0 mol% **MAP/CCH-4** mixture in the temperature region between 23 - 53°C is characterized by a large fairly sharp narrow doublet and a wider much less intense broad doublet(s)(see Figure 3.1b). The temperature dependence (below 53°C) of the dominant narrow doublet of the 3.0 mol% **MAP/CCH-4** sample is similar to what was observed for 3.0 mol% **1/CCH-4** (see Chapter II). The similarity of the temperature dependence of these two solutes at this bulk concentration is demonstrated by a comparison of the $\Delta\nu_Q$ vs T plot for the

1/CCH-4 sample (see Figure 2.1) to a $\Delta\nu_Q$ vs T plot for the large innermost doublet of the 3.0 mol% MAP/CCH-4 sample (see Figure 3.9). A composite plot (Figure 3.10) of the data (only the data for the innermost doublet is shown) for 1.0, 3.0, and 8.0 mol% MAP/CCH-4 is strikingly similar to that observed for the 1/CCH-4 system. Above the bulk N \rightarrow S phase transition temperature, (as indicated by the apex in the plot for each sample concentration) the plot is characterized by 3 approximately parallel curves. The curves are shifted to larger $\Delta\nu_Q$ values (for a given temperature) with decreasing ketone concentration. This is the expected result for a series of homogeneous nematic phases of different bulk concentration.⁸⁷⁻⁹¹ For temperatures below the apices of the plots, the data for all three mixtures fall on the same curve.

Therefore, by analogy to the 1/CCH-4 system we assign the innermost doublet of the 3.0 mol% MAP/CCH-4 system below 53°C as MAP solubilized in a phase separated nematic phase whose composition depends *only* on temperature and *not* on the bulk composition of the mixture.

The behaviour of the 0.6 mol% MAP/CCH-4 sample is substantially different than what was observed for the 3.0 mol% sample. The transition from the bulk nematic phase to the bulk smectic phase (*ca.* 53°C) is marked by the replacement of the fairly sharp nematic phase doublet by two broader doublets (see Figure 3.1a). This is the same spectral pattern that is observed as the minor component of the 3.0 mol% MAP/CCH-4 mixture, and is assigned as MAP dissolved in the smectic phase of CCH-4. The increased linewidth of these doublets (relative to the phase separated nematic doublet) is consistent with a smectic phase assignment.¹¹⁴⁻¹¹⁷

The general appearance of the 0.6 mol% spectrum is characteristic of a uniformly oriented solute experiencing restricted reorientational motions with C - D

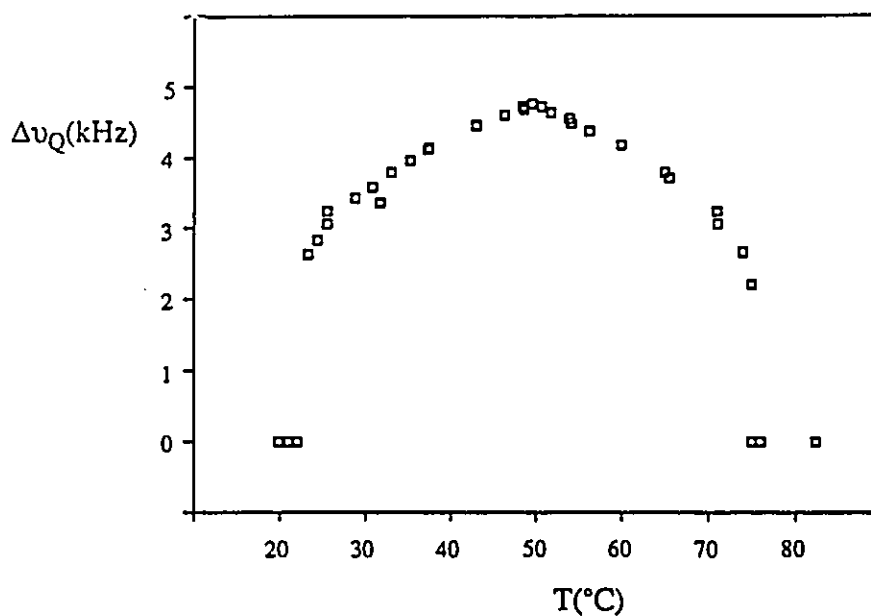


Figure 3.9. Deuterium quadrupolar splitting ($\Delta\nu_Q$) versus temperature for 3.0 mol% MAP in CCH-4.

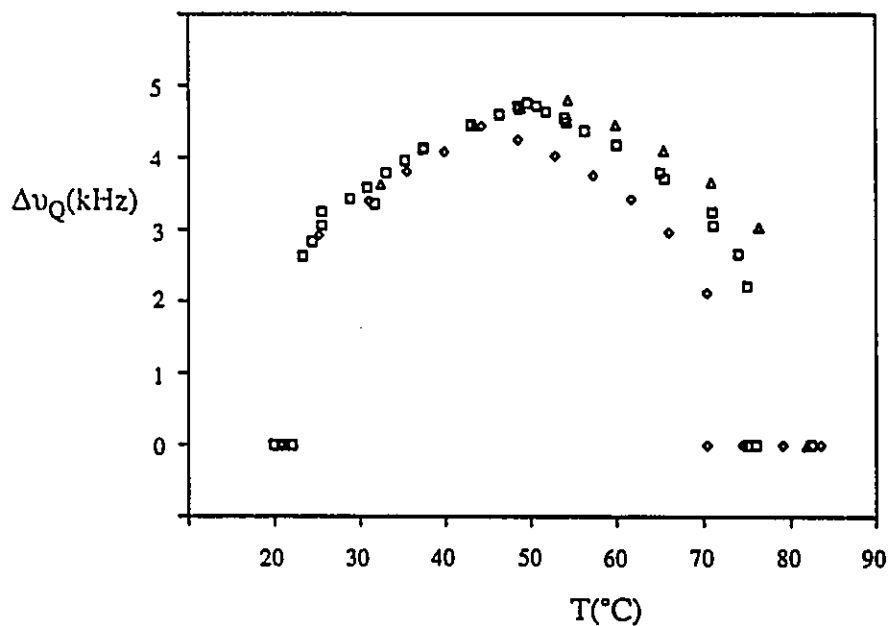


Figure 3.10. Composite plot of $\Delta\nu_Q$ versus temperature for 1.0 (Δ), 3.0 (\square), and 8.0 (\diamond) mol% mixtures of MAP and CCH-4. Only the splittings for the innermost (nematic) doublets are shown.

bonds exchanging relatively slowly.^{116,117} It is possible that the entire smectic phase spectrum (see Figure 3.1a) is the result of MAP solubilized in a single environment within the smectic phase of CCH-4.⁷⁶ However, T_1 experiments determined that the two doublets have different spin-lattice relaxation times. This indicates that the spectrum is most likely due to MAP being solubilized in two non-exchanging environments.

The entire smectic phase spectrum, and/or smectic + phase separated nematic phase spectrum, collapses to an isotropic singlet at *ca.* 23°C, signifying the formation of the "p-phase". This is similar to that observed for 1/CCH-4 (see Chapter II), with the "p-phase" being formed from both the smectic and the phase separated nematic phases. This also adds further support to the assignment that the 0.2 mol% 1/CCH-4 sample is solubilized in the smectic phase of CCH-4 between 35 - 53°C (see Chapter II). Note that the transition temperature for "p-phase" formation is not concentration dependent.

The 1.0 mol% mixture of MAP/CCH-4 exhibits (by ^2H NMR) a biphasic region (phase separated nematic phase doublet and smectic phase spectrum) between 53 - 35°C. Between 35 and 23°C, only the smectic phase spectrum is observed, whereas below 23°C, the spectrum consists solely of the sharp isotropic singlet characteristic of the "p-phase". Based on the results for the 0.6 and 0.7 mol% MAP/CCH-4 samples, these data allow estimation of the solubility limits of MAP in the smectic phase of CCH-4. This has been accomplished by determining (mostly by trial and error) the bulk concentration of MAP in which we can no longer observe the nematic phase doublet for a given temperature. Using this method we estimate that the solubility limit of MAP in the smectic phase of CCH-4 varies between 0.6 - 0.7 mol% for the temperature region 53 - 43°C. Similarly, using the 1.0 mol% MAP/CCH-4 sample, the solubility of MAP in the smectic phase of

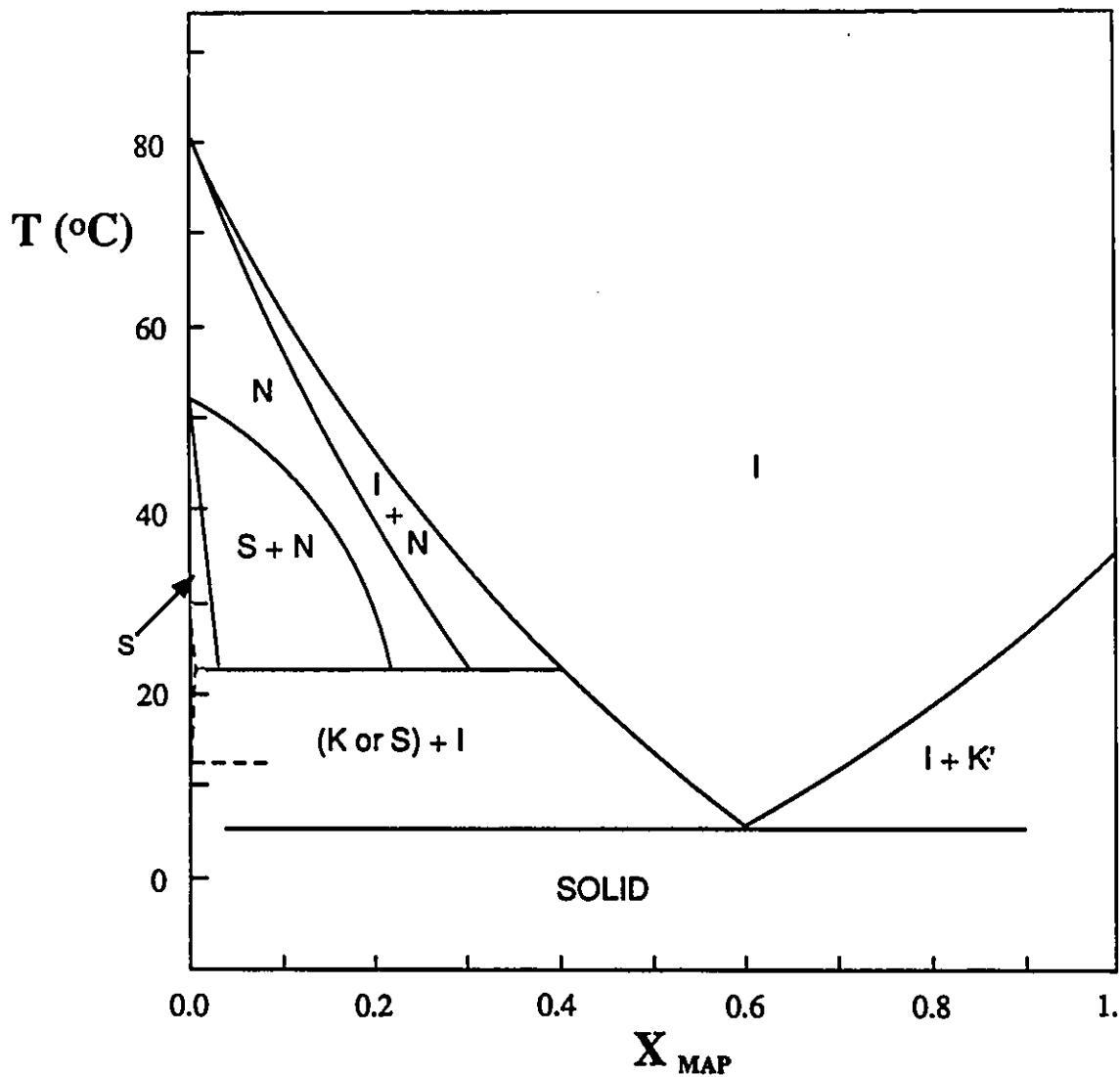


Figure 3.11. Binary phase diagram for the MAP/CCH-4 system, constructed from DSC and thermal microscopy data. Solid lines represent heating data; dashed lines show supercooled behavior. Phase identities: I, isotropic; N, nematic; S, smectic; K, solid. Reproduced with permission from reference 102.

CCH-4 varies between 1.0 and 1.2 mol% for the temperature region 35 - 24°C.

A related study¹⁰² involving DSC and thermal microscopy is in complete agreement with our description of the MAP/CCH-4 binary system between 53 and 20°C. These workers were able to construct a complete binary phase diagram for the MAP/CCH-4 system (see Figure 3.11). The phase diagram very clearly shows the relationship between temperature and bulk concentration for the solubilization of MAP in the smectic phase, or smectic + phase separated nematic phase of CCH-4. Interestingly, they were unable to observe by DSC the transition at 23°C to the "p-phase" (note for comparison the ²H NMR spectrum at 23°C in Figure 3.1a). However, they were able to identify this transition by thermal microscopy. These workers reasoned that the transition of a nematic phase to both an isotropic phase (an exothermic process) and a smectic phase (an endothermic process) might involve a net zero change in enthalpy. This would thereby explain their inability to detect this phase transition by DSC.

The CAP/CCH-4 Binary System

The CAP/CCH-4 binary system is similar in many respects to the MAP/CCH-4 binary system, and as a result will not be discussed in as great detail. There are however a few important differences that should be noted.

Between 52 - 34°C, the ²H NMR spectra of the 2.0 mol% CAP/CCH-4 mixture (see Figure 3.2b) are dominated by a fairly sharp doublet that contains additional broad absorption between the two peaks of the doublet. We assign this doublet to CAP solubilized in the nematic phase of a two phase system; the minor, broad component being due to the smectic phase. This assignment is based on the similarities of the Δv_Q vs T plot (Figure 3.12) for the 2.0 mol% CAP/CCH-4 mixture to that for 3.0 mol% MAP/CCH-4 (see Figure 3.9) As well, a composite plot of the Δv_Q vs T (for the Δv_Q values associated with the prominent doublet) for

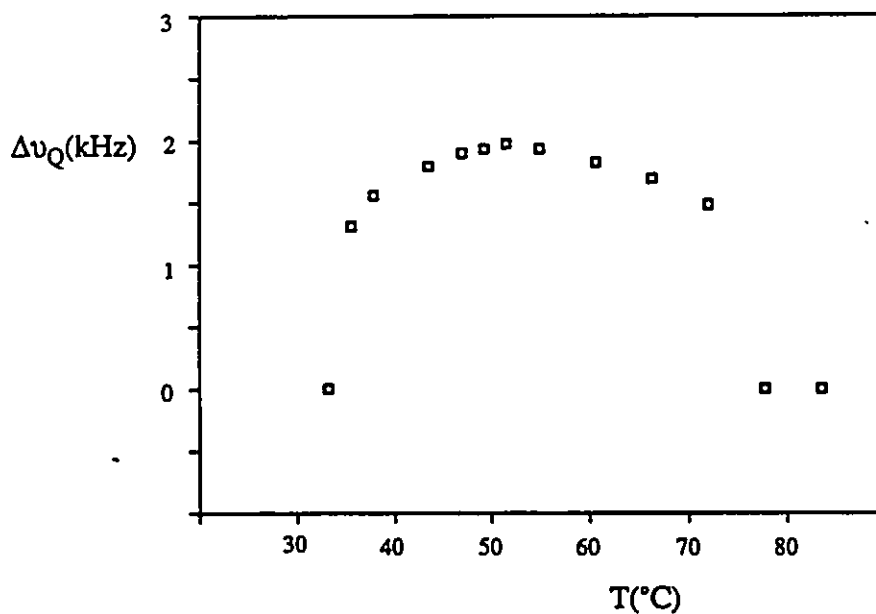


Figure 3.12. Deuterium quadrupolar splitting (Δv_Q) versus temperature for 2.0 mol% CAP in CCH-4.

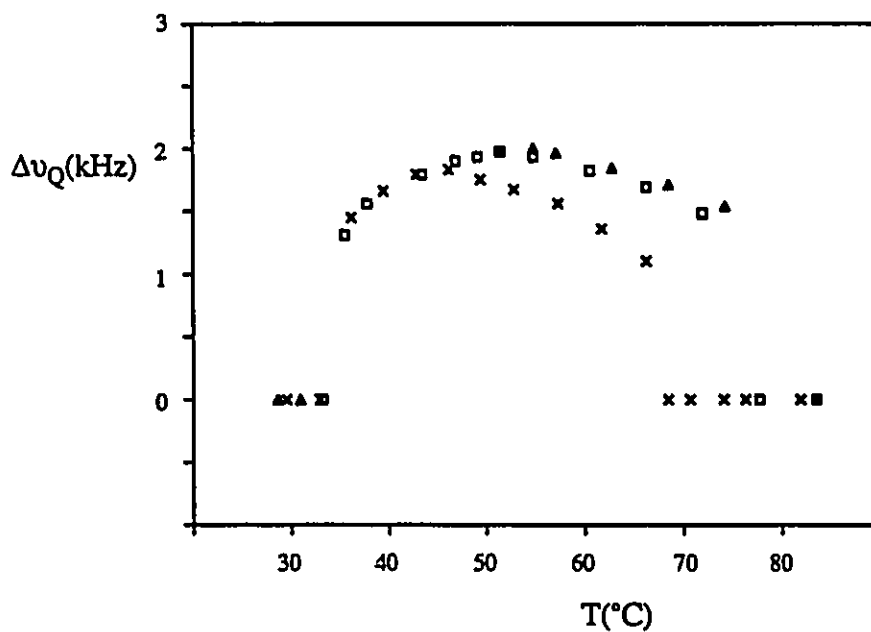


Figure 3.13. Composite plot of Δv_Q versus temperature for 0.6 (Δ), 2.0 (\square), and 8.0 (x) mol% mixtures of CAP and CCH-4. Only the splittings for the nematic doublets are shown.

the 0.6, 2.0, and 8.0 mol% CAP/CCH-4 mixtures (Figure 3.13) is similar to those found for 1 and MAP. The entire spectrum for 2.0 mol% MAP/CCH-4 collapses to a narrow singlet at *ca.* 33°C signifying "p-phase" formation.

The behaviour of the 0.6 mol% sample between the temperatures 52 - 27°C is substantially different from those found for the 2.0 mol% sample. The fairly sharp nematic phase doublet is replaced by a much broader spectral pattern (see Figure 3.2a). We have assigned this spectral pattern to CAP solubilized in the smectic phase of CCH-4. We are unable to discern if the spectral pattern is the result of CAP being uniformly oriented, or is a mixture of oriented (associated with the outer doublet splitting) and randomly oriented (associated with the inner, powder-like spectral pattern) material. It may be possible to distinguish between these possibilities with careful T_1 measurements, by orienting the sample at different angles with respect to the direction of the applied field used for recording the ^2H NMR spectra, or simply by preparing a randomly oriented sample and comparing its spectra to those reported above.

The two spectral patterns respond differently to temperature. The outer doublet *increases* in width with decreasing temperature, while the inner pattern *decreases* in width with decreasing temperature. The relative intensities of the two spectral patterns were not found to be dependent on the rate at which the sample was cooled from the nematic phase. This suggests that the sample may be uniformly oriented. However, these experiments were not exhaustively studied and the results should be viewed with some caution. Similar experiments for PAP *did* show a dependence on the rate at which the sample was cooled (*vide infra*).

The solubility of CAP in the smectic phase of CCH-4 is temperature dependent, and varies between 0.6 (at 46°C; *vide supra*) and *ca.* 0.8 mol% (at 35°C); a result consistent with what was observed for MAP in CCH-4.

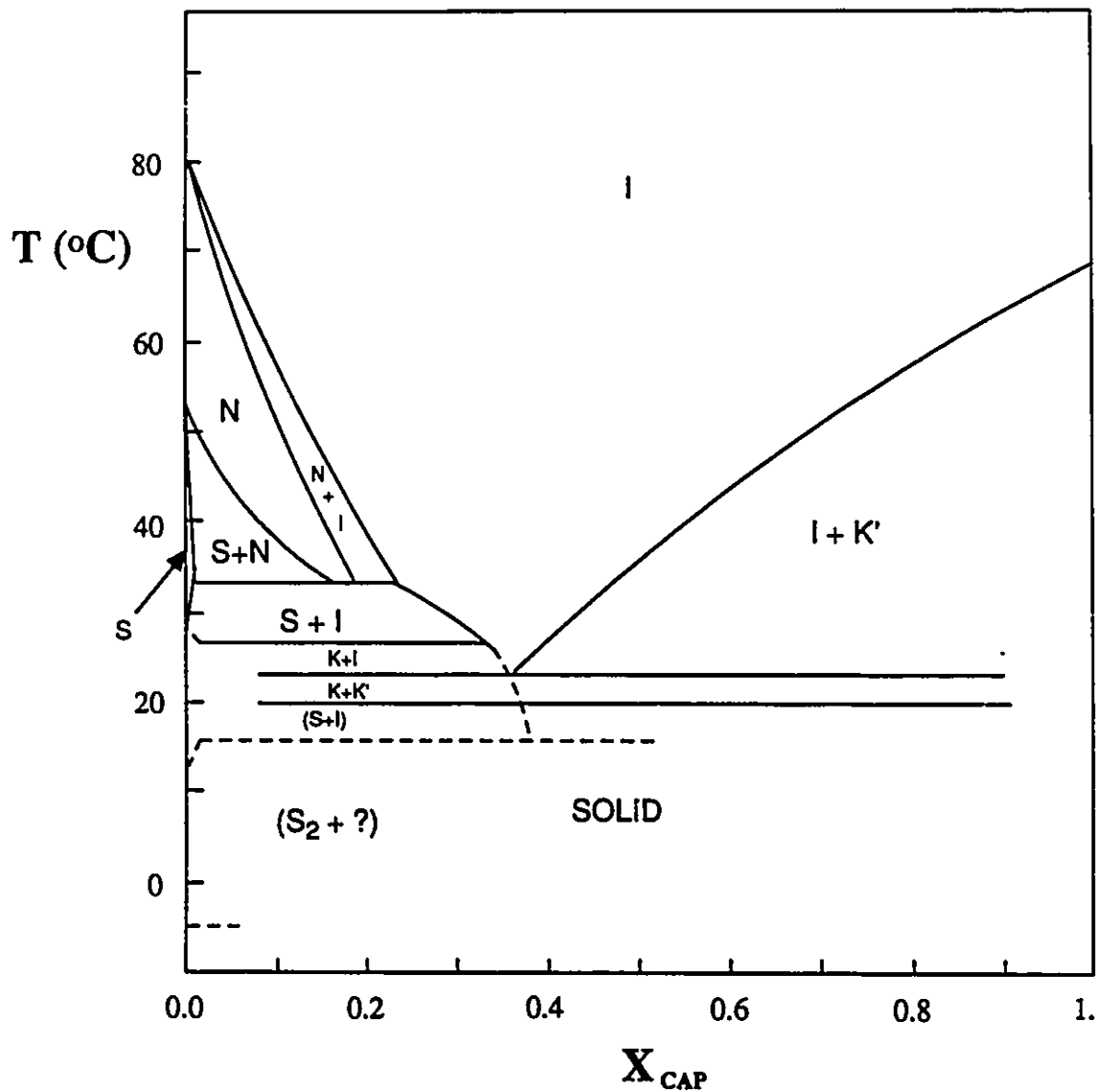


Figure 3.14. Binary phase diagram for the CAP/CCH-4 system, constructed from DSC and thermal microscopy data. Solid lines represent heating data; dashed lines show supercooled behavior. Phase identities: I, isotropic; N, nematic; S, smectic; K, solid. Reproduced with permission from reference 102.

The entire spectrum of the 0.6 mol% sample collapses to a narrow singlet at *ca.* 23°C signifying the formation of the "p-phase". Note that unlike MAP, the temperature at which formation of the "p-phase" occurs is concentration dependent. Again DSC and thermal microscopy data¹⁰² for the CAP/CCH-4 binary system is in complete agreement with our ²H NMR data. The entire temperature-composition binary phase diagram for CAP/CCH-4 is shown in Figure 3.14

The PAP/CCH-4 Binary System

The ²H NMR spectra of 2.0 mol% PAP in CCH-4 (see Figure 3.3b) again reveal that the nematic phase coexists with the smectic phase throughout the 51 - 37°C temperature range. This is indicated by the presence of the fairly sharp nematic phase doublet and the much broader spectral pattern associated with PAP in the smectic phase of CCH-4. Further evidence supporting this assignment is obtained from the $\Delta\nu_Q$ vs. T plot for the nematic phase component for 2.0 mol% PAP (see Figure 3.15). As well, a composite plot of $\Delta\nu_Q$ vs T (for the $\Delta\nu_Q$ values associated with the prominent doublet) for the 0.6, 2.0, and 8.0 mol% PAP/CCH-4 mixtures (see Figure 3.16) is again similar to plots of this type for I, MAP, and CAP. The nematic phase doublet is no longer present in the spectra that are recorded below 37°C. There is no evidence for "p-phase" formation in this sample. Clearly the behaviour of the PAP/CCH-4 binary system below 37°C is somewhat different than observed for MAP and CAP.

In the 0.6 mol% PAP/CCH-4 sample, there is no nematic phase component present observed below 51°C. The broad spectral pattern is assigned to PAP solubilized in the smectic phase of CCH-4. Again we are uncertain if these smectic phase spectra are the result of uniformly oriented PAP, or a mixture of oriented and nonoriented material. However we have observed that there is a marked variation in the relative intensities of the two patterns with the rate at which the sample is cooled

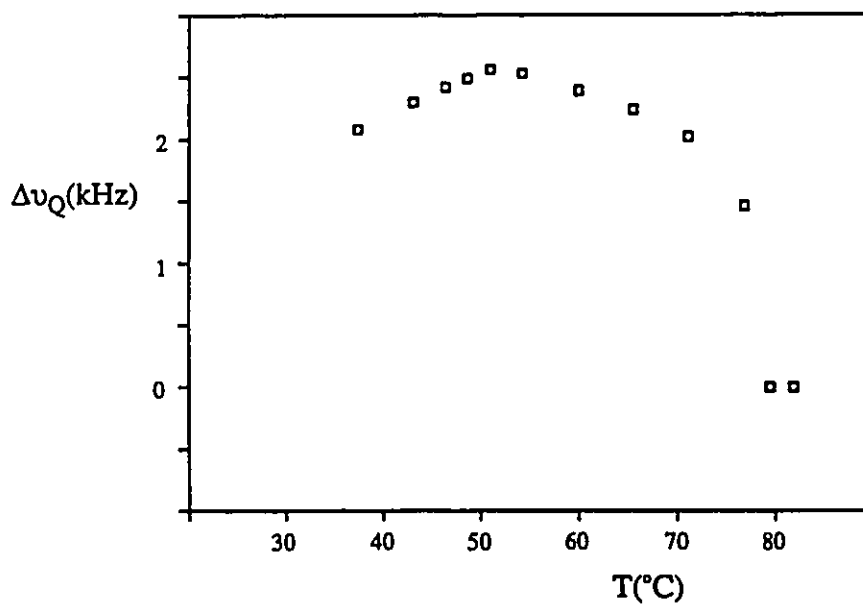


Figure 3.15. Deuterium quadrupolar splitting ($\Delta\nu_Q$) versus temperature for 2.0 mol% PAP in CCH-4.

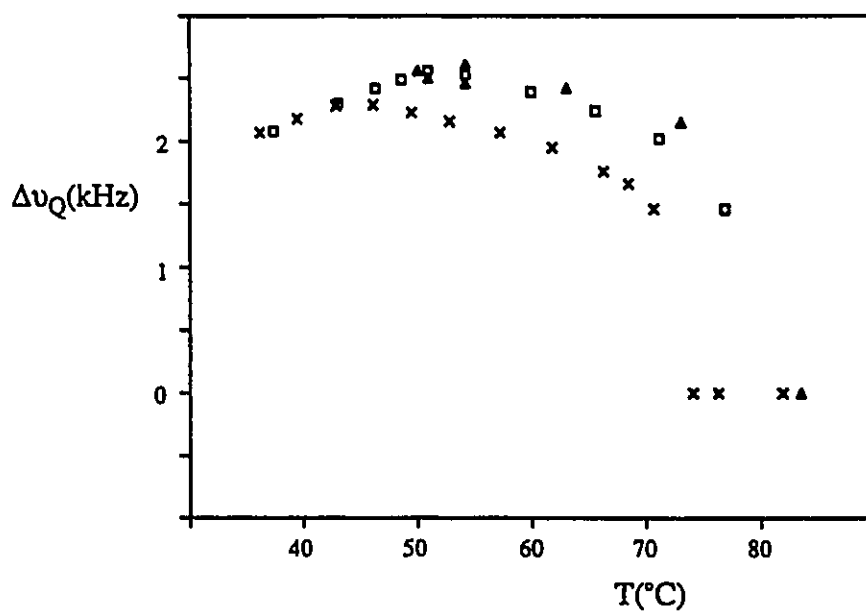
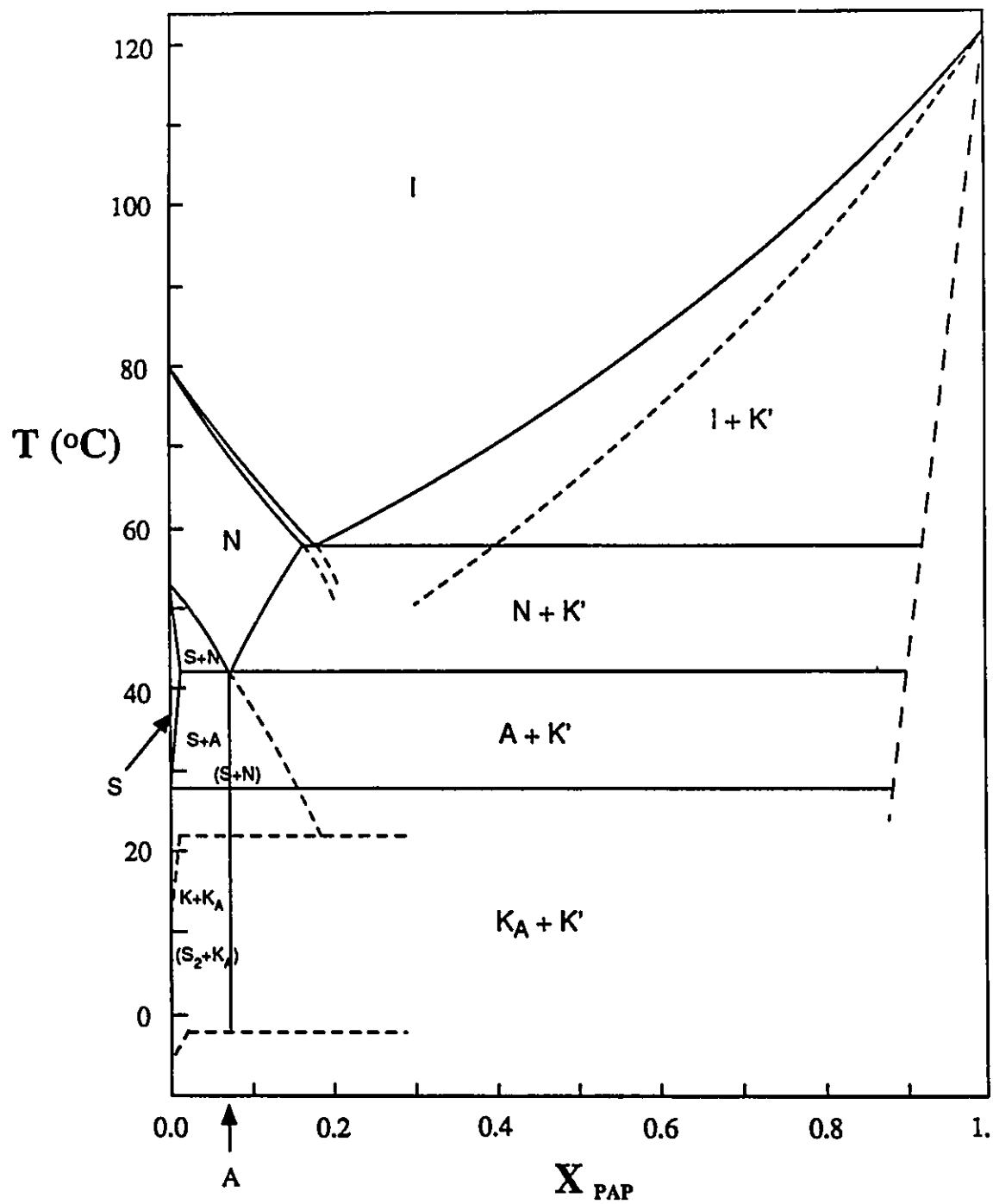


Figure 3.16. Composite plot of $\Delta\nu_Q$ versus temperature for 0.6(Δ), 2.0(\square), and 8.0(x) mol% mixtures of PAP and CCH-4. Only the splittings for the nematic doublets are shown.

Figure 3.17. Binary phase diagram for the PAP/CCH-4 system, constructed from DSC and thermal microscopy data. The light solid lines represent transition temperatures obtained from heating data, the dashed lines represent those obtained from cooling data, and the dark solid lines represent those that are identical in heating and cooling. Phase identities: I, isotropic; N, nematic; S, smectic; K, solid; A, binary solid modification. Reproduced with permission from reference 102.



from the nematic phase. This suggests that the broad inner spectral pattern is probably due to randomly oriented solute. The spectrum broadens considerably below 26°C and takes on the appearance of a polycrystalline solid.⁹⁴

DSC and thermal microscopy studies¹⁰² on the PAP/CCH-4 binary system confirm the solubility of PAP in the smectic phase of CCH-4 (of composition 0.6 - 0.8 mol% ketone) between the temperatures of 53 and 42°C. Below 42°C, the PAP/CCH-4 smectic solution was found to be metastable and eventually partitions into a mixture of a binary solid modification (of *ca.* 7 mol% PAP/CCH-4) and a smectic phase consisting of pure (or almost so) CCH-4. This is likely the phase responsible for the ²H NMR behaviour observed for 2.0 mol% PAP/CCH-4 below 37°C. These studies also confirmed the presence of two phases (nematic and smectic) for the 7.0 mol% PAP/CCH-4 mixture in the temperature range 51 - 42°C. Below 42°C it was reported that progressively more smectic phase separates out. The remaining nematic phase was observed to crystallize at *ca.* 27 - 28°C. Figure 3.17 shows the binary phase diagram obtained from the DSC and thermal microscopy of PAP/CCH-4 mixtures. The phase diagram is consistent with our ²H NMR results.

3.8 The Solubilization of 7 in CCH-4

As would be expected, the behaviour of 7 in the isotropic and nematic phase of CCH-4 is very similar to what was observed for the other ketones presented in this study. The isotropic phase is characterized by a narrow singlet, while in the nematic phase the singlet is replaced by a well defined doublet (see Figure 3.4). As was the case for the other ketones this indicates that 7 is well oriented, with some restrictions to reorientational motions.

In the Results section, it was indicated that the behaviour of 7 in the temperature region corresponding to the bulk smectic phase could not be observed

by ^2H NMR. This is similar to what was observed for the 0.2 mol% sample of **1** in CCH-4. Similarly, we interpret these results as an indication that **7** is completely soluble in the smectic phase of CCH-4 at this concentration. Phase separation was not observed for the temperature range and solute concentration (1 mol%) studied.

Note that this is in contrast to what was observed for the substituted β -phenylpropiophenones. The assignment of **7** as being solubilized in the smectic phase of CCH-4 is in complete agreement with previous photochemical studies in our group.³⁸ This study reported dramatic solvent phase effects on the fragmentation/cyclization ratio of the Norrish II reaction for **7** in CCH-4. Unfortunately, we did not define the solubility limits of **7** in the smectic phase of CCH-4, but it is at least 1 mol%. The fact that it is comparable to or even larger than that for MAP is surprising in view of the general trend to decreasing solubility with increasing solute size.

3.9 The Solubilization of C_6D_6 in CCH-4

While all of the ketones investigated behaved similarly in the isotropic and nematic phases of CCH-4, C_6D_6 yielded completely unexpected results in both the nematic and smectic phases of CCH-4.

Like all of the solutes studied in this thesis the ^2H NMR spectra in the isotropic phase of CCH-4 were characterized by a single narrow singlet. However, once the temperature of the sample was lowered below the I \rightarrow N phase transition temperature, the spectra were characterized by *two* doublets of similar magnitude, varying from *ca.* 11 - 16 kHz (see Figures 3.5 and 3.6). The origin of these two doublets is unknown. It is unlikely that they result from dipolar coupling.^{61,63,118} Related studies with C_6D_6 in other nematic solvents resulted in only a single quadrupolar doublet being observed.¹¹⁹ This would seemingly remove the alternate possibility that the second doublet is the result of C_6D_6 experiencing restricted

rotation about the D_{6h} axis. The possibility that the C_6D_6 may be solubilized in two different phases or solvation sites seems equally unlikely in view of thermal microscopy studies of solutions of C_6D_6 in CCH-4.⁸⁵ This study reported that C_6D_6 was solubilized in a single phase at temperatures corresponding to the bulk smectic phase. While we have shown that thermal microscopy may not be a reliable method for observing two-phase systems, particularly when one phase is in small relative concentration, this result seems reliable in view of the fact that ^{13}C studies of C_6H_6 in CCH-4 showed no evidence for more than one phase.⁸¹

Strangely, the spectrum observed at 52°C has only a single well defined doublet. The reason for the disappearance of the second doublet is unknown.

Once the temperature is lowered below 52°C, a second doublet of much smaller splitting (5.4 kHz) is observed. The larger doublet which was characteristic of the nematic phase remains. We have assigned the inner doublet as C_6D_6 solubilized in the smectic phase of CCH-4, and the outer doublet as C_6D_6 solubilized in a phase separated nematic phase. As was the case for the β -phenylpropiophenones, the doublet assigned to the smectic phase increases in width as the temperature is lowered, while the doublet assigned to the phase separated nematic phase decreases in magnitude. While the exact concentration for the solubility of C_6D_6 in the smectic phase is unknown, comparison of peak intensities (Figure 3.5) indicates that it is somewhere between 1 - 2 mol%. This is in line with what was observed for the smaller acetophenones, and is in keeping with the general trend that the solubility of solutes in the smectic phase of CCH-4 increases with decreasing solute size.

As the temperature was lowered to *ca.* 29°C, the inner doublet, which we have assigned to C_6D_6 solubilized in the smectic phase, splits into two doublets. This is very similar to what was observed in the nematic phase. The phase separated

nematic phase doublet is still present at these temperatures. A complete explanation of the two inner doublets for temperatures between 28 - 23°C still eludes us. However, it is possible that the solute is solubilized in two different solvation sites or phases. As this is near the temperature expected for crystallization of the smectic phase, it may be possible that the second doublet is caused by a modification of the crystal-B smectic phase to a monotropic smectic phase prior to crystallization.

Both inner doublets disappear as the temperature is lowered below 21°C, leaving only the phase separated nematic phase doublet. This is likely the result of crystallization of the smectic phase. We have been unable to observe this phase by ^2H NMR. The phase separated nematic phase doublet continues to decrease in magnitude as the temperature is lowered, until it coalesces to a singlet at ca. 9°C. It is likely that the singlet at 9°C represents formation of the solute induced "p-phase" as observed for this⁸² and other solutes presented in this thesis. Again the "p-phase" is formed, at least in part, from the phase separated nematic phase. We are unable to determine if C_6D_6 solubilized in the crystalline phase also gives rise to "p-phase" formation.

3.10 Summary

All of the solutes investigated in this study (MAP, CAP, PAP, 7, and C_6D_6) were determined to be soluble in the smectic phase of CCH-4. This confirmed our initial hypothesis that MAP was not soluble in the smectic phase of CCH-4 to the same extent or manner as were the β -phenylpropiophenones studied in Chapter II. While the extent to which the three acetophenones, MAP, CAP, and PAP, are solubilized in the smectic phase of CCH-4 is low (≤ 2 mol%), they represent the first conclusive case in which ^2H NMR spectra have been recorded for solutes solubilized in this smectic phase.

In addition to the acetophenones, ketone 7 was also found to be soluble in the

smectic phase of CCH-4 (≥ 1 mol%). This has important ramifications on previous photochemical³⁸ data reported for this solute in the liquid crystalline phases of CCH-4.

While C_6D_6 was also determined to be soluble in the smectic phase of CCH-4 (1 - 2 mol%), there are still many details pertaining to its solubilization in both the nematic and smectic phases of CCH-4 that need to be clarified.

In general, the extent to which a solute can be solubilized, in the smectic phase of CCH-4, increases with decreasing solute size.

a solute in the smectic phase of CCH-4. For example phenyl substitution on the solute appears to limit solubility as is indicated by a comparison of Figures 2.3 and 3.4.

TABLE 4.1
Solubility Limits in the Smectic Phase of CCH-4

Solute	Solubility Limit ^a
C ₆ D ₆	1 - 2
MAP	0.9 - 1
CAP	0.7 - 0.8
PAP	0.6 - 0.8
1	0.2 - 0.5
3	< 3% ^b
4	< 3% ^b
5	< 2% ^c
6a,b,c	< 2% ^c
7	≥ 1%

^areported in mol% for the smectic phase of CCH-4 as determined by ²H NMR

^bThese values represent upper limits as we did not investigate mixtures containing lower concentrations of solutes. It is likely however that the solubility limit is similar to 1.

^cFrom reference 83. These values also represent upper limits.

The exact nature of how the size of the solute influences its solubility in the smectic phase of CCH-4 has yet to be fully understood. However, this work should serve as an impetus for future work.

An equally important consequence resulting from this work, is the demonstration of the power of ²H NMR in investigating systems of these types. Clearly, when one is dealing with low solute concentrations, it is difficult to observe by thermal microscopy the disruptive effects that the solute may have on the mesophase order. ²H NMR provides a sensitive (relative to microscopy experiments) technique for investigating such systems.

Eventually, with the collection of enough ²H NMR data, a general description of the type of spectral features which can be expected from solutes

dissolved in the smectic liquid crystalline phase of CCH-4 (and in fact any other liquid crystals) will be developed. Although the amount of data collected in this thesis is not extensive enough to allow for a complete description, certain generalizations can be made. Deuterated solutes dissolved in the nematic phase of CCH-4 give rise to well defined quadrupolar doublets that are characterized by fairly sharp linewidths. The magnitude of the quadrupolar splitting increases with decreasing temperature throughout the nematic phase. Typical values for the quadrupolar splittings observed for acetyl $-CD_3$ and $-CD_2$ deuterons range between 1 - 5 and 10 - 27 kHz respectively, while aromatic $-CD$ deuterons have splittings ranging from 20 - 45 kHz. It is not uncommon for $\Delta\nu_Q$ values for CD_3 deuterons to be significantly smaller than those observed for CD_2 and aromatic CD deuterons, a result of the internal motion about the C_3 axis that is usually available to methyl groups.

The solubilization of guest solutes in the smectic phase of CCH-4 is much more complex than that observed for the nematic phase. This is not unexpected given the increased order present in the smectic phase relative to the nematic phase. Generally, the solubility in the smectic phase (of the solutes studied) ranged from 0 - 2 mol%. If the bulk concentration of the solute was greater than the solubility limit (for a given solute) in the smectic phase, the excess solute would cause phase separation to occur, giving rise to a solute-rich, phase separated nematic phase which coexists with the bulk smectic phase. The excess ketone which resides in the phase separated nematic phase is characterized by a quadrupolar doublet similar to that observed in the bulk nematic phase. However, unlike the bulk nematic phase, the magnitude of $\Delta\nu_Q$ for the ketone in the phase separated nematic phase *decreases* as the temperature is lowered throughout the bulk smectic phase .

Of the solutes which we have investigated there appears to be no general

features which adequately describe the spectral characteristics of dissolved solutes in the smectic phase. The spectral characteristics seem to be extremely dependent on the individual solute. In all cases however, the spectra are characteristic of C - D bonds which are undergoing *slow* reorientations. Consistent with this is the observation that both the linewidths, and the quadrupolar splittings of the *observed* smectic phase spectra were significantly larger (except in the case of C₆D₆) than those found for the corresponding nematic phase spectra. Those solutes for which we were unable to observe deuterium signals in the smectic phase, (*i.e.* 1 and 7) either have quadrupolar splittings in excess of 50 kHz or have such fast relaxation rates, that it is impossible for us to observe their signals.

At lower temperatures (at or near the K→S phase transition) we have observed, as have others,⁸¹⁻⁸³ a solute-induced "p-phase". While this phase is fairly common, it was not observed for all of the solutes studied *i.e.* PAP and 7. Based on the behaviour of MAP the reason we were unable to observe "p-phase" formation is presumably the result of not cooling the sample to low enough temperatures. We have identified this phase as a *viscous isotropic liquid*, and *not* as a plastic or cubic phase as has been suggested by other workers^{21,81-83}

We have also identified two solutes (1 and PAP) which form stable binary solid and/or smectic modifications with CCH-4. While we have insufficient data at this time to fully characterize whether or not a particular solute will form a binary modification, we have determined that they may be formed either on direct cooling of a smectic solution or by crystallization of the "p-phase".

This work will certainly have important ramifications on previous studies involving the effects of the liquid crystalline phases of CCH-4, and its related homologues (and indeed other liquid crystalline systems), on dissolved solutes. This results from the fact that most previous studies assumed homogeneous solubilization

in the smectic phase of CCH-4, while in fact they had employed solute concentrations that were above the solubility limit of that solute in the smectic phase of CCH-4.

While this work clearly points out the need for workers in this area to take more care in identifying the solubility limits of solutes in liquid crystalline phases, there are other numerous interesting consequences of this work. For example, solutes such as the β -phenylpropiophenones which cause phase separation at very low concentrations provide an easy way of obtaining a low temperature nematic phase of CCH-4 that is unattainable otherwise. Similarly "p-phase" formation also provides an accessible low temperature isotropic phase of CCH-4. Having control over both the phase and the temperature has obvious advantages. In addition to the above, we have only scratched the surface of the potential utility of *solid* binary modifications of smectic liquid crystals.

Finally, now that we have successfully identified some of the limitations of solute solubilization in highly ordered smectic phases, or at least found a reliable method of investigating it, it may be possible to truly exploit these phases in a manner that was initially hoped for, *i.e.* controlling unimolecular or bimolecular chemical reactivity.

CHAPTER V

Experimental

^1H NMR spectra were recorded on a Varian EM390 (90 MHz) or a Bruker AM500 (500 MHz) spectrometer. All ^1H spectra were recorded at 90 MHz in deuteriochloroform unless otherwise noted. ^{13}C NMR spectra were recorded at 62.5 or 125.6 MHz on a Bruker WM250 or AM500 respectively. All measurements are reported in parts per million downfield (high frequency) from tetramethylsilane.

Except where otherwise noted, ^2H NMR experiments were carried out at 76.78 MHz on a Bruker AM500 NMR spectrometer equipped with an Aspect 3000 computer, a Bruker BVT-100 Variable Temperature Unit, and a 10 mm VSP broadband probe. Temperatures were controllable to within $\pm 1^\circ$, and were recorded with a copper-constantan thermocouple. Samples were prepared in 5 mm NMR tubes by adding the appropriate amounts of solute and liquid crystal, and heating to the isotropic phase to ensure complete sample mixing. The sample and probe were allowed to equilibrate at each temperature for as long as was necessary to obtain reproducible spectra. This was generally 5 - 20 min for the samples containing ≤ 5 mol% solute, but extended up to a few hours for those containing higher concentrations of **1**, particularly at temperatures below 45°C .

Deuterium NMR spectra were recorded on stationary samples using the quadrupolar echo pulse sequence [26], generally collecting 8 - 32 K data points per scan over a 40 - 165 kHz sweep width. Typically, 96 - 16000 such scans were collected and averaged (with a 0.15 - 0.8 sec delay between scans, depending on sample temperature). The $\pi/2$ pulse width was *ca.* 27 - 30 μs for **1**, **2**, and MAP, and

14 - 17.8 for all others. The difference in the pulse widths for the two sets of data was a result of instrument maintenance, and is not a result of any intrinsic properties of the solutes. The data were processed using 40 - 150 Hz line-broadening and exponential multiplication, prior to obtaining the Fourier transform. At a given temperature, both the line-width and the observed splitting are approximately independent of the pulse sequence used (quadrupolar echo or single pulse). In addition, no noticeable difference could be observed when spectra collected with the sample spinning were compared to spectra collected with the sample held stationary.

A few experiments (mostly controls) were carried out at 41.3 MHz on a home-built spectrometer at the University of Guelph, with considerable assistance from Dr. K. H. Jeffrey. Samples were sealed under vacuum in 9 X 25 mm Pyrex tubes, and thereafter handled similarly to those described above. The spectrometer has been described in detail elsewhere.¹²⁰

Deuterium T_1 measurements summarized in Figure 7 for 3 mol% samples of **1** in CCH-4 and EB (15 - 108°C) and 3.0 mol% MAP in CCH-4 were carried out on the Bruker AM500, and employed a π - τ -quadecho or $\pi/2$ - τ -quadecho (for T_1 values less than 20 ms) non-selective inversion-recovery pulse sequence. Typically, T_1 values were calculated from least squares analysis of data from 8 - 12 τ values. Errors were calculated as two standard deviations by a statistical method [37], and ranged from *ca.* 1 - 2% for values > 50 ms to *ca.* 20% for those less than 15 ms. Error bars are included in the plot in Figure 7 for those data with associated errors \geq 10%.

T_1 -values at a few representative temperatures in the 77 - 123°C range were measured on a Bruker AC200 NMR spectrometer equipped with a 10 mm broadband probe, with the assistance of Dr. C. Rodger (Bruker Canada). These values are not reported, but were consistently *ca.* 10% smaller than those measured

on the AM500, and showed a similar variation with temperature.

CCH-4, CCH-2 (E. Merck), and benzene- d_6 (MSD isotopes) were used as received from their suppliers. 4-Cyclohexylacetophenone (CAP) was prepared by Friedel-Crafts acetylation of cyclohexylbenzene (Aldrich) with aluminum trichloride in carbon disulfide, and was purified by repeated recrystallizations from ethanol/water, and one treatment with decolorizing charcoal (m.p. = 68 - 69.5°C; lit. = 68 - 70°C¹²¹). Similarly, 4-Methoxyvalerophenone (7) was prepared by Friedel-Crafts acylation of valeryl chloride and anisole (Aldrich) with aluminum trichloride in carbon disulfide. Vacuum distillation (0.1mm, 102°C) resulted in a pure colorless liquid.

β -Phenyl-4-methoxypropiofenone and β -(4-cyclohexylphenyl)-4-methoxypropiofenone were prepared using a previously described method^{25,122} and had melting points of 96 - 97 °C and 89 - 90 °C, respectively. β -Phenyl-4-methoxypropiofenone- α,α - d_2 (1), 4-methoxyacetophenone- α,α,α - d_3 (MAP), 4-Phenylacetophenone- α,α,α - d_3 (PAP) and β -(4-cyclohexylphenyl)-4-methoxypropiofenone- α,α - d_2 (3) were prepared from their protio-analogues (Aldrich) by base-catalysed deuterium exchange. Typically, 0.2 - 1 g of the ketone were refluxed in a mixture of sodium hydroxide (0.2 - 1 g), dioxane (40 - 125 mL), and deuterium oxide (99.8% atom D; 3 - 10 mL) for 12 - 18 hours. The resulting mixture was cooled to room temperature and extracted a few times with ether. After washing once with water, the combined ether extracts were dried over anhydrous sodium sulphate, filtered, and the solvent was evaporated on the rotary evaporator. The deuterated ketones were recrystallized two or three times from ethanol or ethanol/water, and had melting points as follows: 1, 95.5 - 97°C (lit.¹²³ 96 - 97°C); 3, 62.5 - 64°C (lit.^{6f} 63 - 64°C) ; MAP, 35.5 - 37.5°C (lit.⁵¹ 36 - 38°C), CAP, 68.5 - 70°C (lit.⁴¹ 68 - 70°C); PAP, 115.5 - 118°C (lit.⁵¹ 116 - 118°C). Their ¹H NMR

spectra (Varian EM390; chloroform-d) confirmed them to be > 95% deuterated in the α -position in each case.

Benzaldehyde-4-d was prepared from 4-bromobenzaldehyde. A benzene solution (150 ml) of 4-bromobenzaldehyde (5 g, 0.025 mol) and ethylene glycol (1.7 g, 0.027 mol) was refluxed for 14 hours in a 250 ml round bottom flask with a Dean Stark trap attached. The solution was then cooled and washed with 5% NaHCO₃ (3 X 60 ml) and dried over sodium sulphate. The benzene was removed under reduced pressure leaving a pale yellow oil identified as 4-bromo-(2-(1,3-dioxacyclopentyl))benzene (5 g, 0.022 mol).

¹H NMR(EM390; CDCl₃ vs. TMS): δ = 4.05(s, 4H), 5.65(s, 1H), 7.45(m, 4H).

The acetal (2 g, 0.009 mol) was dissolved in dry tetrahydrofuran (THF) (50 ml) and placed in a 100 ml round bottom flask. A 50 ml pressure equalizing dropping funnel was attached to the top of the flask and the entire system was maintained under a positive pressure of dry nitrogen. The acetal solution was cooled in a dry ice/acetone bath and was allowed to equilibrate for 15 minutes. After equilibration was complete, a hexane solution of n-Butyl Lithium (ca. 5 ml of ca. 2.5 M; Aldrich) was added dropwise to the acetal over a 25 minute period. After the addition was complete the solution (red) was allowed to stir for an additional hour. The solution was then quenched by addition of a D₂O/THF solution (3 g D₂O, 15 ml THF) while the flask was still maintained at -78°C. After the addition of the D₂O was complete, the solution was allowed to warm to room temperature. The solution was extracted with ether (3 X 60 mls). The ether solution was then dried over sodium sulfate, filtered, and then the ether was removed under reduced pressure giving a yellow oil (1.1 g, 0.007 mol) identified as 2-(1,3-dioxacyclopentyl)benzene-4-d.

A solution of the deuterated acetal (1g, 0.0065 mol), THF (70 mls), and 5% HCl (30 mls) was added to a 150 ml round bottom flask and refluxed under nitrogen

for 2 hours. The reaction mixture was cooled, extracted with ether (3 X 50 ml) and dried over sodium sulfate. The solution was filtered, and the ether/THF was removed under reduced pressure leaving a yellow oil (0.65 g, 0.006 mol) identified as benzaldehyde-4-d.

$^1\text{H NMR}$ (EM390; CDCl_3 vs. TMS): $\delta = 7.45(\text{d}, 2\text{H}), 7.85(\text{d}, 2\text{H}), 10(\text{s}, 1\text{H})$.

β -(4-Deuteriophenyl)-4-methoxypropiophenone (**2**) was prepared from 4-deuteriobenzaldehyde by the published route.¹²² After isolation and three recrystallizations from ethanol/water, ketone **2** had a melting point of 96 - 97°C, and exhibited the following $^1\text{H NMR}$ spectrum.

$^1\text{H NMR}$ (EM390; CDCl_3 vs. TMS): $\delta = 3.14 (\text{m}, 4\text{H}), 3.83 (\text{s}, 3\text{H}), 6.90 (\text{d}, 2\text{H}), 7.30 (\text{s}, 4\text{H}), 7.93 (\text{d}, 2\text{H})$.

The high resolution $^2\text{H NMR}$ spectrum (76.8 MHz; in CHCl_3 with external CDCl_3 reference) for this compound showed a single resonance at 7.30 ppm.

APPENDIX A

The magnitude of $\Delta\nu_Q$ for a monodeuterated solute in a nematic liquid crystal is given by Equation [A.1] (see Introduction Chapter);

$$[A.1] \quad \Delta\nu = \frac{3}{4} \left[\frac{e^2qQ}{h} \right] \langle 3\cos^2\theta_0 - 1 \rangle \langle 3\cos^2\beta - 1 \rangle$$

where $\Delta\nu$ is the separation of the two doublet peaks in frequency units, θ_0 is the angle between the principal molecular axis and the magnetic field, and β is the angle between the principal component of the electric field gradient tensor and the principal molecular axis.

In the case of freely rotating (fast on the NMR time scale) deuterated methyl groups, all of the angular components that are not along the direction of the C - C bond that attaches the methyl group to the rest of the molecule average to zero. This allows for the principal axis to be defined as that corresponding to the C - C bond which attaches the methyl group to the rest of the molecule. This is the assumption that has been made in Figure A.1.

In both cases θ_0 will be 90° , therefore the calculated values for both *syn*- and *anti*- methoxyacetophenone (based on the above geometries and a quadrupolar coupling constant of 170 kHz) is 32 kHz and -97 kHz respectively. Noting that the absolute value for the *anti* conformer is larger than that found for the *syn* conformer is consistent with the argument presented in Chapter III.

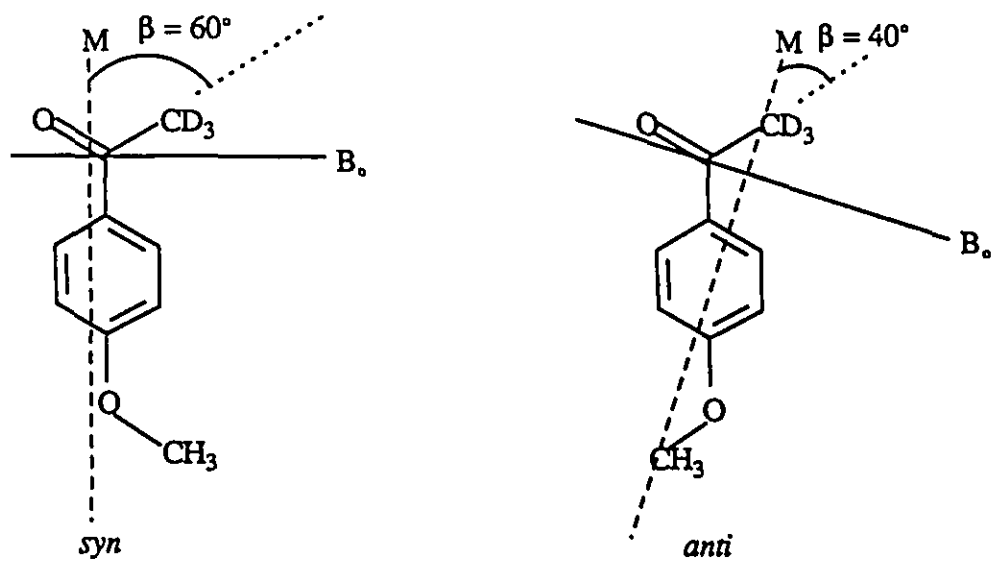


Figure A.1. Illustration of angles used in the calculation of $\Delta\nu$ for *syn*- and *anti*-methoxyacetophenone.

References

- 1) The molecules which make up the class of compounds known as liquid crystals can exist in both crystalline, liquid crystalline, and isotropic phases. Throughout the rest of this thesis the term *liquid crystal(s)* will refer to such molecules while they are in a liquid crystalline phase.
- 2) Doane, J. W. in *Magnetic Resonance of Phase Transitions*; Owens, F. J.; Poole, C. P. Jr.; Farach, H. A., Eds.; Academic Press: New York, 1979. Chapter 4.
- 3) This is not always the case however, recently a new class of thermotropic liquid crystals have been found which are disk-like in their shape. See ref 6 for more details.
- 4) Diele, S.; Brand, P.; Sackmann, H. *Mol. Cryst. Liq. Cryst.* **1972**, *17*, 163.
- 5) de Vries, A.; *Mol. Cryst. Liq. Cryst.* **1973**, *24*, 337.
- 6) Taylor, T. R.; Arora, S. L.; Ferguson, J. L. *Phys. Rev. Lett.* **25**, 722, 1970.
- 7) Wise, R. A.; Smith, D. H.; Doane, J. W. *Phys. Rev. A* **7**, 1366, 1973.
- 8) *Liquid Crystals. The Fourth State of Matter*; Saeva, F. D., Ed.; Marcel Dekker, Inc.: New York, 1979.
- 9) Chistyakov, I. G.; Schabischev, L. S.; Jarenov, R. I.; Gusakova, L. A. *Mol. Cryst. Liq. Cryst.* **1969**, *7*, 279.
- 10) In *Liquid Crystals 2, Part II*, (G. H. Brown ed.) Gordon and Breach, London, 1969, p. 813.
- 11) Bacon, W. E.; Brown, G. H. *Mol. Cryst. Liq. Cryst.* **1971**, *12*, 229.
- 12) Dewar, M. J. S.; Nahlovsky, B. D. *J. Am. Chem. Soc.* **1974**, *96*, 460.
- 13) Nerbonne, J. M.; Weiss, R. G. *Isr. J. Chem.* **1979**, *18*, 266.
- 14) Hrovat, D. A.; Liu, J. H.; Turro, N. J.; Weiss, R. G. *J. Am. Chem. Soc.* **1984**, *106*, 7033.
- 15) Nerbonne, J. M.; Weiss, R. G. *J. Am. Chem. Soc.* **1979**, *101*, 402.
- 16) Samori, B.; Fiocco, L. *J. Am. Chem. Soc.* **1982**, *104*, 2634.
- 17) De Maria, P.; Lodi, A.; Samori, B.; Rustichelli, F.; Torquati, G. *J. Am. Chem. Soc.* **1984**, *106*, 653.
- 18) Otruba III, J. P.; Weiss, R. G. *Mol. Cryst. Liq. Cryst.* **1982**, *80*, 165.
- 19) Eskenazi, C.; Nicoud, J. F.; Kagan, H. B. *J. Org. Chem.* **1979**, *44*, 995.
- 20) Seuron, P.; Solladie, G. *J. Org. Chem.* **1980**, *45*, 715.

- 21) Treanor, R. L.; Weiss, R. G. *J. Am. Chem. Soc.* **1986**, *108*, 3137.
- 22) Zimmermann, R. G.; Liu, J. H.; Weiss, R. G. *J. Am. Chem. Soc.* **1986**, *108*, 5264.
- 23) Treanor, R. L.; Weiss, R. G. *Tetrahedron* **1986**, *43*, 1371.
- 24) Leigh, W. J.; Frendo, D. T.; Klawunn, P. J. *Can J. Chem.* **1985**, *63*, 2131.
- 25) Leigh, W. J. *J. Am. Chem. Soc.* **1985**, *107*, 6114.
- 26) Leigh, W. J. *Can. J. Chem.* **1986**, *64*, 1130.
- 27) Leigh, W. J.; Mitchell, D. S. *J. Am. Chem. Soc.* **1988**, *110*, 1311.
- 28) Schnur, J. M.; Martire, D. E. *Mol. Cryst. Liq. Cryst.* **1974**, *26*, 2113.
- 29) Oweimreen, G. A.; Lin, G. C.; Martire, D. E. *J. Phys. Chem.* **1979**, *83*, 2111.
- 30) Maerlew, S. W. in *"The Molecular Physics of Liquid Crystals."* Edited by Luckhurst, G. R.; Gray, G. W. Academic Press. New York, 1979, Chapter. 11.
- 31) Oweimreen, G. A.; Martire, D. E. *J. Chem Phys.* **1980**, *72*, 2500.
- 32) Porcaro, P. J.; Shubiak, P. J. *J. Chromatogr. Sci.* **1971**, *9*, 690.
- 33) Leigh, W. J. *Can. J. Chem.* **1985**, *63*, 2736.
- 34) Samori, B.; De Maria, P.; Mariani, P.; Rustichelli, F.; Zani, P. *Tetrahedron* **1987**, *43*, 1409.
- 35) Tanaka, Y.; Chiyo, T.; Iijima, S.; Shimizu, T. Kusano, T. *Mol. Cryst. Liq. Cryst.* **1983**, *99*, 255.
- 36) Cassis Jr., E. G.; Weiss, R. G. *Photochem. Photobiol.* **1982**, *35*, 439.
- 37) Otruba III, J. P.; Weiss, R. G. *J. Org. Chem.* **1983**, *48*, 3448.
- 38) Leigh, W. J.; Jakobs, S. *Tetrahedron* **1987**, *43*, 1393.
- 39) Wedel, H.; Haase, W. *Chem. Phys. Lett.* **1978**, *55*, 96.
- 40) Myrvold, B. O.; Klæboe, P. *Acta Chem. Scand.* **1985**, *A39*, 733.
- 41) Haase, W.; Trinquet, O.; Quotschalla, U.; Foitzik, J. K. *Mol. Cryst. Liq. Cryst.* **1987**, *148*, 15.
- 42) Sackman, E. *Chem. Phys. Lett.* **1969**, *3*, 253.
- 43) Saeva, F. D.; Wysocki, J. J. *J. Am. Chem. Soc.* **1971**, *93*, 5928.
- 44) Saeva, F. D. *J. Am. Chem. Soc.* **1972**, *94*, 5135.

- 45) Sackman, E.; Möhwald, H. *J. Chem. Phys.* 1973, 58, 5407.
- 46) Beens, H.; Möhwald, H.; Rehm, D.; Sackmann, E.; Weller, A. *Chem. Phys. Lett.* 1971, 8, 341.
- 47) Anderson, V. C.; Craig, B. B.; Weiss, R. G. *J. Phys. Chem.* 1982, 86, 4642.
- 48) Anderson, V. C.; Craig, B. B.; Weiss, R. G. *Mol. Cryst. Liq. Cryst.* 1983, 97, 351.
- 49) Anderson, V. C.; Weiss, R. G. *J. Am. Chem. Soc.* 1984, 106, 6628.
- 50) Anderson, V. C.; Craig, B. B.; Weiss, R. G. *J. Am. Chem. Soc.* 1981, 103, 7169; 1982, 104, 2972.
- 51) Sackmann, E.; Rehm, D. *Chem. Phys. Lett.* 1970, 4, 537.
- 52) Baur, G.; Stieb, A.; Meier, G. *J. Appl. Phys.* 1973, 44, 1905.
- 53) Cehelnik, E. D.; Cundall, R. B.; Lockwood, J. R.; Palmer, T. F. *J. Chem. Soc., Faraday Trans. II* 1974, 70, 244.
- 54) Krishnamurti, D.; Krishnamurthy, K. S.; Shashidar, R. *Mol. Cryst. Liq. Cryst.* 1969, 8, 339.
- 55) Rao, K. V. S.; Polnaszek, C. F. *Freed. J. H. J. Phys. Chem.* 1977, 81, 449.
- 56) Lin W.; Freed. J. H.; *J. Phys. Chem.* 1979, 83, 379.
- 57) Meirovitch, E.; Igner, D.; Igner, E.; Moro, G.; Freed. J. H. *J. Chem. Phys.* 1982, 77, 3915.
- 58) Broido, M. S.; Belsky, I.; Meirovitch, E. *J. Phys. Chem.* 1982, 86, 4197.
- 59) Meirovitch, E.; Broido, M. S.; *J. Phys. Chem.* 1984, 88, 4316.
- 60) Meirovitch, E.; Freed. J. H. *J. Phys. Chem.* 1984, 88, 4995.
- 61) Luz, Z. In *Nuclear Magnetic Resonance of Liquid Crystals*. NATO ASI Series Ser. C. Vol. 141. Edited by Emsley, J. W.; D. Reidel Publishing Co., Dordrecht. 1985. Chapt. 13.
- 62) Vaz, N. A. P.; Doane, J. W. *J. Chem. Phys.* 1983, 79, 2470.
- 63) Avent, A. G.; Emsley, J. W.; Ng, S.; Venables, S. M. *J. Chem. Soc. Perkin Trans. II*, 1984, 1855.
- 64) Fung, B. M.; Sigh, R. V.; Alcock, M. M. *J. Am. Chem. Soc.* 1984, 106, 7301.
- 65) Vold, R. R.; Vold, R. L. In *Liquid Crystals and Ordered Fluids* Vol. 4. Edited by Giffin, A. C. and Johnson, J. F. Plenum Publishing Corp. 1984. p. 561.

- 66) Blinc, R.; Marin, B.; Pirs, J. Doane, J. W. *Phys. Rev. Lett.* **1985**, *54*, 438.
- 67) Samulski, E. T. *Polymer* **1985**, *26*, 177.
- 68) Luckhurst, G. R. *Quart. Rev.* **1968**, 179.
- 69) Englert, G.; Saupe, A. *Z. Naturforsch.* **1964**, *19a*, 172.
- 70) *Licristal Liquid Crystals* EM Chemicals, Hawthorne, N.Y. (1986).
- 71) Rahimzadeh, E.; Tsang, T.; Yin, L. *Mol. Cryst. Liq. Cryst.* **1986**, *139*, 291.
- 72) Brownsey, G. J.; Leadbetter, A. J. *J. Phys. (Paris)* **1981**, *42*, L135.
- 73) The cubic structure has been assigned on the basis of x-ray diffraction and optical microscopy studies. See reference 6 for more details.
- 74) Kelker, H.; Hatz, R. *Handbook of Liquid Crystals*. Verlag Chemie, Weinheim. 1980
- 75) Gray, G. W.; Goodby, J. W. *Smectic Liquid Crystals. Textures and Structures*. Leonard Hill, Glasgow. 1984
- 76) Mitchell, D. S.; Leigh, W. J. *Liquid Crystals* **1989**, *4*, 39.
- 77) Wagner, P. J.; Kelso, P. A.; Kemppainen, A. E.; Haug, A.; Graber, D. R. *Mol. Photochem.* **1970**, *2*, 81.
- 78) Scaino, J. C.; Perkins, M. J.; Sheppard, J. W.; Platz, M. S.; Barcus, R. L. *J. Photochem.* **1983**, *21*, 137.
- 79) Whitten, D. G.; Punch, W. E. *Mol Photochem.* **1970**, *2*, 77.
- 80) These *assumptions* were based on thermal microscopy inspection of the solute/CCH-4 mixtures.
- 81) Fung, B. M.; Gangoda, M. *J. Am. Chem. Soc.* **1985**, *107*, 3395.
- 82) Gangoda, M.; Fung, B. M. *Chem. Phys. Lett.* **1985**, *120*, 527.
- 83) Treanor, R. L.; Weiss, R. G. *J. Phys. Chem.* **1987**, *91*, 5552.
- 84) Leigh, W. J. In *Photochemistry on Solid Surfaces*; Matsuura, T.; Anpo, M., Eds.; Elsevier: Amsterdam, in press.
- 85) Fahie, B. J.; Mitchell, D. S.; Leigh, W. J. *Can. J. Chem.* **1989**, *67*, 148.
- 86) Fujiwara, H.; Hirai, J.; Sasaki, Y.; Takahashi, K. *Mol. Cryst. Liq. Cryst.* **1987**, *150B*, 387.
- 87) Emsley, J. W.; Hashim, R.; Luckhurst, G. R.; Shilstone, G. N. *Liq. Cryst.* **1986**, *1*, 437.

- 88) Janik, B.; Samulski, E. T.; Toriumi, H. *J. Phys. Chem.* **1987**, *91*, 1842.
- 89) Pohl, L.; Eidenschink, R. *Anal. Chem.* **1978**, *50*, 1934.
- 90) Khetrapal, C. L.; Arun Kumar, B. S.; Ramanathan, K. V.; Suryaprakash, N. *J. Magn. Res.* **1987**, *73*, 516.
- 91) Ambrosetti, R.; Catalano, D.; Forte, C.; Veracini, C. A. *Z. Naturforsch.* **1986**, *41A*, 431.
- 92) We recognize that such external factors as the phase (solvent or neat) that the molecule is in can have a *small* effect on the energy of these transitions.
- 93) This also applies for ESR spectroscopy.
- 94) Fyfe, C. A. *Solid State NMR for Chemists*. C.F.C. Press, Ontario, Canada, 1983.
- 95) For an excellent review of this see reference 2.
- 96) Davis, J. H.; Jeffrey, K. R.; Bloom, M.; Valic, M. I.; Higgs, T. P. *Chem. Phys. Lett.* **1976**, *42*, 390.
- 97) Bloom, M.; Davis, J. H.; Valic, M. I. *Can. J. Phys.* **1980**, *58*, 1510.
- 98) Davis, J. H. *Biochim. Biophys. Acta* **1983**, *737*, 117.
- 99) Smith, I. C. P. in *NMR of Newly Accessible Nuclei*; Laszlo, P., Ed.; Academic Press: New York, 1983; Vol. 2, Chapt. 1.
- 100) *Advances in Nuclear Quadrupole Resonance*; Smith, J. A. S., Ed.; Heyden and Son Lts.: New York, 1974; Part VII.
- 101) Hwang, J. S.; Rao, K. V. S.; Freed, J. H. *J. Phys. Chem.* **1976**, *80*, 1490.
- 102) Fahie, B. J.; Mitchell, D. S.; Workentin, M. S.; Leigh, W. J. *J. Am. Chem. Soc.*, In Press.
- 103) *Nuclear Magnetic Resonance of Liquid Crystals*. NATO ASI Series, Ser. C, Vol. 141; Emsley, J. W., Ed.; D. Reidel Publishing Co.: Dordrecht, 1985.
- 104) Vold, R. L.; Vold, R. R. *Isr. J. Chem.* **1983**, *23*, 315.
- 105) Doane, J. W. *Isr. J. Chem.* **1983**, *23*, 323.
- 106) Samulski, E. T. *Isr. J. Chem.* **1983**, *23*, 329.
- 107) Dong, R. Y. *Isr. J. Chem.* **1983**, *23*, 370. (h) Dong, R. Y. *Bull. Magn. Res.* **1987**, *9*, 29.
- 108) Dong, R. Y. *Bull. Magn. Res.* **1987**, *9*, 29.

- 109) Samulski, E. T. *Polymer* 1985, 26, 177.
- 110) Veracini, C. A.; Longeri, M. in ref. 34a; p. 123.
- 111) Allinger, N. L.; Maul, J. J.; Hickey, M. J. *J. Org. Chem.* 1971, 36, 2747.
- 112) Emsley, J. W.; Lindon, J. C.; Street, J. M.; Hawkes, G. E. *J. Chem. Soc., Faraday Trans. 2* 1976, 72, 1365.
- 113) The long molecular axis of CAP and PAP is taken as the 1,4-axis as well.
- 114) Luz, Z.; Hewitt, R. C.; Meiboom, S. *J. Chem. Phys.* 1974, 61, 1758.
- 115) Vaz, M. J.; Yaniv, Z.; Dong, R. Y.; Doane, J. W. *J. Magn. Res.* 1985, 62, 461.
- 116) Dong, R. Y.; Schmiedel, H.; Vaz, N. A. P.; Yaniv, Z.; Neubert, M. E.; Doane, J. W. *Mol. Cryst. Liq. Cryst.* 1983, 98, 411.
- 117) Vaz, N. A.; Vaz, M. J.; Doane, J. W. *Phys. Rev. A* 1984, 30, 1008.
- 118) Hsi, S.; Zimmermann, H. Luz, Z. *J. Chem. Phys.* 1978, 69, 4126.
- 119) Rowell, J. C.; Phillips, W. D.; Melby, L. R.; Panar, M. *J. Chem. Phys.* 1965, 43, 3442.
- 120) Jeffrey, K. R.; Wasylishen, R. E. *Can. J. Phys* 1986, 64, 833.
- 121) *Aldrich Catalog Handbook of Fine Chemicals*; Aldrich Chemical Co., Inc.; Milwaukee, 1988.
- 122) Netto-Ferreira, J. C.; Leigh, W. J.; Scaiano, J. C. *J. Am. Chem. Soc.* 1985, 107, 2617.
- 123) Zasadov, Y. A.; Mitel'kova, E. I.; Milanova, S. N. *Zh. Obs. Khim.* 1957, 26, 2499; *Chem. Abstr.* 1957, 51, 4994d.

PHOTOCHEMISTRY OF CYCLOPROPENES

CHAPTER I

Introduction

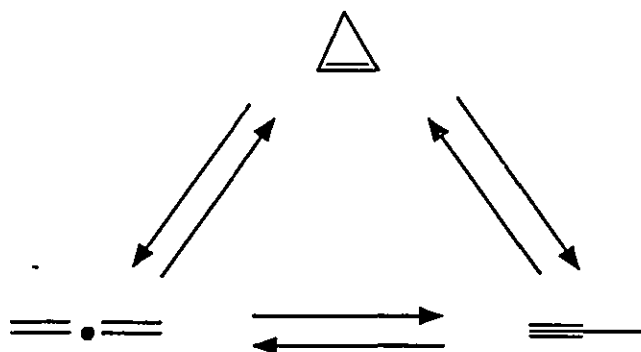
1.1 General Background

Cyclopropene is the smallest of the cyclic alkenes. Since normal unstrained sp^3 and sp^2 carbon-carbon bond angles are 109.5° and 120° ¹ respectively, it is not surprising that cyclopropene, with C-C bond angles of 51° and 64.5° ,² has a very high strain energy. The strain energy of cyclopropene has been calculated to be 222 kJ/mol,^{3,4} which is nearly 142 kJ/mol higher than cyclopropane.^{3,4} As a result, cyclopropene is thermally labile.

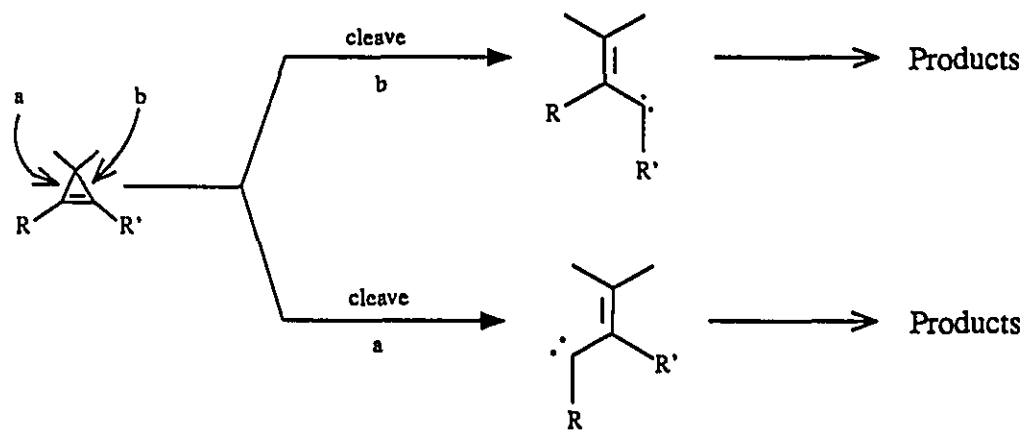
The cyclopropene double bond provides easily accessible excited states to initiate ring opening or fragmentation reactions. A major deactivation pathway for acyclic and larger ring cyclic alkenes is *cis-trans* isomerization.⁵ Although cyclopropene is in principle a substituted ethylene, the restricted rotation about the double bond caused by the ring, coupled with the release of ring strain on ring opening, allows for molecular transformations that are not observed in simple alkenes. Interestingly, not all reactions of cyclopropene derivatives result in ring opening, a somewhat unexpected result in view of the above.⁶

The past 25 years have witnessed an intense interest in the thermal,⁷ photochemical⁸⁻¹⁰ (both singlet and triplet excited-state reactions) and catalytic¹¹ (using transition metals) rearrangements of cyclopropene and/or cyclopropene derivatives. In addition, the unimolecular reactions of cyclopropene have been extensively investigated theoretically.¹²⁻¹⁸ Considering the overwhelming interest that this small molecule has generated, it is somewhat

surprising that a complete mechanistic understanding of the C_3H_4 surface, which involves interconversions of allene, cyclopropene and methylacetylene, is lacking (Scheme 1.1).



Scheme 1.1. Allowed thermal and photochemical interconversions on the C_3H_4 surface.



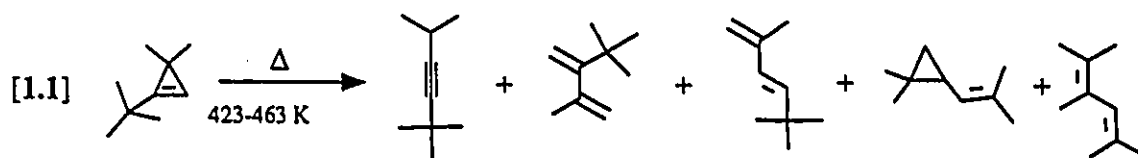
Scheme 1.2 Vinylcarbene formation from cyclopropenes.

It has been well established that ring-opening to yield vinylcarbenes, a result of cleavage of the $C_1 - C_2$ (bond "a") or $C_2 - C_3$ (bond "b"), is the major

decomposition pathway for cyclopropenes both thermally and photochemically (see Scheme 1.2).

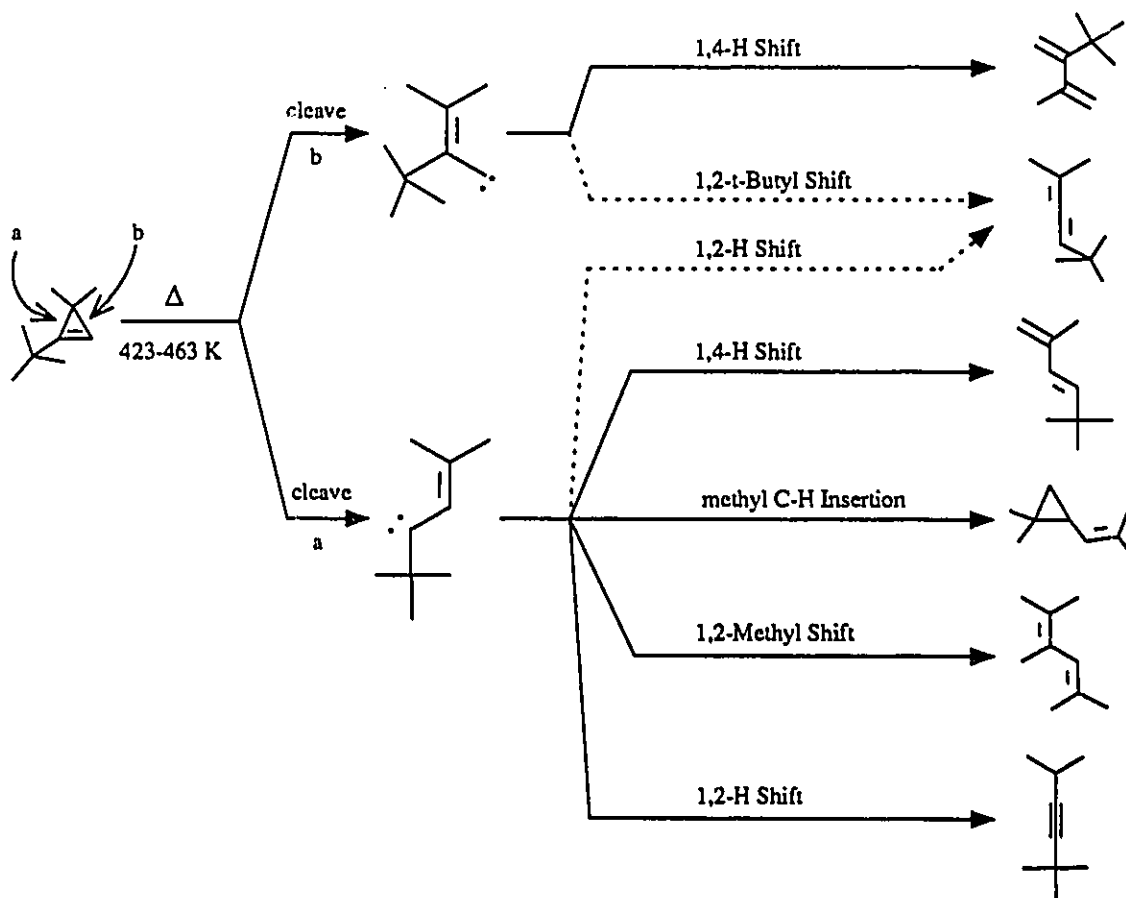
1.2 Ground-State Reactions

The thermal chemistry of cyclopropenes has been extensively investigated⁷ and is well understood. These studies clearly demonstrate that the major ground-state reaction pathway leading to products involves vinylcarbene intermediates. Convincing evidence for the involvement of vinylcarbene intermediates in the thermal chemistry of cyclopropenes was first presented with the thermolysis of 1-*t*-butyl-3,3-dimethylcyclopropene by Streeper and Gardner in 1973¹⁹ (Equation [1.1]).

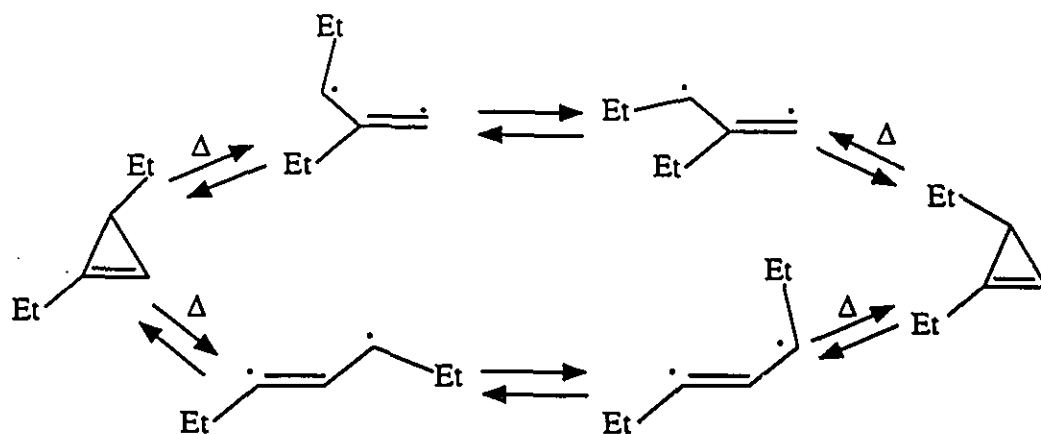


These products are all derivable from secondary reactions (H-migration or C-H/C-C bond insertion) of the vinylcarbenes to yield allenes, acetylenes or 1,3-dienes (see Scheme 1.3). A characteristic trend in the thermal chemistry of cyclopropenes is that product formation is dominated by the more stable of the two possible vinylcarbenes that can be formed on ring opening.

In an energy wasting step, the vinylcarbenes can revert back to starting material. This can be a significant reaction pathway as was demonstrated in the elegant work of Bergman and coworkers who studied the thermolysis of optically active 1,3-diethylcyclopropene²⁰ (Scheme 1.4). They found that k_{rac} (rate constant for racemization) was approximately 9 times larger than k_p (rate constant for product formation). This result is consistent with the fact that the most common method for

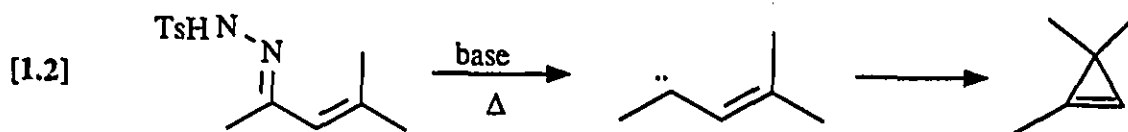


Scheme 1.3. Illustration of postulated vinylcarbene intermediates formed on thermolysis of 1-*t*-butyl-3,3-dimethylcyclopropene. Note the allene (as indicated by dashed lines) can be formed from both possible vinylcarbenes, however it was not observed as a product in the thermolysis.



Scheme 1.4. Thermal isomerization of an alkylcyclopropene.

preparing cyclopropenes is via the vinylcarbene intermediate (Equation [1.2]).



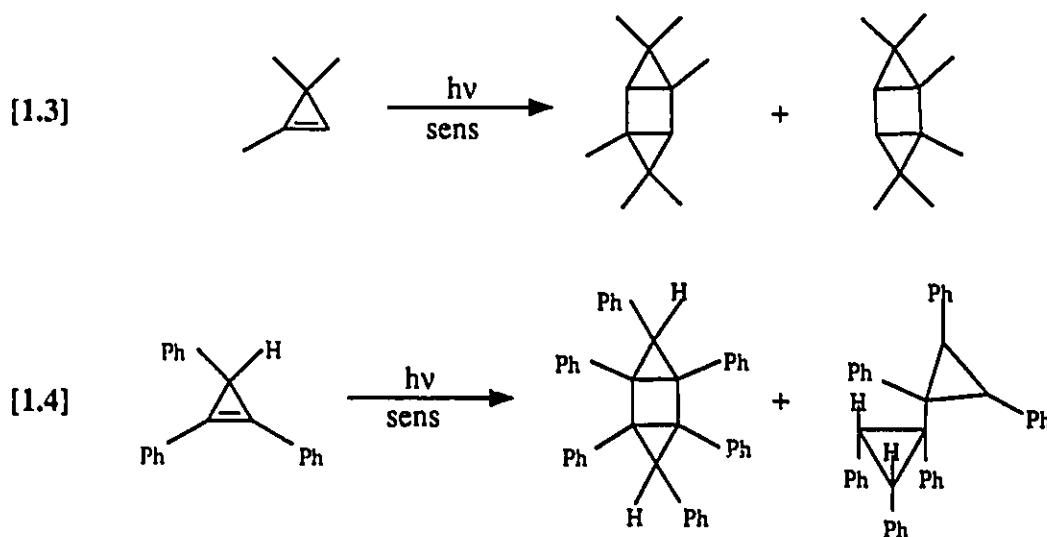
1.3 Excited-State Reactions

An excellent review of the photochemical reactions of cyclopropenes has been provided by Padwa.⁹ Singlet and triplet sensitized excitation of cyclopropenes leads to observable photochemistry which is very characteristic of the reacting state (singlet or triplet).

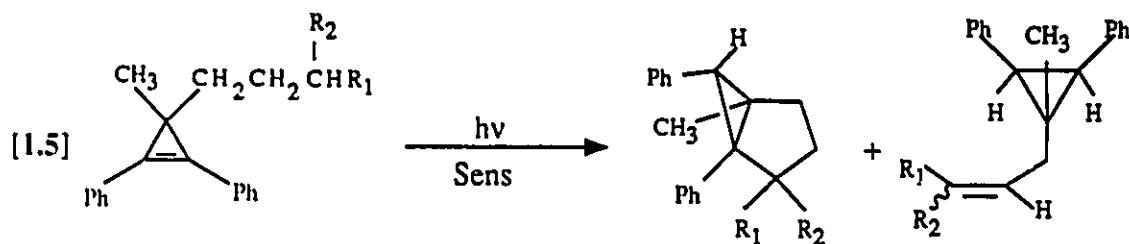
Triplet-State Reactions

Like other simple alkenes, singlet excited cyclopropenes do not intersystem cross efficiently, and as a result triplet states must be accessed by using triplet

sensitizers. In contrast to the (thermal) ground-state behaviour of cyclopropene derivatives which ring open to form vinylcarbenes, the excited triplet state of cyclopropenes either decays back to the ground-state, dimerizes,²¹⁻²⁵ or in certain cases undergoes intramolecular hydrogen transfer reactions.²⁶ Dimerization is the major reaction for both alkyl²² and phenyl²³⁻²⁵ substituted cyclopropenes as is shown in Equation [1.3] and [1.4].



Triplet states of tetrasubstituted cyclopropenes do not dimerize, a consequence of severe steric interactions. However, tetrasubstituted cyclopropenes which possess γ -hydrogens undergo intramolecular hydrogen transfer upon triplet excitation (Equation 1.5).²⁶



Theory has shown that there is a large activation barrier (54 kJ/mol) to ring opening on the triplet excited-state surface²¹ which accounts for the lack of ring opened products.

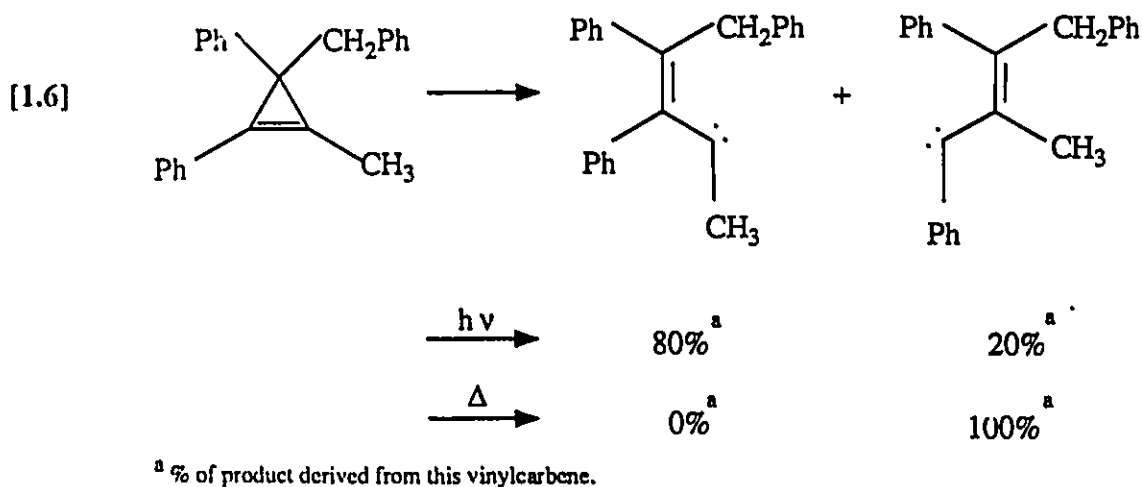
Singlet-State Reactions

The vast majority of direct photochemical (*i.e.* singlet excited-state) investigations of cyclopropenes have involved cyclopropenes containing substituents (*i.e.* phenyl or carbonyl)⁷⁻¹⁰ which extend (*via* conjugation) their UV absorption further into the near UV region (> 230 nm) of the ultraviolet spectrum. In fact, only two reported investigations of the direct solution photochemistry of simple alkylcyclopropenes,²⁷⁻²⁸ which typically absorb at wavelengths shorter than 220 nm, have been reported.

The experimental difficulties associated with doing solution photochemistry at <220 nm are many. The choice of inexpensive, readily available light sources is limited to the low pressure mercury lamp which emits chiefly at 253.7 nm with a minor emission line at 184.9 nm comprising only 8 - 10% of the total output, and the zinc resonance lamp which emits chiefly at 214 nm. Once a suitable light source is found, transmission of the photons to the molecule of interest is not a trivial problem as much of the light, if not all, can be absorbed by any one of the solvent (or impurities in the solvent), the reaction vessel, water or air. The use of scrupulously pure hydrocarbon solvents such as n-pentane and a reaction vessel made with Suprasil quartz is necessary if one is to successfully study the far-UV photochemistry of simple alkylcyclopropenes.

The reactivity of singlet excited phenylcyclopropenes parallels the observed ground-state reactivity of phenylcyclopropenes, with ring opening to give vinylcarbenes as the major reaction pathway. As is the case on the ground-state surface, the major reaction of the vinylcarbenes that are generated from singlet

excited phenylcyclopropene is reversion back to starting material.²¹ There is however, one important difference which distinguishes the thermal and direct photochemical generation of vinylcarbenes from phenylcyclopropenes; in general, product formation from singlet excited phenylcyclopropenes is dominated by the least stable vinylcarbene, whereas product formation in the thermolysis of phenylcyclopropenes is dominated by the more stable vinylcarbene^{9,29} (Equation [1.6]).



The observed difference between the ground- and excited-state chemistry of phenylcyclopropenes has been explained using the "funnel theory"³⁰ of excited- to ground-state conversions⁹ (Figure 1.1). Funnel theory predicts that excited-state molecules should preferentially deactivate from the excited-state surface to the *highest* energy ground-state surface. In Figure 1.1, the vinylcarbene derived from cleavage of bond "b" should be less stable (or higher in energy) than the vinylcarbene derived from cleavage of bond "a". Using funnel theory, ground-state reactions should then preferentially cleave bond "a", while excited-state reactions should preferentially cleave bond "b". This is in complete agreement with

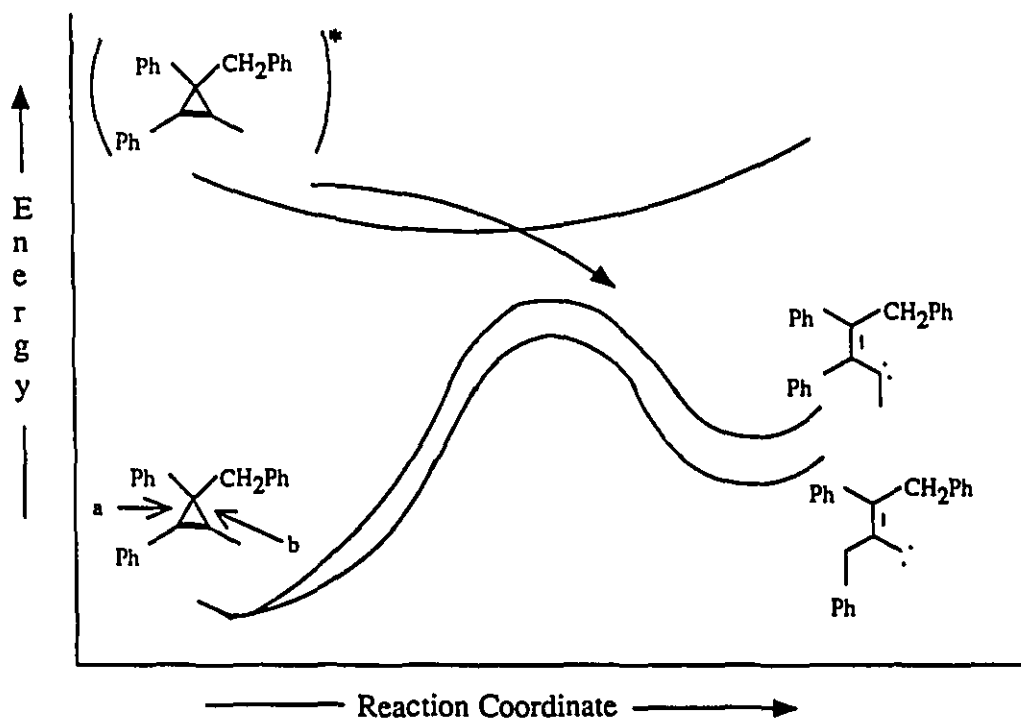
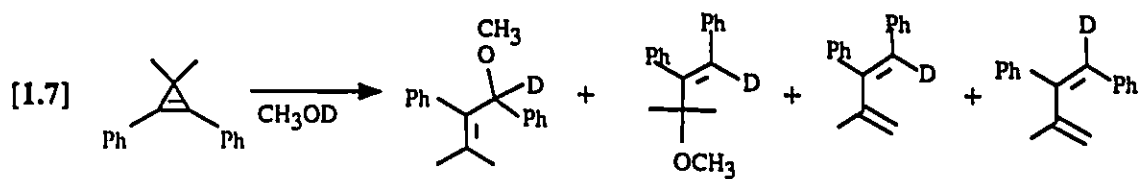


Figure 1.1. Funnel theory diagram showing preference for formation of least stable vinylcarbene on ring-opening of excited phenylated cyclopropenes.

experimental results (see Equation [1.6]).

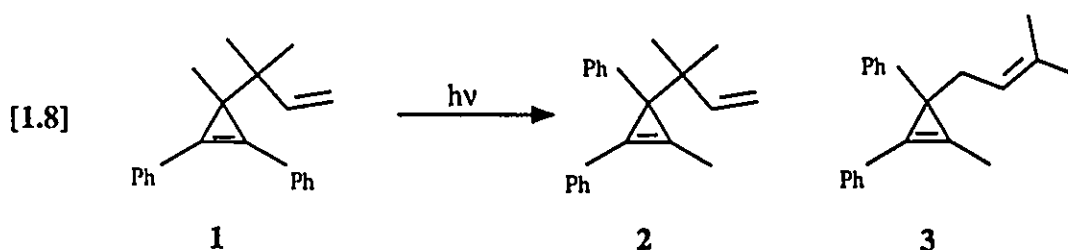
It should be noted that these experiments have relied on product distribution as a means of obtaining information regarding vinylcarbene formation. If however, both vinylcarbenes do not reclose to give starting material with the same rate, then the product distribution does not accurately reflect the relative yield of each vinylcarbene formed on ring opening. Should this be the case, then funnel theory may not adequately explain observed experimental results for these systems.

Evidence which supports the intermediacy of vinylcarbenes in the singlet photochemistry of phenylcyclopropenes was provided by Arnold and coworkers³¹ (Equation [1.7]). The vinylcarbene that was formed upon photolysis of 1,2-diphenyl-3,3-dimethylcyclopropene in deuterated methanol was efficiently trapped by the solvent.



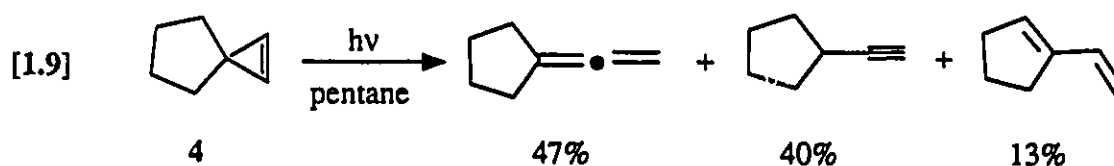
The wide variety of subsequent reactions that have been observed for vinylcarbenes, formed *via* photochemical ring-opening of phenylcyclopropenes, are too numerous to cover within the context of this document but have been reviewed in detail by Padwa.⁹

Although ring-opening to give vinylcarbenes is by far the major reaction pathway for singlet excited phenylcyclopropenes, cleavage of the substituent in the 3-position can be a significant, if not a major, decomposition pathway if the substituent can sufficiently stabilize the ensuing radical species⁶ (Equation [1.8]).

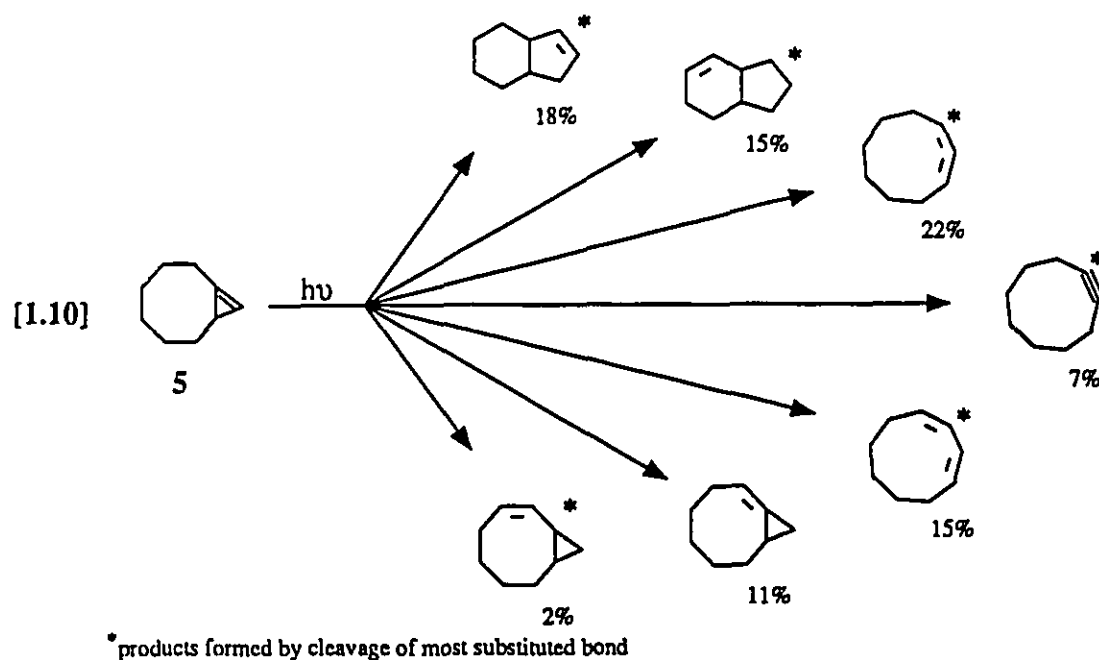


Thus, photolysis of **1** affords a 1:1 mixture of **2** and **3** as the exclusive photoproducts. Even after very careful examination of the crude photolysate of **1**, no evidence for products derived from ring opening could be found.

An understanding of the excited-state behaviour of simple alkylcyclopropenes (as a model for cyclopropene itself) is essential to the development of a unified mechanistic picture of the C_3H_4 surface. However, despite the number of investigations of the excited-state behaviour of cyclopropene derivatives, there have been only two reports concerning the photochemistry of simple alkylcyclopropenes.^{27,28} (Equation [1.9] and [1.10]).



As with phenylcyclopropenes, the products of the photolysis of **4** and **5** can be explained *via* the intermediacy of a vinylcarbene. Compound **5** is asymmetrically substituted and as a result can provide information on vinylcarbene selectivity in alkylcyclopropenes. In the case of **5**, more than 70 - 90% of the products are derived from the more substituted (more stable) vinylcarbene (*vide infra*). This contrasts what has generally been observed for phenylcyclopropenes (see above).



1.4 Theoretical

The C_3H_4 surface is comprised of three stable isomeric hydrocarbons: cyclopropene, allene and methylacetylene. The simplicity of this surface (only 3 heavy atoms and 4 light atoms), coupled with the very significant structural differences in the geometry of each isomer, makes it an ideal system for theoretical studies of molecular isomerization. Numerous theoretical studies have been carried out in an effort to understand the nature of the reactive states involved. Considering that the majority of theoretical studies that have been carried out have been confined to the parent C_3H_4 system, while experimental studies have mostly concentrated on phenylated systems, the agreement between the two approaches has been remarkable.

Theoretical investigations at both the semi-empirical^{13,32,33} and *ab initio*^{12,13,34} level have been reported for cyclopropene and verify the importance of

vinylcarbene formation to the decomposition of cyclopropenes. Calculations^{12,14,16} have consistently shown that the triplet is the lowest energy ground-state for vinylmethylene (vinylmethylene denotes the unsubstituted vinylcarbene obtainable from simple cyclopropene, while vinylcarbene refers to substituted vinylmethylenes in general). The electronic structure of the triplet has been denoted $^3A''$ or $^3\sigma\pi$ (to indicate the structure has three π electrons and an s electron in the σ plane, see Figure 1.2). It has also been shown that there are two low lying singlet states for vinylmethylene.^{12,14,16} The lowest energy singlet has been denoted $^1A'$ or σ^2 , and lies 33 - 67 kJ/mol above the triplet (Figure 1.2). Just slightly higher in energy is a second singlet state, $^1A''$ or $^1\sigma\pi$ (Figure 1.2).¹² All of the atoms (both carbons and

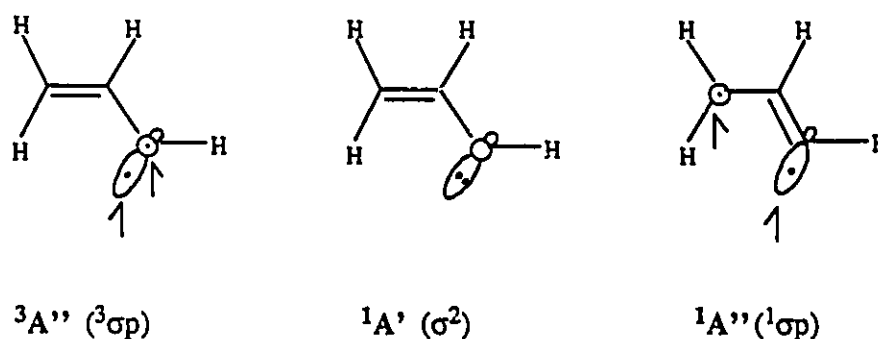


Figure 1.2. Electronic structures of ground and excited vinylmethylene.

hydrogens) for the three vinylmethylenes lie within a common plane.

Singlet ($^1A'$) vinylmethylene has been calculated to lie 153.2 kJ/mol above the ground-state of cyclopropene.¹² The final electronic state of vinylmethylene, $^1A'$ (σ^2), is independent of the reacting state from which it was formed (*i.e.* the ground- or excited-state of cyclopropene).⁷

Calculations¹² reveal an overall energy barrier of 178.3 kJ/mol for ring opening on the ground-state surface to give vinylmethylene. The calculated energy for the lowest excited singlet ($^1\pi,\pi^*$) and triplet ($^3\pi,\pi^*$) states of cyclopropene are

1080 kJ/mol and 523 kJ/mol respectively.¹⁶ Ring-opening from the singlet excited-state to give vinylmethylene intermediates is exothermic with no activation barrier,⁷ while the triplet excited-state is non-reactive to ring opening, a result of an energy barrier on the reaction coordinate for ring opening.

In addition, detailed theoretical mechanistic studies of the reactivity of cyclopropene on the ground- and excited-state surfaces, particularly those involving interconversions of cyclopropene to allene and acetylene, have been reported.¹⁶⁻¹⁸

Theoretical Investigations of Ground-State Reactions

Yoshimine and coworkers have reported the most complete description of ground-state reactions involving cyclopropene.^{17,18} Their findings reveal a barrier height (activation energy) for the cyclopropene → methylacetylene rearrangement of 174.5 kJ/mol which is in excellent agreement with the experimentally determined value.³⁵ In addition a barrier of 195.6 kJ/mol has been calculated for the cyclopropene → allene rearrangement (Figure 1.3), which is also in excellent agreement with the experimentally determined value.³⁵

Note that the cyclopropene → allene rearrangement involves vinylcarbene **6** which is an allylic-like structure, similar in structure to those in Figure 1.2, except that the terminal hydrogen is positioned above or below the plane of the three carbon atoms. *Cis* and *trans*-**6** were found to be isoenergetic. Since the terminal hydrogen can either be above or below the plane defined by the three carbon atoms for both the *cis* and *trans* isomer, this means there are 2 possible reacting geometries for vinylcarbene **6**, both of which are isoenergetic. However, the barriers to ring closure were found to differ considerably; 20.1 kJ/mol for *trans*-**6** and less than 5.0 kJ/mol for *cis*-**6**. This difference in the barriers to ring closure may ultimately play an important role in whether *trans*-**6** or *cis*-**6** is more important to allene formation from cyclopropene. No planar or bisected vinylcarbenes were found to be stable

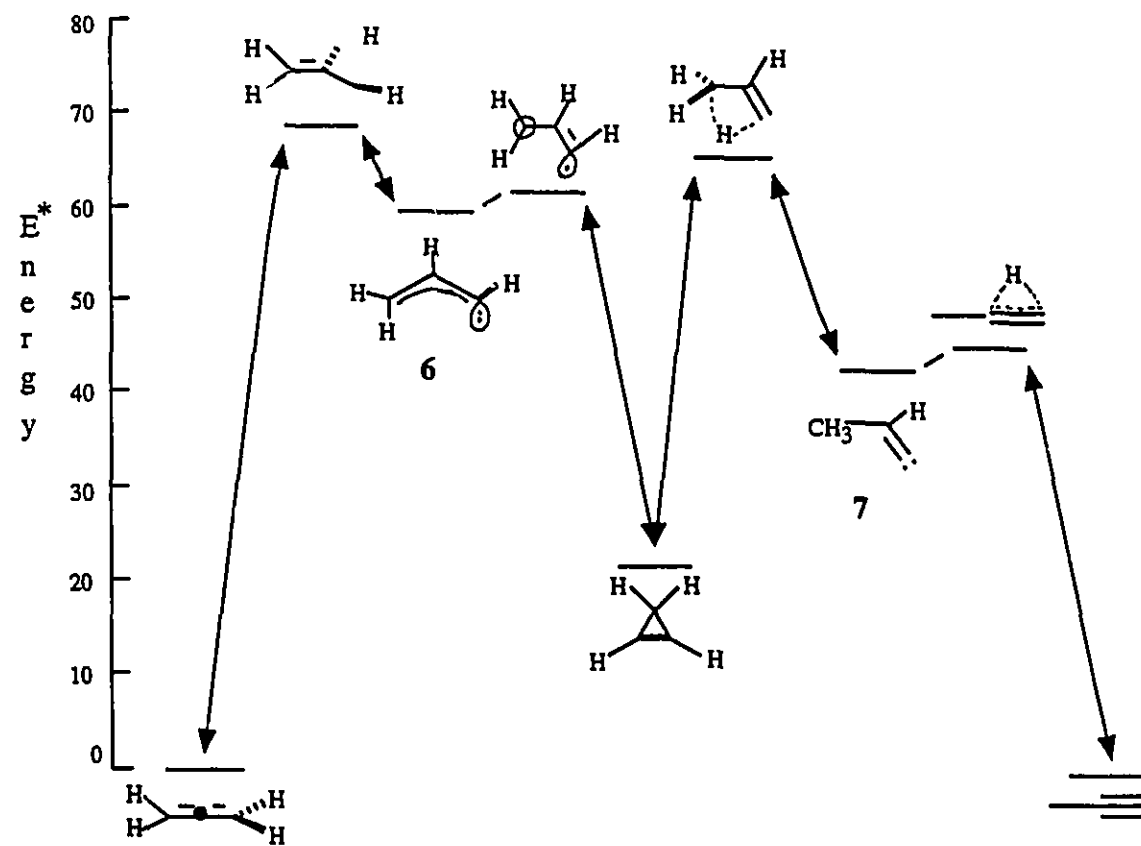


Figure 1.3. Lowest energy reaction path for conversion of cyclopropene to allene and acetylene. (Energy in kcal/mol)

intermediates on the cyclopropene to allene ground-state surface (see Figure 1.4 for structure of bisected vinylmethylene).

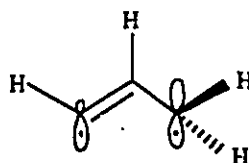
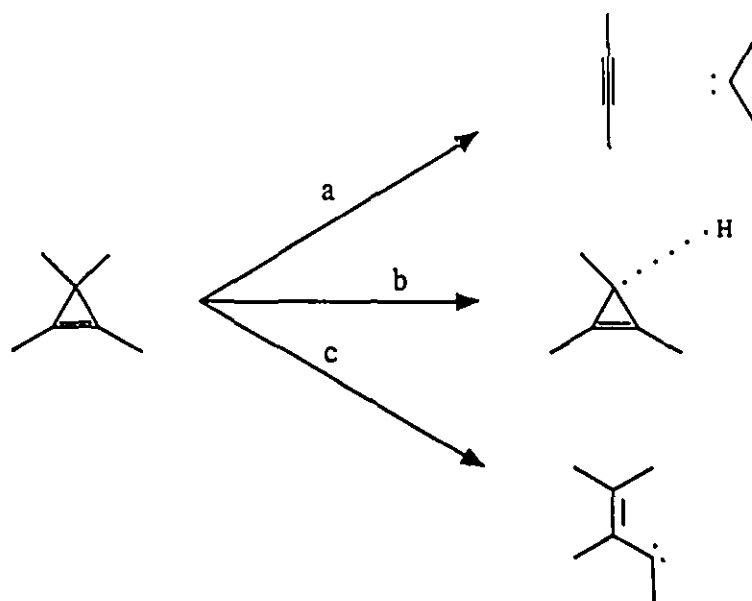


Figure 1.4. Structure of bisected vinylmethylene.

One interesting result is that the lowest energy pathway for the cyclopropene \rightarrow methylacetylene rearrangement involves the intermediacy of propenylidene **7** which is formed by stepwise or concerted [1,2]-hydrogen migration/ring-opening. All other pathways for the cyclopropene \rightarrow methylacetylene rearrangement investigated by Yoshimine and coworkers, including those involving the lowest singlet states of vinylmethylene, were found to be *ca.* 67 kJ/mol higher in energy. To date, there has been no experimental evidence which supports the intermediacy of **7** in the cyclopropene \rightarrow methylacetylene rearrangement. As a result, the importance of **7** in the cyclopropene \rightarrow methylacetylene rearrangement on the excited-state surface is unknown.

Theoretical Investigations of Excited-State Reactions

A complete theoretical investigation of the unimolecular reactions involving the excited-state of cyclopropene was carried out by Sevin and coworkers.¹⁶ The results of this study found that the low lying $^3\pi,\pi^*$ state is non reactive to ring opening, confirming previous semi-empirical investigations.¹⁴ Three possible reaction pathways for the thermal decomposition of cyclopropene were investigated (Scheme 1.5).



Scheme 1.5. Description of various theoretically investigated excited-state reaction pathways for cyclopropene.¹⁶

The major reaction pathway was found to be ring-opening (as is observed experimentally for both phenyl- and alkyl-substituted cyclopropenes) through an overall synchronous cleavage of the C_1-C_3 or C_2-C_3 bond and methylene rotation (path "c", Scheme 1.3). This results in formation of a high energy vinylcarbene which is able to reclose (photochemical racemization) or lead to further reactions. Side-chain cleavage was also found to be a potential reaction pathway for cyclopropene decomposition (path "b", Scheme 1.3) if the $^1\pi,\pi^*$ excited-state is lowered in energy by a substituent on the C_1 or C_2 carbon, and if a stabilizing group is attached to the C_3 position in order to stabilize the final diradical species. This finding is in excellent agreement with experimental results.⁶ Finally, it was suggested that direct formation of methylene and acetylene from cyclopropene may be able to compete with the above-mentioned types of ring cleavage when the lowest lying singlet state is high in energy (path "a", Scheme 1.3). To date there has been no experimental confirmation of the importance of this path in the excited-state

chemistry of cyclopropenes.

1.5 Objectives

The photochemistry of two alkyl-substituted cyclopropenes (**8** and **9**) was investigated with the intent of providing a much needed link between the photochemical behaviour of phenylated cyclopropenes and the parent unsubstituted system. As well, these compounds afford the possibility of testing the significance



of recent theoretical work by Arnaud-Danon¹⁶ and Yoshimine^{17,18} on the excited-state chemistry of cyclopropenes. In addition, the asymmetrical substitution of the cyclopropene double bond in these compounds allows for investigation of substituent effects on the mode of cyclopropene bond-cleavage in alkyl systems (*i.e.*, the competition between ring-opening to yield substituted *vs.* unsubstituted vinylcarbene intermediates), and provide a basis for comparison with the analogous behaviour of phenylated cyclopropenes. Finally, the thermal chemistry of both compounds has been previously reported^{19,36} and is available for comparison to their photochemical behaviour.

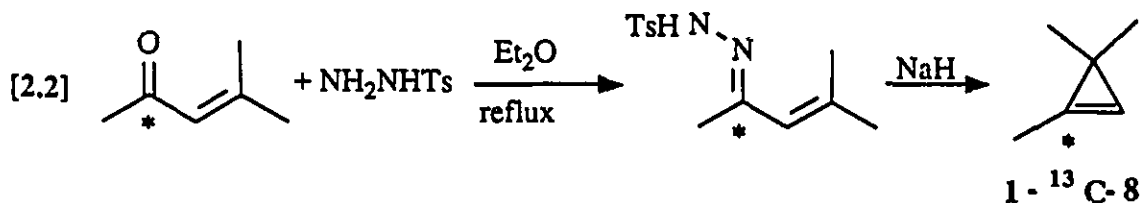
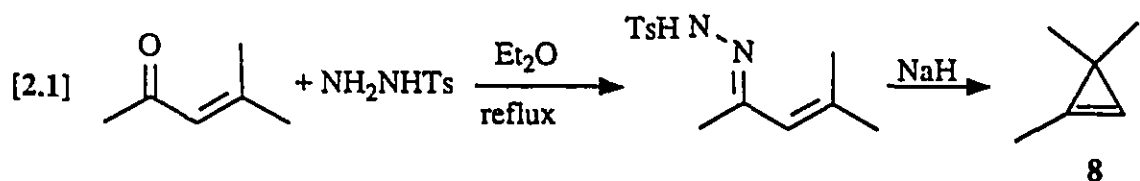
CHAPTER II

Results

2.1 Preparation of Compounds

1,3,3-Trimethylcyclopropene (8)

1,3,3-trimethylcyclopropene(8) and 1-¹³C-1,3,3-trimethylcyclopropene(1-¹³C-8) were synthesized by base-catalyzed decomposition of the tosylhydrazone of mesityl oxide and 2-¹³C-mesityl oxide respectively, with only minor changes to the previously reported experimental procedure³⁷ (Equation [2.1] and [2.2]).

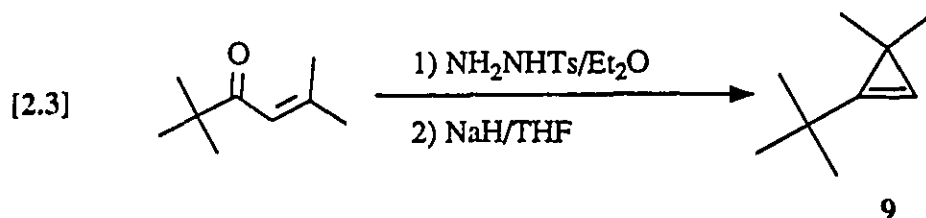


¹³C-labelled mesityl oxide was synthesized using a literature procedure³⁸ starting with 2-¹³C-sodium acetate.

1-*t*-Butyl-3,3-dimethylcyclopropene (9)

1-*t*-Butyl-3,3-dimethylcyclopropene (9) was prepared from the

tosylhydrazone of 2,2,5-trimethylhex-4-ene-3-one in a manner similar to that used for **8** (Equation [2.3]).



Compounds **8** and **9** were purified by semi-preparative gas chromatography (vpc). Compound **8** exhibited spectral characteristics similar to those reported for this compound.³⁷ The structure of **9** was assigned on the basis of its ¹H NMR (90 and 250 MHz), IR, mass and UV spectra.

2.2 Ultraviolet Absorption Spectra of **8** and **9**

Ultraviolet absorption spectra of **8** and **9** were recorded in deoxygenated pentane. All measurements were obtained using 0.1cm cells and are summarized in Table 2.1.

TABLE 2.1
Solution UV Absorption Data^{a,b,c}

Cyclopropene	λ_{\max} (nm)	E_{\max} (kcal/mol) ^d	ϵ_{\max}
3	194	147	4400
4	196	146	6800

^a ca 0.0004M solutions in pentane. ^b solutions deoxygenated with nitrogen
^c 0.1 cm path length. ^d energy at λ_{\max} .

2.3 Description of Light Sources

Irradiations were performed using one of the following light sources:

10W Low Pressure Mercury Lamp. The two principle emission lines from this lamp are at 184.9 nm and 253.7 nm, accounting for 10% and 78% of the total lamp output respectively.

Pulsed Excimer Laser. The output of the excimer laser consists of monochromatic light at 193nm (10ns pulse width, 20 - 100 mJ, 0.25 Hz repetition rate) when filled with an Ar/F₂/He mixture.

16W Zinc Resonance Lamp. The principle emission from this lamp is at 214 nm.

Cadmium Spectral Lamp. The principle emission from this lamp is at 228 nm.

For more detail on the light sources, see the Experimental section (Chapter IV).

2.4 Relative Product Yield Determinations

Relative product yields (RPY) for the products in the photolysis of **8** and **9** (Table 2.2 and 2.3) were determined in triplicate directly from the integration of the vpc traces (Equation [2.4]) at several light dosages between *ca.* 0.5% and 5% conversion.

$$[2.4] \quad \text{RPY} = \frac{\text{Integrated Area For Peak of Interest}}{\Sigma(\text{Integrated Area of all Product Peaks})}$$

No correction or calibration factor was employed in these determinations. This was not expected to result in large errors since all of the photoproducts in the photolysis of **8** (except methyl acetylene), and in the photolysis of **9**, are isomeric hydrocarbons.

(See the Experimental section (Chapter IV) for more details.)

2.5 Quantitative ¹³C Determinations

Although ¹H NMR is quite often used to obtain quantitative information on

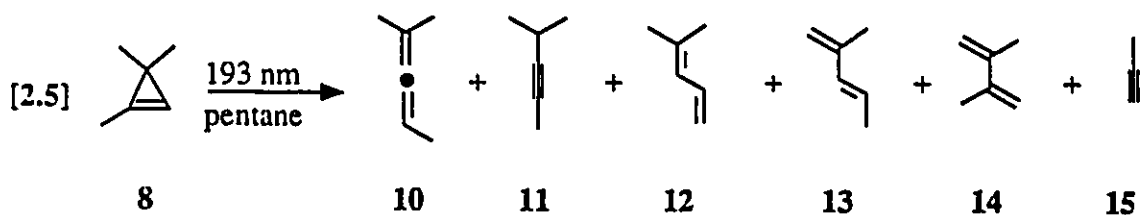
the relative number of protons in a molecule, integration of ^{13}C NMR spectra to obtain quantitative information regarding the relative number of ^{13}C 's contributing to a particular signal is less common.

Two different NMR experiments (Method I and II) were used to obtain the quantitative ^{13}C data presented in this chapter (see section 2.6). Method I involved recording the spectrum in the presence of $\text{Cr}(\text{acac})_3$ (to shorten the carbon spin-lattice relaxation time³⁹), using inverse gate decoupling (NOE is suppressed by decoupling the protons only during the acquisition of the signal),⁴⁰ and a delay of $>5T_1$ between pulse sequences to ensure complete relaxation. Method II involved a much more rigorous approach which is described in complete detail in Appendix A. Method II affords significantly lower errors as compared to Method I.

2.6 Direct Photolysis of 8 and 9 in Solution

Photolysis of 8 in Pentane

Photolysis of a deoxygenated, 0.041M pentane solution of 8 with the unfocussed pulses from the Ar/F₂ excimer laser (193nm; *ca.* 8ns; 20-80 mJ) produced 6 primary products as shown in Equation [2.5].

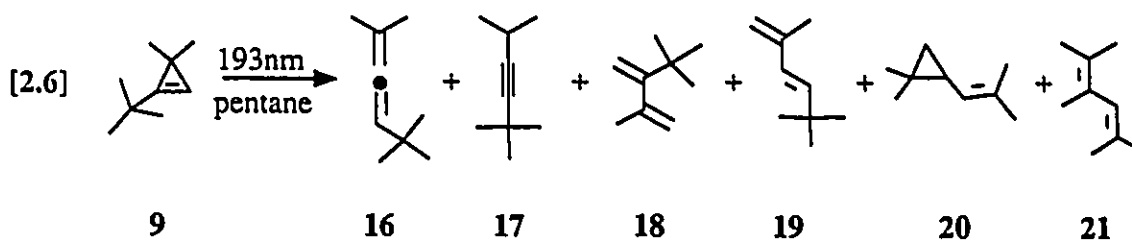


Each compound was identified by co-injection of the photolysate and an authentic sample on at least two vpc columns. *Cis*-13 could not be detected in the photolysis mixture up to *ca.* 10% conversion. Propyne was detected using a column specifically designed for $\text{C}_1 - \text{C}_4$ hydrocarbons and its presence was established by

co-injection of an authentic sample. However propene, while resolvable under these conditions was not detected. The yield of propyne could not be accurately determined, but it is estimated to be in the 0.3 - 2% range.

Photolysis of 9 in Pentane

Similarly, 193 nm photolysis of a deoxygenated 0.018M pentane solution of 9 produced the 8 primary products shown in Equation [2.6].



Products 20 and 21 were identified by co-injection of the photolysate with authentic samples on at least two vpc columns. Products 16 - 19 were isolated by semi-preparative vpc from larger scale runs carried to *ca.* 20% conversion, and identified by NMR spectroscopy (^1H and ^{13}C), and IR spectroscopy, GC/MS analysis, and comparison to literature data in the cases of 16 and 17. The photolysate also contained two additional minor products (each in < 8% yield) for which sufficient quantities to enable identification could not be obtained.

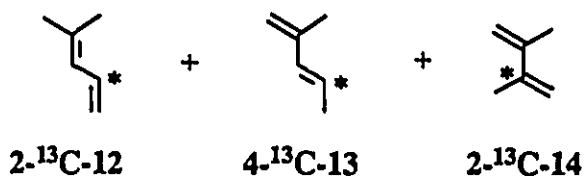
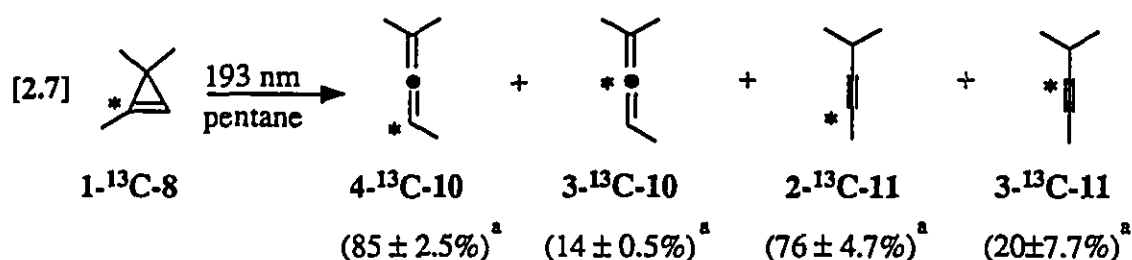
2,2-dimethyl-1-butyne could not be detected in the photolysis mixture. We estimate our limit of detection to be $\leq 0.5\%$.

Preparative Photolysis of 1- ^{13}C -8 in Pentane

A deoxygenated, 0.25M pentane solution of 1- ^{13}C -8 was photolyzed (193 nm) to approximately 25% conversion, and the labelled products 10 - 14 were

isolated by semi-preparative vpc. The formal product distribution from the photolysis of 1-¹³C-8 was indistinguishable from that obtained from 8.

The distribution of the ¹³C label for compounds 12 - 14 was determined (qualitatively) by integration of the ¹³C NMR spectrum and comparison to the spectrum of the corresponding unlabelled material recorded under identical conditions (see Experimental section). A detailed quantitative analysis



of compounds 12 - 14 is lacking, and as a result the error in these determinations may be as high as ± 25%. However, much more rigorous quantitative analyses were employed for 10 and 11. Method I was used for 10, while Method II was used

^aThe error limits for the allene were calculated from the average of three independent acquisitions (Method I). Method I however does not allow the assignment of meaningful error limits for each independent acquisition, and as a result non were. In doing this however we are ignoring a potentially large source of error in these determinations. Method II however, which was use for calculation of the errors for the alkyne, does allow assignment of errors to each independent calculation. This increases the calculated error obtained using Method II as compared to Method I, but Method II is a much more reliable approach. See Appendix-A for more details. Errors quoted are ±σ.

for 11. The distribution of the label in 10 that is quoted in Equation [2.7] is the average of three independent determinations using Method I, and the error quoted is a single standard deviation from the mean. Method II is described in complete detail in Appendix A.

Photolysis of 8 in Methanol and 1-Hexene

Deoxygenated 0.05M methanol and 1-hexene solutions of 8 were irradiated in an attempt to trap vinylidene 22 (R = H, Scheme 3.1) using the Zinc(214 nm) and Cadmium(228 nm) lamps respectively. Analysis of both photolysis solutions by vpc (column a) did not reveal the presence of any new compounds in addition to those identified when 8 was irradiated in pentane.

Photolysis of pentane solutions of both 8 and 9 with a low pressure mercury lamp (185 + 254 nm) resulted in product distributions similar to those observed with the laser. This was good evidence that the laser experiments were not subjected to conditions in which two-photon photochemistry could take place.

TABLE 2.2
Relative Product Yields For Photolysis^a and Thermolysis^b of 8^c

	10	11	12	13	14
hν(193 nm) ^d	31%	14%	37%	11%	7%
Δ(491-518°K)	—	—	—	71% ^e	21%

^aIn pentane, 23°C; methyl acetylene was identified in the photolysis but an accurate yield could not be determined. We estimate it to be in the 0.3 - 2% range. ^bsee reference 36. ^cRelative product yields for photolysis data is reproducible to ± 1%. ^dAr/F₂ excimer laser. ^eIt was not reported if 13 was *cis* or *trans* or a mixture of both.

TABLE 2.3
Relative Product Yields For Photolysis^a and Thermolysis^b of 9^c

	16	17	18	19	20	21
hν(193 nm) ^{d,e}	37%	8%	9%	15%	7%	9%
Δ(423-463°K)	—	22%	4%	13%	26%	35%

^aIn pentane, 23°C. ^bsee reference 19. ^cRelative product yields for photolysis data is reproducible to ± 1%. ^dAr/F₂ excimer laser. ^eTwo minor products (each in < 8% yield) were not identified.

TABLE 2.4
Contribution of Paths "a" - "d" (Scheme 3.1) to the Ground-^a and Excited-State Chemistry of 8

	"a"	"b"	"c"	"d"
Excited-State	84%	10%	<0.5%	6% ^b
Ground-State	71%	21%	—	— ^c

^asee reference 36. ^bsee Discussion for explanation of this value. ^c11 was not observed in the thermolysis of 8 which would indicate that path "d" cannot be contributing to the ground-state chemistry of 8, however there were minor products (each < 5%) that were not identified.

TABLE 2.5
Contribution of Paths "a" - "d" (Scheme 3.1) to the Ground-^a and Excited-State Chemistry of 9

	"a"	"b"	"c"	"d"
Excited-State	88%	9%	—	3% ^b
Ground-State	96%	4%	—	— ^c

^asee reference 19. ^bsee Discussion for explanation of this value. ^cThe thermal data available for 9 does not allow us to determine the importance of this pathway.

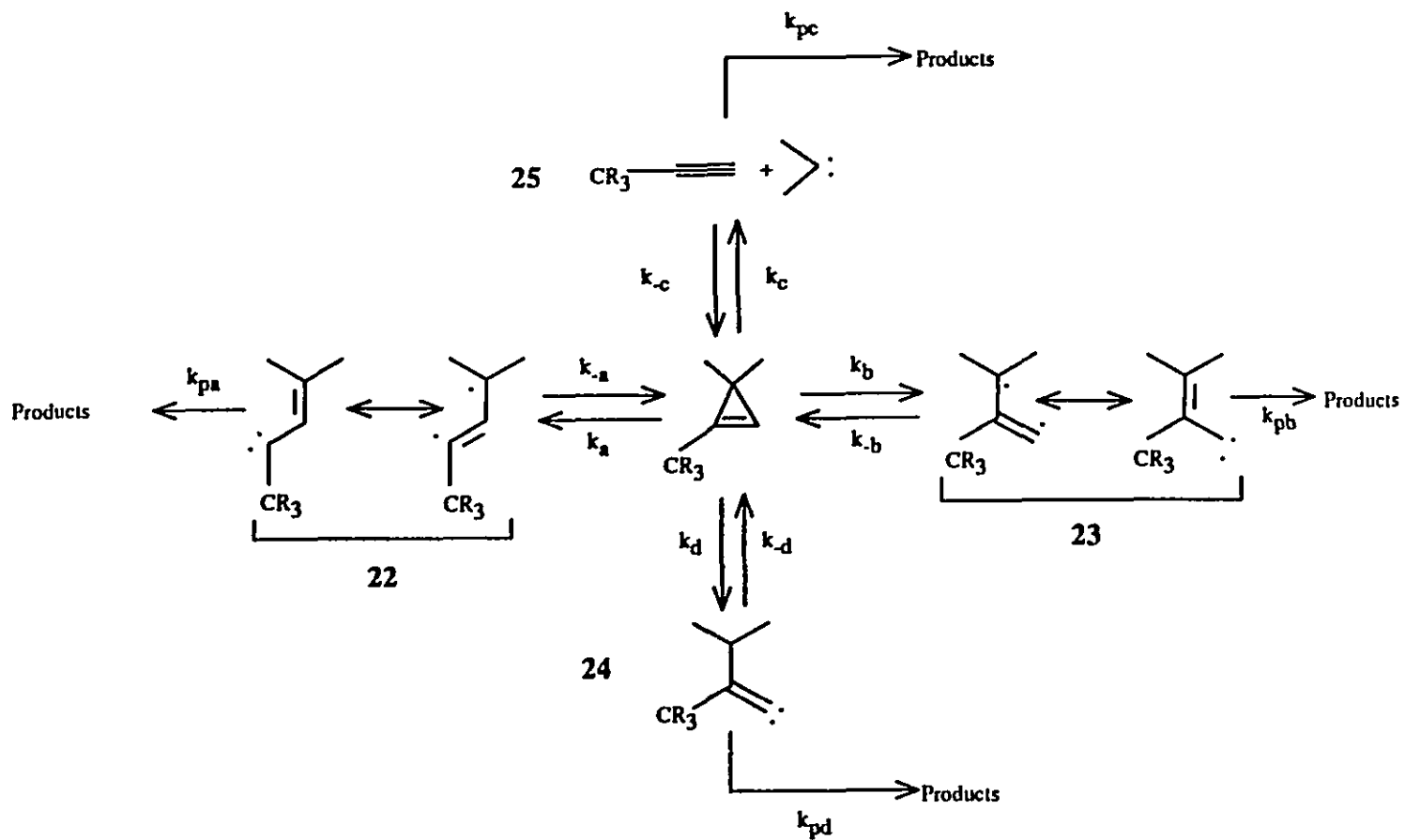
CHAPTER III

Discussion

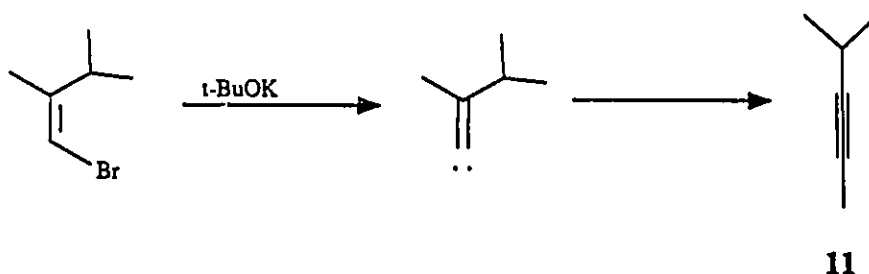
Four potential reaction pathways have been postulated to account for the excited-state reactivity of cyclopropene. These pathways have been applied to compounds **8** (R = H) and **9** (R = CH₃) in Scheme 3.1.

Previous studies^{7,8-10,41} have convincingly established that vinylcarbenes play an important role in the photochemistry of cyclopropenes (paths "a" and "b", Scheme 3.1). The reversibility of paths "a" and "b" has also been well established in photochemical studies of optically active cyclopropenes.²¹ The qualitatively observed low reaction efficiencies for **8** and **9** are in good agreement with this. Although paths "c" and "d" are reversible in principle, the efficiency of these processes has not been well characterized. The reversibility of path "c" is not expected to be so efficient as to preclude product formation. Carbene elimination from cyclopropanes^{9,42} is a very similar reaction, which yields products despite any solvent cage effects which may be reducing the efficiency of this reaction. Solvent cage effects for carbene elimination from cyclopropenes should be similar to those for cyclopropanes.

Precedence for the reversibility of path "d"⁴³ has been reported by Wolinsky and coworkers⁴⁴ who observed cyclopropene formation from independently generated alkylidenes. However, evidence which suggests a low efficiency of cyclopropene formation from alkylidene **24** (R = H) was also reported in the same study.⁴⁴ Compound **11** was the only hydrocarbon product that was formed in the reaction of 1-bromo-2,3-dimethyl-1-butene with potassium tert-butoxide in high



Scheme 3.1. Possible ring-opening reaction mechanisms for an alkyl-substituted cyclopropene.



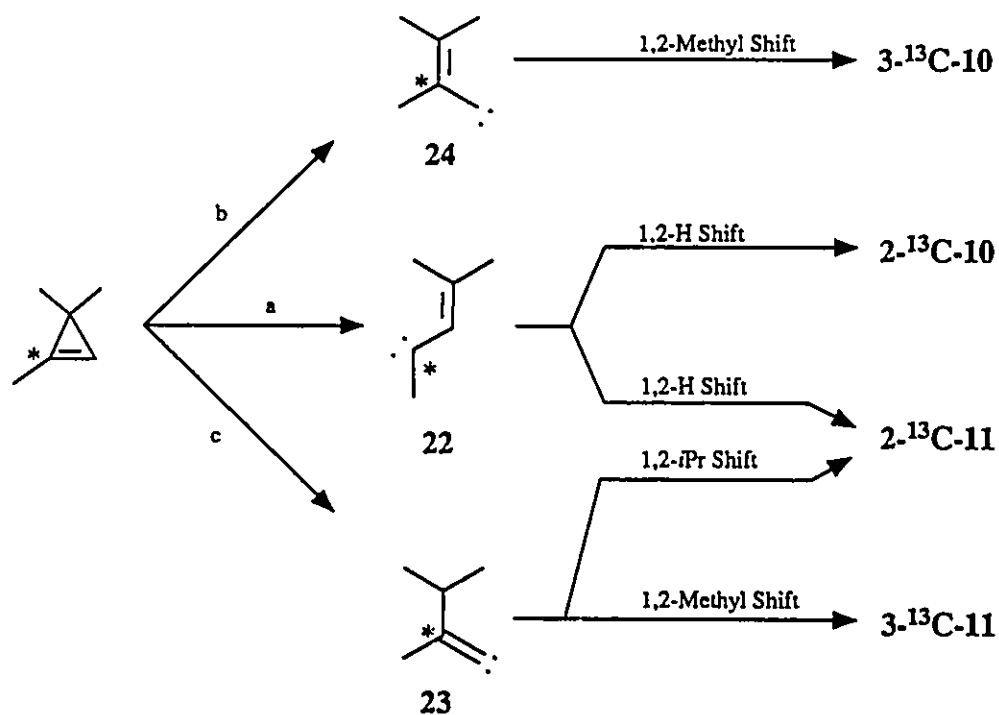
enough yield to allow for identification. No mention is made as to whether other minor products were formed in low yield. We suggest, by analogy, that the reversibility of alkylidene **24** ($R = \text{CH}_3$) to give **9** is also low in efficiency. The following discussion will concentrate on the role of each of the four pathways presented in Scheme 3.1 to the observed photochemistry of **8** and **9**.

1,3,3-Trimethylcyclopropene (8):

Careful vpc analysis (column c) of the photolysis mixture of **8**, immediately after the photolysis was complete, indicated that methyl acetylene was a primary photoproduct. Although the yield of methyl acetylene was low, its presence in the photolysis mixture is significant. This represents the first experimental evidence that simultaneous two-bond cleavage in alkylcyclopropenes (path "c", Scheme 3.1) can occur (albeit as a very minor reaction pathway) as predicted by Sevin.¹⁶

The mechanism or mechanisms that are important in the formation of **10** and **11** could only be determined using ^{13}C labelled starting material (Scheme 3.2). The traditional methods used for the quantitative analysis of the ^{13}C content in labelling studies proved to be unacceptable for analysis of **11**. The important mechanistic implications associated with the location of the ^{13}C label in **11** necessitated a more thorough NMR analysis which has been discussed in detail in Appendix A.

Although the mechanism by which alkynes are formed from excited-state

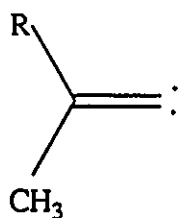


Scheme 3.2. Possible carbene intermediates in the formation of 10 and 11.

cyclopropenes has received a significant amount of interest in the literature,^{7-10,16,45} most of the discussion has dealt with the nature of the vinylcarbene, *i.e.* planar vinylmethylene diradical or bisected vinylmethylene diradical. Comparatively little attention has focussed on the possibility that vinylidene formation from cyclopropene (as postulated by Yoshimine and coworkers^{17,18}) may be a significant reaction pathway for alkyne formation.

Analysis (¹³C NMR) of **11** clearly indicated that the ¹³C label was partitioned between the 2 and the 3 positions. The presence of the ¹³C label in the 3 position (via methyl group migration in **24**, Scheme 3.2) provides the first experimental evidence that suggests that vinylidene **24** is an important intermediate in the photochemistry of alkylcyclopropenes. This pathway accounts for a minimum of 20% of alkyne **11** formation (Equation [2.7]).

To our knowledge, the relative migrating abilities of methyl vs. isopropyl in alkylidene carbenes is unknown. However, it seems reasonable to suggest that they may be approximately equal, or even in favor of isopropyl group migration⁴⁶ (a result of the electrophilic nature of alkylidene carbenes⁴⁷). Stang has investigated the electrophilic/nucleophilic nature of alkylidene carbenes in a study involving the relative reactivity (addition) of (CH₃)₂C=C: with a series of ring-substituted styrenes.⁴⁷ The results of this study clearly indicated that the moderate electrophilicity of alkylidene carbenes is comparable in magnitude to Cl₂C:.⁴⁷ Stang has also reported the following trends for alkyne formation from dialkyl vinylcarbenes:



R = t-butyl > Ethyl > isopropyl

It is difficult to interpret the significance of this data relative to our system since it is unclear whether this reflects increasing migratory aptitude of the substituent or an increasing tendency to promote migration of the methyl group. As well, Stang's work involves the ground state surface and it is not known whether alkyl group migration in **20** occurs on the ground state surface or on the excited state surface.

If the assumption is accurate that the rate of migration of the isopropyl group is equal to or larger than that of methyl migration in **24**(R = H), then at least another 20% (total equals 40%) of **11** is formed *via* vinylcarbene **24**(R = H, Scheme 3.2). Alkyne **11** accounts for 14% of the total product mixture in the photochemistry of **8** (Table 2.2). Since 40% of alkyne **11** is formed *via* alkylidene **24**(R = H), this constitutes 5 - 6% of the total product mixture (Table 2.4). Clearly this represents an important mechanistic pathway for alkyne formation in the photochemistry of **8**. This result indicates that vinylidene intermediates may play a vital role in alkyne formation in the photochemistry of all alkylcyclopropenes that are unsubstituted in the 2-position. Although alkylidene **24** accounts for 5 - 6% of the total product mixture, this does not represent a ratio of the unimolecular rate constants ($k_d/k_a + k_b + k_c + k_d$) for formation of the various intermediates, as the rate constants for the reverse reactions to give back starting material are not known.

Attempts to provide additional support (*via* trapping experiments with methanol and 1-hexene) for the intermediacy of **24**(R = H) in the formation of **11** were unsuccessful. There are several possible reasons why these experiments may have failed. Alkylidene **24**(R = H) would provide a trapped product in only 5 - 6% (relative to **8**) yield, assuming a trapping efficiency of 100%.⁴⁸ A trapping efficiency of less than 50% would make it extremely difficult to identify the trapped product. Similar attempts to trap vinylcarbenes from the photolysis of **5** have also failed.²⁸

A more traditional quantitative analysis (see Equation [2.7]) of the position of the ^{13}C label in **10** enabled us to determine that 85% of the allene was being formed by path "a", and only 15% was being formed by path "b". This is consistent with that expected based on the relative migrating abilities of methyl vs hydrogen in both saturated⁴⁹ and vinylcarbenes.⁷ Vinylcarbene **23**(R = H, Scheme 3.1) has two available pathways for product formation: a 1,4-hydrogen shift to form **11**, or a 1,2-methyl shift to form **10**. Since hydrogen migration is much more facile in vinylcarbenes relative to methyl migration,⁷ the yield of **10** relative to **14** from **23**(R = H) should be low. However, **10** can readily be formed by a 1,2-hydrogen shift from vinylcarbene **22**(R = H, Scheme 3.1) making this pathway more feasible. Since the ^{13}C analysis indicated that **10** was almost exclusively formed *via* **22**(R = H), no further effort was made to obtain more accurate ^{13}C values.

Intermediate **22**(R = H, Scheme 3.1) can account for formation of compounds **12** and **13** by evoking a 1,2 and a 1,4 hydrogen shift respectively. Our qualitative ^{13}C data (Equation [2.7]) is in agreement with this assignment, and it seems unlikely that any other intermediates are involved in their formation. No *cis*-**13** is formed in the photolysis of **8**. This would indicate that the initially formed "*trans diradical like*" resonance structure of **22** is strongly contributing to the *overall* electronic structure of **22**. This is consistent with recent theoretical studies.^{7,12} Similarly, intermediate **23**(R = H, Scheme 3.1) can account for formation of compound **14** by evoking a 1,4 hydrogen shift. Again, our qualitative ^{13}C data is in agreement with this.

1-t-Butyl-3,3-dimethylcyclopropene (9):

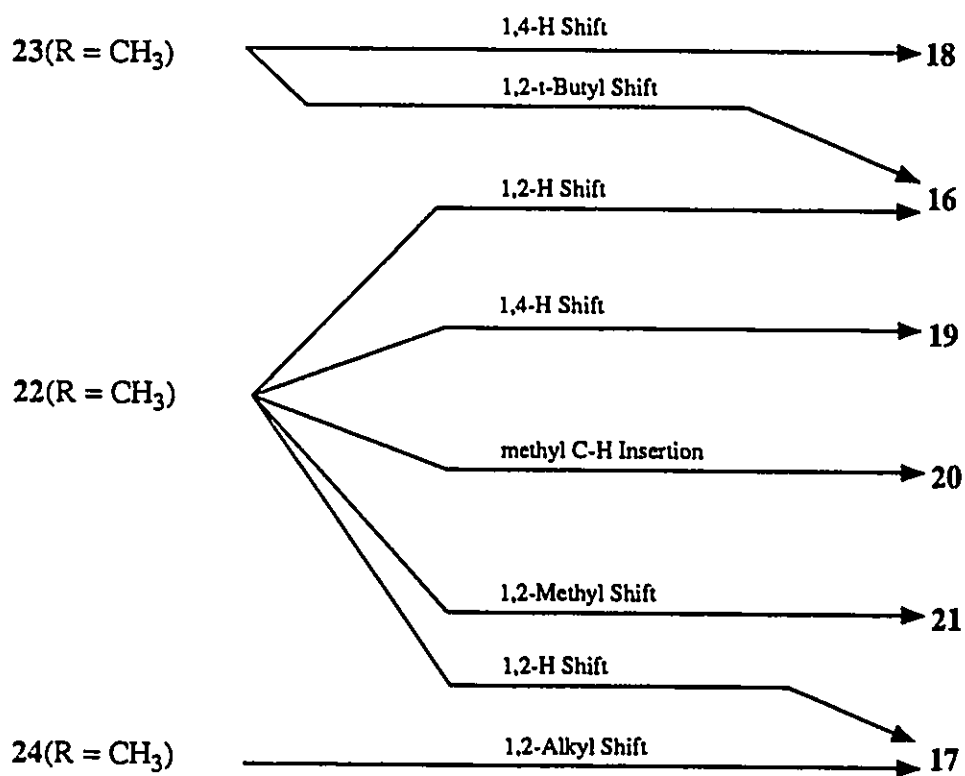
The photochemistry of **9** was not as extensively investigated as the

photochemistry of **8**. Analysis of the photolysis mixture indicated that there were 8 primary products. We were only able to identify 6 of the products, but the two unidentified products accounted for less than 15% of the product mixture.

Probable pathways for product formation are outlined below (based on the intermediates proposed in Scheme 3.1). The mechanistic arguments are similar to those presented for **8** (Scheme 3.3). Note that, as was the case for **8**, there are two possible intermediates in the photochemistry of **9** that can lead to the formation of allene **16** and alkyne **17**. Intermediate **22**(R = CH₃) should account for most of allene **16**. We see no obvious reason why intermediate **24**(R = CH₃) should not be as important in the photochemistry of **9** as it(R = H) was in the photochemistry of **8** (*i.e.*: accounting for approximately 40% of the alkyne formed).

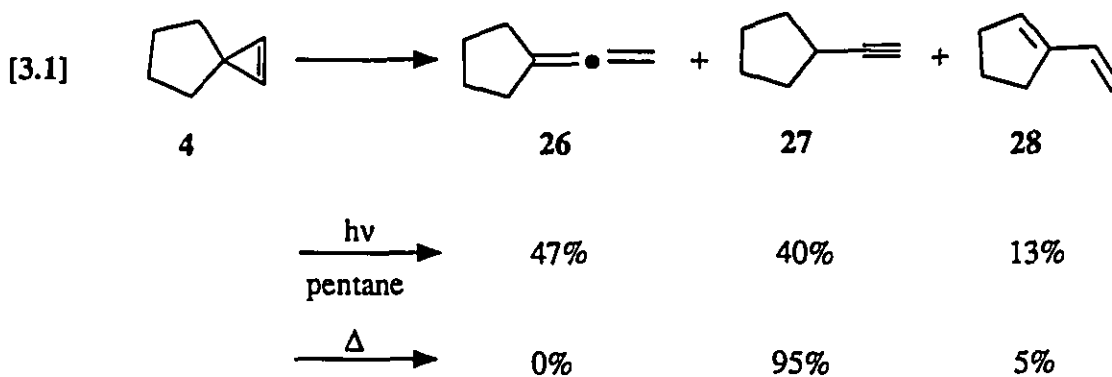
Two bond cleavage resulting in formation of *t*-butylacetylene was not observed. This is not overly surprising as this was a very minor pathway in the photochemistry of **8**.

Tables 2.2 and 2.3 summarize the product distributions for the thermolysis and photolysis of **8** and **9**. Although all of the products can be rationalized with a general reaction Scheme (see Scheme 3.1), there are clearly some important differences in the reactivity of intermediates **22** and **23** depending on whether they are generated thermally or photochemically. These differences are reflected in the product distribution that arises from a given vinylcarbene (**22** or **23**). For instance, allenes **10** and **16** are almost certainly formed *via* **22**, and represent major components of the photolysis mixture but are not observed thermally. It is uncertain what factors (*i.e.* the initial geometry, electronic structure or energy of the intermediates) are responsible for causing the reactivity of **22** and **23** to be dependent on the method by which they are formed (thermal or photochemical). Similar observations have been reported for related systems.²⁷ For example



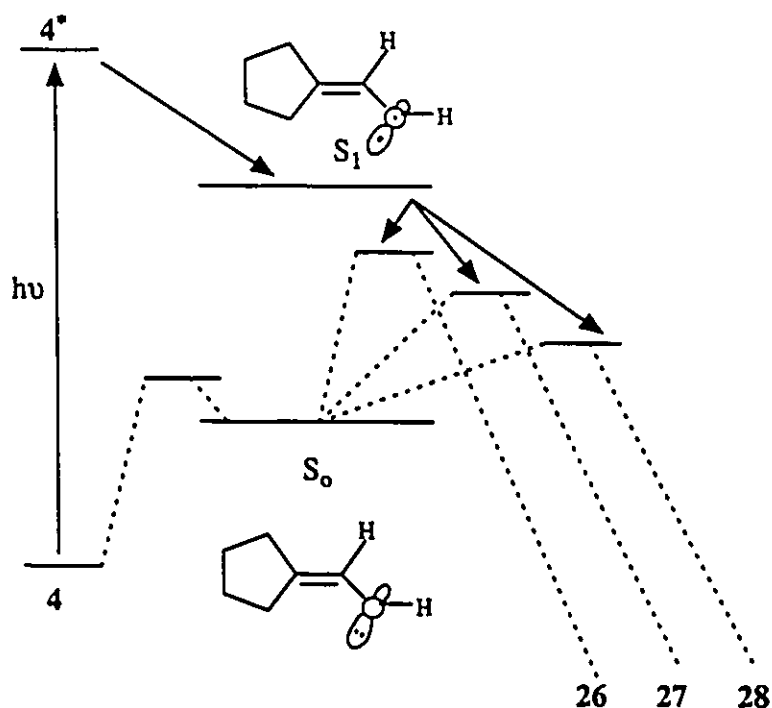
Scheme 3.3. Possible intermediates involved in the primary photoproducts of 9.

Steinmetz has reported on the photolysis and thermolysis of **4**. Since **4** is symmetrical, only one vinylcarbene is formed in both the thermolysis and photolysis. However, the product distribution obtained from the thermolysis and photolysis is significantly different (Equation [3.1], see also Equation [1.9])



Steinmetz suggested that the thermal chemistry was dominated by the ground-state (S_0) $^1A'$ vinylcarbene. However, photochemically he proposed that **4** ring-opened to initially form the excited-state (S_1) $^1A''$ vinylcarbene which subsequently decayed to a maximum on the ground-state surface, which corresponded to the transition state for the $^1A'$ vinylcarbene \rightarrow product rearrangement (see Scheme 3.4). It was also concluded that the transition state energy leading to **28** was the lowest of the three possible transition states since **28** was the major thermal product. Likewise, since **26** was not observed thermally it must have the highest transition state energy for product formation. Using funnel theory, it then seems reasonable that **26** would be the major photochemical product, owing to the close proximity of its ground-state surface to the excited-state surface.

It is worth noting that alkyne formation was a significant reaction pathway in the photochemistry of both **8** and **9** (Tables 2.2 and 2.3), similar to that observed for other alkylcyclopropenes.^{27,28} In contrast, alkyne formation is generally not



Scheme 3.4. Possible thermal and photochemical decomposition pathways for **4**.

observed for phenyl cyclopropenes.²⁷ A detailed theoretical investigation of the importance of alkylidene formation in the photochemistry of cyclopropenes is lacking.

Table 2.4 and 2.5 outline the contribution of the available reaction pathways (Scheme 3.1) to the ground- and excited-state chemistry of cyclopropenes **8** and **9**. Observe that path "a" dominates product formation in both the ground- and excited-state chemistry of **8** and **9**. This is in contrast to what has been observed for phenyl cyclopropenes^{9,10,50} where the more stable vinylcarbene ($\text{CR}_3 = \text{phenyl}$, path "a" Scheme 3.1) dominates product formation on the ground-state surface and the least stable vinylcarbene ($\text{CR}_3 = \text{phenyl}$, path "b" Scheme 3.1) dominates product formation on the excited-state surface. This observed difference between the ground- and excited-state chemistry of phenyl cyclopropenes has been explained

using the "funnel theory"³⁰ of excited- to ground-state conversions.⁹

There are potential theories that can account for the dominance of path "a" in both the ground- and excited-state chemistry of **8** and **9**. One possible explanation is that the energy difference between **22** and **23** may not be very large, a result of the inability of an alkyl group to significantly stabilize a vinylcarbene. If **22** and **23** are similar in energy, then their respective ground-state surfaces should approach the excited-state surface of the cyclopropene in a similar manner. In this situation, the excited cyclopropene should only have a small preference, if any, to which ground state surface it funnels to.³⁰ Alternatively, the observed product distribution for the photolysis of **8** and **9** may not accurately reflect the rate of formation of **22** or **23**. If k_{pb}/k_b is not equal to k_{pa}/k_a (Scheme 3.1) then the observed product distribution does not reflect which intermediate (**22** or **23**) is preferentially formed on ring opening. Johnson has shown that this is the case for at least one phenylcyclopropene⁴⁵ and one alkylcyclopropene.^{27,28}

Summary

Direct photolysis of two simple alkylcyclopropenes in pentane solution with far-UV light results in the formation of allenes, alkynes, and 1,3-dienes; a result of bond cleavage to yield vinylcarbene intermediates. Vinylcarbenes derived from cleavage of the most substituted bond (C_1 - C_3) account for more than 80% of the observed products in each case.

Quantitative ¹³C NMR analysis of alkyne **11** formed in the photolysis of ¹³C labelled **8** suggests the intermediacy of alkylidene carbenes, (**24**), in the photochemistry of alkylcyclopropenes. These results enable us to assign upper (40%) and lower (20%) limits for the contribution of **24** in the formation of **11** (*ca.* 3% of the overall photochemistry of **8**).

CHAPTER IV

Experimental

4.1 General

^1H NMR spectra were recorded on a Varian EM390 (90 MHz) or a Bruker AM500 (500 MHz) spectrometer. All ^1H spectra were obtained at 90 MHz in deuteriochloroform unless otherwise noted. ^{13}C NMR spectra were acquired at 62.5 or 125.6 MHz on a Bruker WM250 or AM500 respectively. All are reported in parts per million downfield (higher frequency) from tetramethylsilane. Mass spectra were recorded on a Finnigan 4000 mass spectrometer with a 4500 ion source. The mass spectrometer was interfaced with a Finnigan gas chromatograph, equipped with a 60m X 1.0 μ DB1-30W (Chromatographic Specialties, Inc.) fused silica capillary column. Ultraviolet absorption spectra were acquired in pentane solution using a Perkin-Elmer Lambda 9 spectrometer equipped with a Model 3600 Data Station. Infrared spectra were recorded on a Perkin-Elmer 283 spectrometer in carbon tetrachloride or chloroform solution, and are reported in wavenumbers calibrated using the 1601.9 cm^{-1} polystyrene absorption.

Analytical vpc separations were carried out using a Varian 3700 gas chromatograph (injector temp. = 80 $^{\circ}$ -120 $^{\circ}$ C) equipped with a flame ionization detector, a Hewlett-Packard HP-3393a integrator, and one of the following columns: (a) 1.0 μ m SPB-1 wide-bore capillary (30m X 0.75mm ID borosilicate; Supelco, Inc.); (b) 20% β,β -oxydipropionitrile (ODPN) on 80/100 Chromosorb PNAW (14ft X 1/8 in stainless steel; Supelco, Inc.); or (c) 23% SP-1700 on 80/100 Chromosorb PAW (15ft X 1/4in stainless steel; Supelco, Inc.). Relative detector responses were

not calibrated. This was not expected to introduce large errors as all of the photoproducts in the photolysis of **8** (except methylacetylene) and in the photolysis of **9** are isomeric hydrocarbons. Experimentally determined relative ratios (analyzed under identical experimental conditions as the photolystates) were calculated for solutions of **11**, **13** and **14** in various relative quantities at concentrations similar to those in the photolysis experiment. The ratios obtained from the standard solutions of **11**, **13** and **14** did not vary from the actual ratios (obtained from the photolysis experiments) by more than 5%.

Semi-preparative vpc separations employed a Hewlett-Packard 5750B gas chromatograph equipped with a thermal conductivity detector (detector temp. = 150 - 170°C) and one of the following stainless steel columns: (d) 3.8% UC W982 on 80/100 Supelcoport (24ft X 1/4in); or (e) 20% $\beta\beta$ Oxidipropionitrile (ODPN) on Chromosorb 100/120 PNAW (24ft X 1/4in; Supelco Inc.).

4.2 Commercial Solvents, Reagents and Chemicals Used

n-Pentane (Baker Photrex), and methanol (Caledon HPLC) were used as received from the supplier. Mesityl oxide (Aldrich Chemical Co.) was distilled once before use. 1-Hexene (Aldrich Chemical Co.) was distilled four times prior to use (optical density in 0.1 mm cells \rightarrow <210 nm, >5; 220 nm, 0.74; 230 nm, 0.53). *p*-Toluenesulfonylhydrazide, 3,3-dimethyl-2-butanone (pinacolone), *trans*-4-methyl-2,4-pentadiene(**13**), 2,3-dimethyl-1,3-butadiene(**14**), 3-methyl-2-butanone, 2,5-dimethyl-2,4-hexadiene, and sodium hydride were all used as received from the Aldrich Chemical Co. As well bromine (BDH), diiodomethane (Baker), 4-methyl-2,3-pentadiene (**10**, ICN Pharmaceuticals Inc.), 4-methyl-2-pentyne (**11**, Farchan), zinc-copper couple (Alfa). and 2-¹³C-sodium acetate (MSD Isotopes) were all used as received.

4.3 Photolysis of Cyclopropenes

Photochemical experiments employed the pulses (193 nm, ca. 10ns, 20-100 mJ, 0.25 Hz repetition rate for quantitative photolysis experiments, 2 Hz for preparative experiments) from a Lumonics TE-861M excimer laser filled with an argon/fluorine/helium mixture, a 10W Osram HNS 10W/U OZ low pressure mercury lamp (185 + 254nm), a 16W Philips 93106E zinc resonance lamp (214 nm, methanol carbene trapping experiments), or a George W Gates and Company Inc. 220V 1.5 amp Cadmium Spectral Lamp (228nm, 1-hexene carbene trapping experiments). The lamps were given a 20 minute warmup period before each experiment and cooled with a stream of dry nitrogen.

Quantitative photolyses were carried out at ambient temperature (ca. 23°C) in 10 X 25 mm cylindrical Suprasil quartz cells (Hellma). Preparative photolyses were carried out (using the laser) in rectangular cells constructed from 10 X 20 mm rectangular Suprasil tubing (Vitro Dynamics). In all cases, the sample was agitated during irradiation with a small magnetic stirrer, or with a mechanical shaker. Solutions were deoxygenated before irradiation by bubbling dry nitrogen or argon through the cooled (to ca. 0°C) solutions for 5 - 15 min. Photolysis solutions were monitored between 0.25 and 5% conversion, with aliquots being withdrawn at suitable time intervals (every 50 - 100 laser pulses) for vpc analysis on column b. Relative product yields were determined directly from the integration of the vpc traces.

4.4 Identification of Photoproducts

The products obtained from photolysis of **8** were identified by co-injecting photolysates carried to ca. 5% conversion with authentic samples on at least two vpc columns, and by comparison of the ^1H NMR spectra of isolated (from preparative runs carried to 20 - 25% conversion, by vpc with column e) samples with those of

the authentic samples.

The labelled products **10 - 14** were isolated by semi-preparative vpc (column e) from the preparative photolysis of **1-¹³C-8**. Identification was made on the basis of their NMR (¹H and ¹³C). The position of the ¹³C label in **10 - 14** is indicated with boldface text (see below) and was determined from their ¹³C spectra.

Products **16 - 19** from the preparative photolysis of **9** were isolated by semi-preparative vpc (column e) and were identified on the basis of their NMR (¹H and ¹³C), IR, and GC/MS spectra (see section 4.7).

Compounds **20** and **21** were prepared by an independent synthesis (see section 4.7) and were identified as primary photolysis products by co-injection with photolysates carried to ca. 5% conversion on at least two vpc columns. In addition, the GC/MS of **20** and **21** from the photolysis mixture and the synthesized compounds agreed favorably.

4.5 Carbene Trapping Experiments

Vinylidene trapping experiments were attempted in methanol (0.1M **8**, Zn lamp) and 1-hexene (0.1M **8**, Cd lamp). The pure methanol and methanol/**8** solution had U.V. absorbances of 0.15 and >5 respectively at 214 nm. Similarly, the 1-hexene and 1-hexene/**8** solution had UV absorbances of 0.7 and >5 respectively at 228 nm. All absorbances were recorded in 0.1 cm cells. In both cases aliquots were taken at appropriate times during the irradiation (ca. each 1% conversion of **8** to products) and analyzed by vpc (column a). In each case irradiation of **8** was carried to 6 - 10% conversion. At no time during the photolysis were any new products observed by vpc.

4.6 Preparation and Purification of Cyclopropenes

1,3,3-Trimethylcyclopropene (8). Freshly distilled mesityl oxide (5.4g, 0.055 mol)

was added dropwise to a slurry of 4-(methylsulfonyl)-phenylhydrazine (10.2 g, 0.055 mol) in anhydrous ether (350 ml) in a 500 ml two-necked, round bottom flask fitted with a reflux condenser. After addition was complete, the reaction was refluxed with stirring for 24 hours. The reaction flask was then cooled in an ice bath and the white solid was collected by suction filtration. The product was recrystallized from ether yielding a colourless precipitate (10 g, 0.038 mol). The melting point and spectral characteristics of the product were consistent with those previously reported³⁷ for mesityl oxide tosylhydrazones. A suspension of the tosylhydrazone (10 g, 0.038 mol) in o-dichlorobenzene (40 ml) was slowly added over a period of 1 hour to a solution of NaH (1.8 g, 0.076 mol) in refluxing o-dichlorobenzene (150 ml) in a two-necked, round bottom flask fitted with a small Vigreux column. The column head was connected to three traps (connected in series) which were immersed in a dry ice/acetone bath. The addition rate of the solution of the tosylhydrazone, and the heating of the reaction flask were controlled in such a manner so as not to allow any solvent vapours to be condensed in the cold traps. After the addition of the tosylhydrazone was complete, the reaction flask was heated for an additional 30 minutes. The contents of the cold traps were combined (3.1 g, ca. 50% II by vpc). After bulb to bulb distillation, compound 8 was purified (>99.9% purity) by semi-preparative vpc (column D, column temp = 30°C). The material exhibited spectral characteristics similar to those previously reported.⁵¹

1-¹³C-1,3,3-Trimethylcyclopropene (1-¹³C-8)(10 atom % ¹³C by ¹³C NMR). To a suspension of anhydrous sodium acetate (2.25 g, 0.027 mol), 2-¹³C-sodium acetate (0.25 g, 0.003 mol, 99.6 atom% ¹³C) lithium (1g, 0.15 mol), glass beads, in ether (500 ml), a solution of 1-bromo-2-methylpropene⁵² (12 g, 0.088 mol) was added dropwise over 20 minutes. A dry argon atmosphere was maintained over the reactants during the entire reaction. After 24 hours of vigorous stirring the reaction

mixture was cooled in an ice bath. Any remaining pieces of lithium were removed from the flask and the solution was treated with an excess of saturated aqueous ammonium chloride. The ether was separated and dried over sodium sulphate, and subsequently removed on a rotary evaporator while maintaining the round bottom flask at 0°C. This left a mixture of 2-¹³C-4-methyl-3-penten-2-one) and 2,5-dimethyl-2,4-hexadiene (2.6 g, ca. 75% mesityl oxide by ¹H NMR). No effort was made to purify or to quantify the percent of ¹³C in the mesityl oxide, although it was assumed to be approximately 10 atom % ¹³C.

1-¹³C-8 was prepared from 2-¹³C-4-methyl-3-penten-2-one in the same manner as unlabelled 8.

¹³C NMR δ = 131.00, 112.56, 27.0, 9.97.

1-*t*-Butyl-3,3-dimethylcyclopropene (9) A solution of glacial acetic acid (25 mls), water (100 mls) and pinacolone (40 g, 0.40 mol) was placed in a 500 ml three-neck, round bottom flask equipped with a reflux condenser, a thermometer (immersed in aqueous solution) and a 100 ml dropping funnel. Bromine (22 mls, 0.38 mol) was placed in the dropping funnel. The acetic acid solution was heated to 85°C and the bromine was added dropwise, without allowing too much unreacted bromine to build up in the reaction flask. After addition of the bromine was complete, the solution was allowed to react further until it was a pale yellow. It was then cooled to 10°C and quenched with sodium carbonate. The resulting oil was separated from the aqueous layer, and distilled under water aspirated vacuum at 73°C to give a colourless liquid (44 g, 0.25 mol). This liquid was identified as 1-bromo-3,3-dimethylpropan-2-one on the basis of its ¹H NMR spectrum.

¹H NMR δ = 1.25(s, 9H), 4.23(s, 2H).

A dioxane solution (100 mls, freshly distilled from sodium), of the above ketone (10 g, 0.056 mol, dried over 4A molecular sieves) and acetone (5 g, 0.086 mol, dried

over 4A molecular sieves) was placed in a 250 ml two-necked, round bottom flask fitted with a reflux condenser. A dry nitrogen atmosphere was maintained over the reactants. Using a powder funnel, freshly activated zinc⁵³ (5.6 g, 0.086 mol) was added slowly to the flask, while the solution was being stirred. After the addition of the zinc was completed, the contents of the flask were stirred for an additional hour, then cooled to room temperature. The solution was dried and most of the dioxane was removed under reduced pressure, leaving a pale yellow solution of dioxane and 2,2,5-trimethylhexan-5-ol-3-one which was identified on the basis of its ¹H NMR spectrum.

¹H NMR δ = 1.15(s, 9H), 1.25(s, 6H), 2.65(s, 2H).

Dehydration by the previously published method⁵² yielded 2,2,5-trimethylhex-4-enone (3.5 g, 0.025 mol, 45% overall). Identification was made on the basis of its ¹H NMR spectrum.

¹H NMR δ = 1.12(s, 9H), 1.90(s, 3H), 2.10(s, 3H), 6.33(s(broad), 1H).

A solution of the alkenone (5 g, 0.035 mol) and 4-(methylsulfonyl)-phenylhydrazine (6.5 g, 0.035 mol) in methanol (50 mls) was refluxed for 6 hours in a 100 ml round bottom flask. At the end of the 6 hours the reflux condenser was removed and the methanol was allowed to evaporate until the solution became turbid. Following this, the flask was removed from the heat source and enough methanol was added to the solution to remove the turbidity. The solution was allowed to cool slowly to room temperature and the hydrazone was allowed to precipitate giving 2,2,5-trimethylhex-4-ene-3-one tosylhydrazone (2.3 g, 0.0074 mol, 21%, mp = 108 - 113°C) which was identified on the basis of its ¹H NMR spectrum.

¹H NMR δ = 1.40(s, 3H), 1.80(s, 3H), 2.40(s, 3H), 5.30(s, 1H), 7.25(s, 1H), 7.35(s, 1H), 7.78(s, 1H) 7.88(s, 1H).

Thermal decomposition of the tosylhydrazone (4g, 0.013 mol) using a previously published method⁵⁴ gave a colourless liquid identified as

1-*r*-butyl-3,3-dimethylcyclopropene (0.24 g, 0.0019 mol) in greater than 99.9% purity after bulb to bulb and vpc purification (column b, column temperature = 85°C).

$^1\text{H NMR}(\text{CCl}_4) \delta = 1.08(\text{s}, 15\text{H}), 6.55(\text{s}, 1\text{H}).$

The singlet at 1.08 ppm can be resolved at high field (250 MHz) into a singlet and a doublet which integrate 9:6 respectively.

$^1\text{H NMR}(\text{C}_6\text{D}_6) \delta = 1.18(\text{s}, 9\text{H}), 1.37(\text{s}, 6\text{H}), 6.65(\text{s}, 1\text{H}).$

$^{13}\text{C NMR}(\text{C}_6\text{D}_6) \delta = 28.5, 29.0, 33.0, 109.2, 143.2.$

$\text{MS } m/e (I) 124(2), 109(82), 91(15), 81(64), 79(40), 77(22), 69(27), 68(18), 67(100), 65(20).$

$\text{IR}(\text{CDCl}_3, \text{cm}^{-1}) 3068, 2960, 2930-2875, 1755, 1700, 1588, 1519, 1396.$

4.7 Synthesis and/or Identification of Photoproducts

The ^{13}C NMR data listed below for compounds **10** - **14** were obtained from the ^{13}C spectra of the isolated products from the photolysis of **1- ^{13}C -8**. The chemical shifts that are highlighted with boldface text were found to be enriched with ^{13}C .

2-methyl-2,3-pentadiene (10).

$^{13}\text{C NMR } \delta = 203.43, \mathbf{93.86}, 83.57, 20.61, 14.90.$

4-Methyl-2-pentyne (11).

$^{13}\text{C NMR } \delta = \mathbf{84.97}, \mathbf{74.37}, 23.19, 20.34, 3.29.$

4-Methyl-1,3-pentadiene (12).

$^{13}\text{C NMR } \delta = 135.64, \mathbf{133.35}, 125.84, 113.98, 25.74, 18.09.$

trans-2-Methyl-1,3-pentadiene (13).

$^{13}\text{C NMR } \delta = 142.05, 134.07, \mathbf{125.27}, 113.69, 18.56, 17.98.$

2,3-Dimethyl-1,3-butadiene (14).

^{13}C NMR $\delta = 143.29, 112.71, 20.36.$

4-Methyl-1,3-pentadiene (12) and cis-2-methyl-1,3-pentadiene (cis-13) were

prepared by dehydrating 2-methyl-2,4-pentanediol by a previously described method.⁵³ Subsequent vpc purification (2 X col d, 3 X col e) gave both compounds in greater than 99% purity. *Cis-13* exhibited the following spectral data:

^1H NMR(CCl_4) $\delta = 1.64(\text{d}, 3\text{H}), 1.70(\text{s}, 3\text{H}), 4.67(\text{s}, 1\text{H}), 4.78(\text{s}, 1\text{H}),$
 $5.35(\text{m}, 1\text{H}), 5.67(\text{d}, 1\text{H}).$
 ^{13}C NMR(CCl_4) $\delta = 140.85, 131.83, 124.78, 115.05, 23.29, 14.43.$
 IR($\text{CCl}_4, \text{cm}^{-1}$) 3082, 2950, 1790, 1640, 1600, 1450, 1370, 885, 665,
 515.

The spectral data listed below were obtained from products isolated from the photolysis of 9.

2,2,5-Trimethyl-2,3-hexadiene (16).

^1H NMR $\delta = 1.10(\text{d}, 6\text{H}), 1.51(\text{s}, 9\text{H}), 2.50(\text{m}, 1\text{H})$

Note the ^1H NMR agrees favorably with previously reported data.⁵⁵

MS *m/e* (*I*) 124(38), 109(42), 81(22), 79(17), 77(18), 68(35), 67(100),
 65(15).

2,2,5-Trimethyl-3-hexyne (17).

^{13}C NMR $\delta = 87.64, 83.93, 31.17, 30.60, 23.27, 20.07.$

Note, the ^{13}C chemical shifts for the two sp hybridized carbons agree well with previously reported data.⁵⁶

MS *m/e* (*I*) 124(7), 109(39), 81(33), 79(19), 77(39), 67(100).
 ^1H NMR agreed favorably with previously reported data.⁵⁵

2-Methyl-(3-t-butyl)-1,3-butadiene (18).

^1H NMR(500 MHz) $\delta = 1.09(\text{s}, 9\text{H}), 1.87(\text{t}, 3\text{H}), 4.64(\text{m}, 1\text{H}),$
 $4.71(\text{d}, 1\text{H}), 4.84(\text{m}, 1\text{H}), 4.86(\text{d}, 1\text{H});$
 ^{13}C NMR $\delta = 25.8, 29.8, 35.4, 108.7, 113.0, 147.4, 161.4.$
 MS *m/e* (*I*) 124(12), 109(100), 81(29), 79(15), 68(36) 67(92).

trans-2,5,5-Trimethyl-1,3-hexadiene (19).

$^1\text{H NMR } \delta = 1.06(\text{s}, 9\text{H}), 1.80(\text{s}, 3\text{H}), 4.87(\text{s}, 2\text{H}), 5.6(\text{d}, 1\text{H}), 6.05(\text{d}, 1\text{H});$
 $^{13}\text{C NMR } \delta = 18.5, 29.5, 32.7, 114.2, 127.4, 141.3, 142.0$
 $\text{IR}(\text{CDCl}_3, \text{cm}^{-1}) 2962, 2865, 1607, 1551, 1437, 1364, 1263, 1202,$
 $1007;$
 $\text{MS } m/e (I) 124(28), 109(100), 81(29), 79(18), 67(77).$

1-(2,2-Dimethylcyclopropyl)-2-methylpropene (20) was synthesized using an adaptation of a previously described method⁵⁷ for the generation of cyclopropanes from alkenes. A mixture of 2,5-dimethyl-2,4-hexadiene (0.5 g, 0.0045 mol), diiodomethane (1.20 g, 0.0045 mol), zinc copper couple (0.47 g, 0.0065 mol), a crystal of iodine and anhydrous ether (50 ml) was refluxed with stirring while maintaining anhydrous conditions. After 12 hours the mixture was cooled and decanted into a separatory funnel and the solids were washed with ether (2 X 20 mls). The combined ether extracts were washed with 5% hydrochloric acid, 5% sodium bicarbonate solution, and water. The remaining ether was dried over magnesium sulfate and removed using a rotary evaporator, leaving a pale yellow oil (0.38 g, 0.0031 mol) 87%. A bulb to bulb distillation, followed by semi-preparative vpc (column D, column temp. = 80°C) gave **20** in greater than 99% purity.

$^1\text{H NMR } \delta = 0.13(\text{t}, 1\text{H}), 0.60(\text{dd}, 1\text{H}), 1.03(\text{d}, 6\text{H}), 1.18(\text{dd}, 1\text{H}),$
 $1.67(\text{s}, 6\text{H}), 4.83(\text{d}, 1\text{H}).$
 $^{13}\text{C NMR } \delta = 18.54, 18.91, 21.55, 22.95, 24.5, 26.41, 27.29, 125.44,$
 132.97

Note the ^1H and ^{13}C NMR was similar to previously reported data.⁵⁷

$\text{MS } m/e (I) 124(35), 109(79), 81(33), 79(16), 67(100).$

2,3,5-Trimethyl-2,4-hexadiene (21). Finely chopped lithium (0.23 g, 0.033 mol) was added to anhydrous ether (100 ml) in a two-necked round bottom flask that was fitted with a reflux condenser and a 50 ml dropping funnel. A slight positive pressure of dry argon was maintained inside the reaction flask. The lithium/ether

suspension was vigorously stirred using a magnetic stirring bar and ca 50 glass beads. An ether solution (30 ml) of 1-bromo-2-methyl propene⁵⁸ (4 g, 0.03 mol) was added dropwise to the reaction flask. A gentle reflux was maintained by controlling the addition rate of the bromide. After addition of the bromide was complete, the reaction was stirred for an additional 15 minutes. Following this an ether solution (30 ml) of 3-methyl-2-butanone (2.6 g, 0.03mol) was added dropwise to the reaction flask. The reaction was stirred at room temperature for an additional 1 hour after addition of the ketone was complete. The reaction mixture was quenched with 5% HCl, the ether layer was separated and the remaining aqueous layer was extracted with ether (3 X 25 mls). The combined ether extracts were washed with water and dried over sodium sulphate. The ether was then removed using a rotary evaporator leaving a pale yellow oil (3.5 g 0.025 mol, 82%) identified as 2,3,5-Trimethylhex-4-en-3-ol on the basis of its crude ¹H NMR.

¹H NMR δ =0.86(d, 6H), 1.22(s, 3H), 1.65(s,3H), 1.80(s, 3H), 5.15(s, 1H).

Product purity did not allow assignment of the proton on the isopropyl group. The alkenol (3.5 g, 0.025 mol) and p-toluenesulfonic acid (a single crystal) was dissolved in benzene (150 mls) in a 250 ml round bottom flask fitted with a Dean Stark trap and a reflux condenser. The solution was refluxed for 4 hours after which the reaction flask was cooled to room temperature and the benzene was removed on the rotary evaporator, leaving a yellow oil (2.7 g, 0.022 mol, 87%). A bulb-to-bulb distillation followed by semi-preparative vpc (column b, col temp = 80°C) gave a colourless liquid in greater than 99.5% purity which was identified as 2,3,5-trimethyl-2,4-hexadiene.

¹H NMR(500 MHz) δ = 1.50(s, 3H), 1.51(s,3H), 1.55(s, 3H), 1.64(s, 3H), 1.72(s, 3H), 5.59(s, 1H).

Note this agrees well with previously reported data.^{59,60}

^{13}C NMR (62.9 MHz) δ = 18.55, 19.10, 19.77, 21.55, 25.06, 126.29
127.33 131.61;
MS *m/e* (I) 124((53), 109(39), 81(39), 79(20), 77(17), 67(100).
IR(CDCl₃, cm⁻¹) 2985, 2910, 2856, 1448, 1372, 1194, 1123, 1058.

4.8 Quantitative ^{13}C Determinations

^{13}C NMR measurements were recorded in deuterated chloroform with Cr(acac)₃ (4 - 5 mg) added to shorten the spin lattice relaxation time. Carbon T₁ measurements were carried out on the Bruker AM500, and employed a π - τ - $\pi/2$ non-selective inversion-recovery pulse sequence, for both **10** and **11**. In the presence of the Cr(acac)₃ the carbon T₁ values were found to be between 0.6 and 1.1 seconds. A delay of 7 seconds was used between all pulse sequences employed.

For further details regarding Method I and Method II see Appendix A.

Appendix A⁶¹

The idea of obtaining quantitative information pertaining to the number of nuclei present in a molecule from an NMR spectrum (*integration*) has been a very attractive concept to the experimental chemist. In fact it is quite common to integrate routine proton NMR spectra in order to obtain numerical data regarding peak areas. For proton spectra it is reasonably easy to obtain accurate enough integrals (10 - 15% accuracy) to allow for the determination of the relative number of protons contributing to each peak. This works well (even with the large uncertainty in the peak areas) because in most situations the difference in the number of protons present in two peaks is $\geq 25\%$ (*i.e.* CH₃ vs CH₄). The concept of using quantitative NMR information for applications other than structure determination (*i.e.* product purity determinations or kinetic measurements) is quite tempting. However, the accuracy needed for such determinations usually ranges between 0.1 - 2%, and obtaining integral values with this type of accuracy is extremely difficult if not impossible.

During the acquisition of an NMR spectrum the nuclei of interest are disturbed from equilibrium. In order to obtain accurate quantitative information from an NMR experiment it is critical that *all* of the nuclei of interest be in thermal equilibrium prior to the onset of each experiment. This is imperative because the observed signals for those nuclei that are not at equilibrium prior to the experiment will be artificially depressed relative to those that are at equilibrium.

The rate at which nuclei return to their equilibrium population (*i.e.* return from their excited spin state to their ground spin state) is governed by their

spin-lattice relaxation time (T_1). The T_1 for a given nuclei is dependent on a number of variables. For example the most important mechanism in ^{13}C NMR is dipole-dipole relaxation.⁶¹ The mechanism for dipole-dipole relaxation is related to the number of hydrogens on or adjacent to the carbon of interest, as well as involving molecular motions pertaining to the motions of these individual C - H bonds. It is therefore not unusual for different carbons within the same molecule to have significantly different T_1 values. As a result it is important that the longest T_1 for the nuclei of interest in a molecule be known.

For ^{13}C spectra, the delay between pulses can become very long if one is attempting to obtain quantitative information. It is not uncommon for carbon relaxation times to be longer than 30 seconds and this would require waiting 2.5 (5 $\times T_1$) minutes between pulses.⁶³ To obtain quantitative information from a ^{13}C NMR spectrum requires significantly more pulses (*i.e.* $10^4 - 10^5$) than is required for a ^1H NMR spectrum for a similar signal-to-noise ratio. Thus for a *single determination*, under reasonably favorable conditions, the acquisition time for the spectrum would be between 7 - 70 hours (assuming that the T_1 values for the sample of interest are known). Obviously the time constraints for quantitative ^{13}C measurements can become prohibitive very quickly!

For ^{13}C spectra it is traditional to apply broadband decoupling in order to saturate the proton transitions. This may result in a nuclear Overhauser effect which can affect the intensity of a carbon signal by as much as a factor of 2. In order to avoid this problem it is important to decouple the protons only during the acquisition of the signal. This is called *inverse gated decoupling*.⁴⁰ Finally, it is important to ensure that the data is collected with enough digital resolution to enable an accurate description of the peak profile used for integration.

In summary, in order to obtain acceptable quantitative NMR data the

following conditions must be met.

- 1) A delay between pulses of $> 5 \times T_1$ must be employed. If the T_1 values for the sample are unknown, then they must be measured prior to collection of any NMR data that will be used for quantitative analysis.
- 2) For ^{13}C spectra, decoupling of the protons can only be done during the acquisition of the signal.
- 3) Appropriate digital resolution must be used so that the NMR peak is sufficiently well defined to obtain an accurate integral.

These conditions were met and successfully employed (Method I) for ^{13}C labelled **10** and these results are described in Chapter II. In order to obtain error limits regarding the *precision* of the determination, Method I was repeated 2 additional times and the results of each determination were averaged to give a mean and a standard deviation about the mean. While the error limits appear reasonable, they are in fact a gross underestimation of the true error involved in these measurements. This results from the fact that it is impossible to assign meaningful error limits to each individual peak integration, and as a result none were. This limitation of Method I could be overcome by reintegrating the same spectrum several times, but even this may not result in a truly unbiased indication of the error in the integrations.

The uncertainty in the error limits provided by Method I were unacceptable for determination of the ^{13}C distribution in **11**, a result of the important mechanistic conclusions that will be based on this data. This led to the development of Method II.⁶⁴

It is traditional to quantify an NMR signal by integrating the *area* under the peak and/or peaks of interest. This has been shown to be reasonably inaccurate because of problems associated with digital resolution as well as problems in determining the point (on or near the baseline) that you start and/or stop the integration. This is particularly a problem with ^{13}C NMR spectra as they cover such

a large frequency range it is often difficult to obtain sufficient digital resolution as well as an adequate signal-to-noise ratio. While it can be an arduous task to accurately determine the integral of an NMR signal, the peak height of an NMR signal can be easily and precisely determined. Method II makes use of the precision obtainable for measurements of peak heights of ^{13}C signals and correlates them directly with the number of carbons associated with the peak of interest.

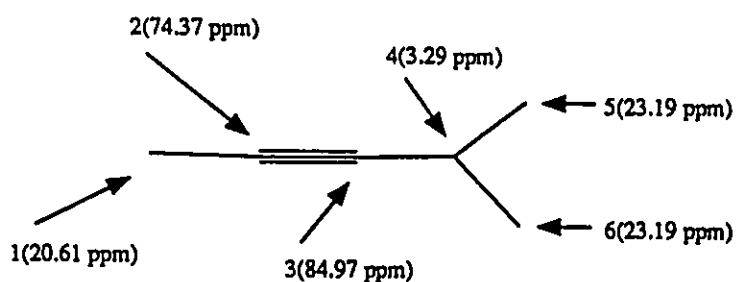
One of the problems associated with using peak height as a means of quantifying an NMR signal is that not all signals in an NMR spectrum will have identical linewidths. If the linewidths of the signals of interest vary considerably (as they may) then their peak heights will not accurately reflect the number of carbons which are responsible for that signal. We have circumvented this problem by acquiring the spectrum with good resolution (16 K) followed by zero filling (64 K data points) before processing. During the processing of the data, we artificially increased the linewidth of each signal to (40 Hz) so as to make any subtle difference in the natural linewidth of each signal insignificant. As a result, we feel that under these conditions the peak height is an accurate measure of the number of carbons which are responsible for the signal of interest.

In addition to eliminating differences caused by variation in the linewidth of the NMR signals, it is also extremely critical that any curvature or irregularities in the baseline of the NMR spectrum be removed before quantification of the data is attempted. We performed baseline correction on all of our spectra in order to ensure that the differences in peak height which we observed were not an artifact of a non zero baseline.

Rather than accumulate a single spectrum of 10^4 pulses, we opted to record 10 spectra, each of 10^3 pulses. This requires the same amount of spectrometer time but has the added advantage of allowing for a determination of the precision of this

method as the peak height for the signals of interest were determined for each of the 10 spectra. With 10 determinations the standard deviation obtained for the precision of the peak height should be reliable and was less than 4% for all determinations.

We were better able to determine the accuracy of our measurements by incorporating an external standard in the NMR tube while recording the ^{13}C spectra. By accurately measuring the amount of external standard that was placed in the NMR tube, we were able to correlate the ^{13}C data obtained for labelled **11** with that obtained for the external standard. In addition, 6 different concentrations of the external standard were used allowing for a check of the linearity of the method (*i.e.* ensuring that the values obtained were not dependent on external standard concentration). This was achieved by plotting the ratio of the mean values obtained for the peak height of the signal of interest (*i.e.* the signal at 84.97 ppm) and the peak height of the external standard *versus* the inverse of the concentration of the external standard used for each spectrum. Under ideal conditions the resulting plot



11

should be a straight line which passes through the origin. The data obtained for labelled **11** is listed in Table A.1 and the plot of this data is shown in Figure A.1. The lines in Figure A.1 are clearly linear. The slope of each line is directly related to the number of carbons responsible for the signal (carbon #) at the chemical shift

TABLE A.1
Relative Peak Height Data^a

84.97 ^b (3) ^g	74.37 ^b (2) ^g	57.5 ^c	23.19 ^b (5,6) ^g	20.34 ^b (1) ^g	3.29 ^b (4) ^g	[ES] ^{d,e}	1/[ES] ^f
0.937	2.614	1	0.804	0.459	0.376	1.2950	0.772
2.760	7.580	1	2.400	1.327	1.127	0.4641	2.154
0.365	1.081	1	0.316	0.160	0.137	3.1000	0.322
0.625	1.805	1	0.526	0.267	0.230	1.9677	0.508
1.306	3.930	1	1.151	0.586	0.464	0.9342	1.070
2.013	5.561	1	1.740	0.939	0.775	0.6023	1.660

^aThe relative peak height data listed in this table represents the ratio of the mean value of the peak height for a given signal (chemical shift) and the mean value of the peak height of the external standard signal. ^bChemical shift values (ppm) corresponding to signals observed for labeled II. ^cChemical shift (ppm) of signal used from external standard. ^dThe concentration of the external standard (ES) used for each determination. ^eThe external standard used was ethanol. ^fThe reciprocal of the concentration of the external standard used for each determination. ^gCarbon number for chemical shift indicated.

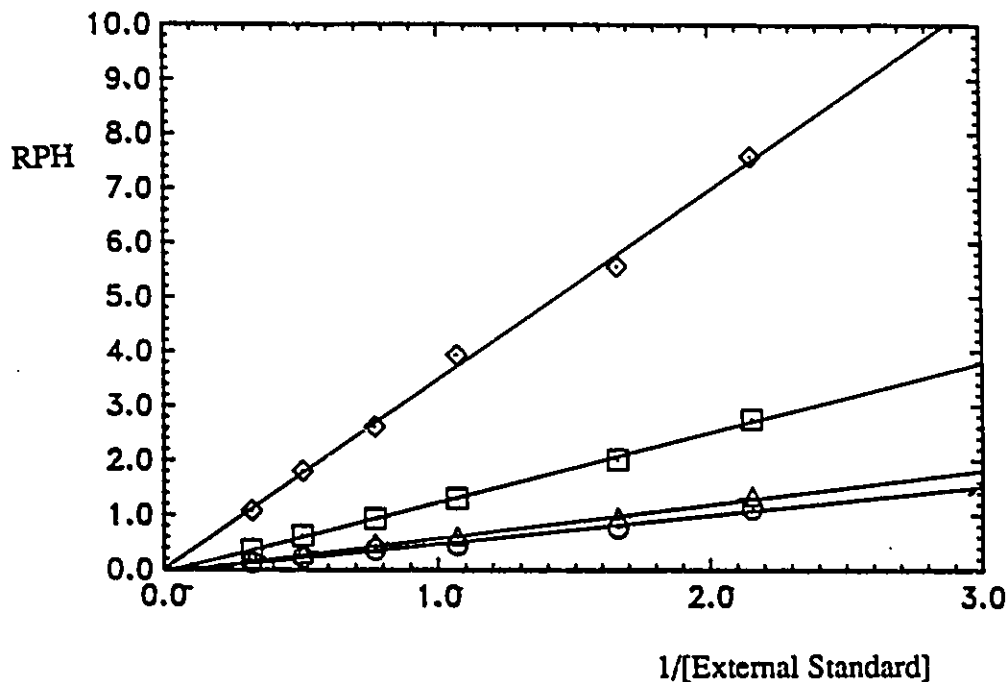


Figure A.1. Relative Peak Height (RPH) versus reciprocal of the concentration of the External Standard (Ethanol) for carbon 1(20.34 ppm, Δ), 2(74.37 ppm, \odot), 3(84.97 ppm, \square), and 4(3.29 ppm, \diamond) in labelled 11.

Carbon #	Slope ^a	Intercept
1	0.622 ± 0.024	-0.049
2	3.477 ± 0.111	0.002
3	1.282 ± 0.031	-0.052
4	0.523 ± 0.028	-0.048
5,6 ^{b,c}	0.893 ± 0.022	0.049

^aError limits are ± 1 standard deviation

^bData for these carbons is not shown on the above graph.

^cSince both carbons 5 and 6 have the same chemical shift, the slope represents 2 X natural abundance ^{13}C .

indicated. The standard deviation of the slope is representative of the error contained in the quantification of the ^{13}C .

In order to determine what carbon positions were enriched with ^{13}C we had to assume that one of the five observed signals found for labelled **11** was not ^{13}C enriched. Since the mechanisms that we were investigating would only cause the ^{13}C label to be found at position 2 or 3, it was reasonable to choose one of the signals which resulted from carbons 1, 4 or 5 and 6 (see Figure A.1). We verified the validity of this assumption by checking the relative peak intensities for carbons 1, 4, 5 and 6 in unlabeled material and found that their relative intensities were the same as those found in the labelled compound. Therefore, using the slope determined for carbon 4 as being representative of natural abundance ^{13}C , the enrichment at each position of labeled **11** can be determined as follows:

$$\text{Enrichment at Carbon X} = \text{Slope (for Carbon X)} - \text{Slope (for Carbon 4)}^{65}$$

These results are tabulated below in Table A.2.

Table A.2
 ^{13}C Enrichment at each Carbon Position of Labelled **11**

Carbon #	Enrichment ^a	Std Deviation ^b
1	0.045(2.5%)	0.024(53%)
2	1.356(76.2%)	0.064(4.7%)
3	0.349(19.6%)	0.027(7.7%)
4	0.0	-----
5,6	0.033(1.9%)	0.026(79%)

^aarbitrary units. ^bStandard Deviations are $\pm \sigma$

The total enrichment in labelled **11** can be determined by dividing the sum of the enrichment found for each carbon by the slope found for carbon 4 (*i.e.* the slope which is representative of natural abundance ^{13}C).

Total Enrichment = $\frac{\Sigma \text{Enrichment found for Carbons 1-6}}{\text{Natural Abundance (Slope found for Carbon 4)}}$

$$= \frac{1.783 \pm 0.141}{0.240 \pm 0.013}$$

$$= 7.409 \pm 0.988\%$$

REFERENCES

- 1) Becker, R. S.; Wentworth, W. E. *General Chemistry* Houghton Mifflin Company, Boston, 1973 pp. 203.
- 2) Radom, L.; Lathan, W. A.; Hehre, W. J.; Pople, J. A. *J. Am. Chem. Soc.* 1971, 93, 5340.
- 3) Wiberg, K. B.; Fenoglio, R. A. *J. Am. Chem. Soc.* 1968, 90, 3395.
- 4) Benson, S. W. *Thermodynamic Kinetics*, Wiley Interscience New York, N. Y. 1968 p.179.
- 5) Saltiel, J.; D'Agostino, J. Megarity, E. D.; Metts, L.; Neuberger, K.R.; Wrighton, M.; Zafiriou, O. C. *Organic Photochemistry, Vol. 3*; Chapman, O. L., Ed.; Marcel Dekker, Inc., New York, 1973.
- 6) Padwa, A.; Blacklock, T. J.; Cordova, D. M.; Loza, R. *J. Am. Chem. Soc.* 1980, 102, 5648.
- 7) Steinmetz, M. G.; Srinivasan, R.; and Leigh, W. J. *Rev. Chem. Intermediates* 1984, 5, 57 and references cited therein.
- 8) Padwa, A. *Acc. Chem. Res.* 1979, 12, 310.
- 9) Padwa, A. *Organic Photochem.* 1979, 4, 261.
- 10) Steinmetz, M. G. *Organic Photochemistry* 1987, 8, 67.
- 11) Bishop, K. C. *Chem. Rev.* 1976, 76, 461.
- 12) Davis, J. H.; Goddard III, W. A.; Bergman, R. G. *J. Am. Chem. Soc.* 1976, 98, 4015; 1977, 99, 2427.
- 13) Salem, L.; Rowland, C. *Angew. Chem. Int. Ed.* 1972, 11, 92.
- 14) Pincock, J. A.; Boyd, R. J. *Can. J. Chem.* 1977, 55, 2482.
- 15) Peyerimhoff, S. D.; Buenker, R. J. *Theor. Chem. Acta* 1969, 14, 305.
- 16) Sevin, A.; Arnaud-Danon, L. *J. Org. Chem.* 1981, 46, 2346.
- 17) Honjou, W.; Pacansky, J.; Yoshimine, M. *J. Am. Chem. Soc.* 1984, 106, 5361.
- 18) Honjou, W.; Pacansky, J.; Yoshimine, M. *J. Am. Chem. Soc.* 1985, 107, 5332.
- 19) Streeper, R. D.; Gardner, P. D. *Tetrahedron Lett.* 1973, 767.
- 20) York, E. J.; Dittman, W.; Stevenson, J. R.; Bergman, R. G. *J. Am. Chem. Soc.* 1972, 94, 2882; 1973, 95, 5680.
- 21) Pincock, J. A.; Moutsokapas, A. A. *Can. J. Chem.* 1977, 55, 979.

- 22) Stecil, H. H. *Chem. Ber.* **1964**, *97*, 2681.
- 23) DeBoer, C.; Breslow, R. *Tetrahedron Lett.* **1967**, 1033.
- 24) Dürr, H. *Liebigs Ann. Chem.* **1969**, *723*, 102.
- 25) Dürr, H. *Tetrahedron Lett.* **1967**, 1649.
- 26) Padwa, A.; Chiacchio, U.; Hatanaka, N. *J. Am. Chem. Soc.* **1978**, *100*, 3928.
- 27) Steinmetz, M. G.; Yen, Y. P.; Pock, G. K. *J. Chem. Soc., Chem. Commun.* **1983**, 1504.
- 28) Stierman, T. J.; Johnson, R. P. *J. Am. Chem. Soc.* **1985**, *105*, 2492; **1985**, *107*, 3971.
- 29) Padwa, A.; Blacklock, T. J.; Getman, D.; Hatanaka, N.; Loza, R. *J. Org. Chem.* **1978**, *43*, 1481.
- 30) Michl, J. *J. Mol. Photochemistry* **1972**, *4*, 243; **1972**, *4*, 257.
- 31) Pincock, J. A.; Morchat, R.; Arnold, D. R. *J. Am. Chem. Soc.* **1973**, *95*, 7536.
- 32) Pancir, J.; Zahradnik, R. *Tetrahedron* **1976**, *32*, 2257.
- 33) Bingham, R. C.; Dewar, M. J. S.; Lo, D. H. *J. Am. Chem. Soc.* **1975**, *97*, 1298.
- 34) Ha, T. K.; Graf, F.; Guenthard, H. H. *J. Mol. Struct.* **1973**, *15*, 335.
- 35) Bailey, I. M.; Walsh, R. *J. Chem. Soc., Faraday Trans. 1* **1978**, *74*, 1146.
- 36) Srinivasan, R. *J. Chem. Soc., Chem. Commun.* **1971**, 1041.
- 37) Closs, G. L.; Closs, L.E.; Böll, W. A. *J. Am. Chem. Soc.* **1963**, *85*, 3796.
- 38) Braude, E. A.; Coles, J. A. *J. Chem. Soc.* **1950**, 2012.
- 39) Derome, A. E. *Modern NMR Techniques for Chemistry Research*; Baldwin, J. E., ED.; Pergamon Press, 1987.
- 40) Freeman, R.; Hill, H. D. W.; Kaptein, R. *J. Mag. Res.* **1972**, *7*, 327.
- 41) Padwa, A.; Blacklock, T. J.; Getman, D.; Hatanka, N.; Loza, R. *J. Org. Chem.*, **1978**, *43*, 1481. References 4 - 24 of this paper are an excellent compilation of work that has suggested the intermediacy of viny-carbenes in the thermal and photochemical reactions of cyclopropenes.
- 42) Griffin, G. W. *Angew. Chem., Int. Ed. Engl.* **1971**, *10*, 537.
- 43) We recognize that these are ground state reactions and **20** may be reacting on the excited state surface.

- 44) The generality of the alkylidene to cyclopropene rearrangement is unknown. This is further complicated because under the reaction conditions used to generate the alkylidene the cyclopropene rearranged to methylenecyclopropane. In some cases the yield of methylenecyclopropane is quite high. See: Wolinsky, J.; Clark, G. W.; Thorstenson, P. C. *J. Org. Chem.* 1976, 41, 745.
- 45) Klett, M. W.; Johnson, R. P. *J. Am. Chem. Soc.*, 1985, 107, 3963.
- 46) Apeloig, Y.; Karni, M.; Stang, P. J.; Fox, D. P. *J. Am. Chem. Soc.* 1983, 105, 4781.
- 47) Stang, P. J.; Mangum, M. G. *J. Am. Chem. Soc.* 1975, 97, 6478. Stang, P. J. *Acc. Chem. Res.* 1978, 11, 107.
- 48) Although Stang was able to trap **20** quite efficiently (see ref 18) direct comparison to our work is dangerous since it has not been established if **20** is reacting on the ground or the excited state surface.
- 49) For numerous examples of hydrogen vvs. alkyl migration in dialkyl carbenes see Kirmse, W. *Carbene Chemistry* Academic Press, New York, 1964.
- 50) See ref 2 of ref 7.
- 51) Closs, G. I.; Closs, L. E. *J. Am. Chem. Soc.* 1961, 83, 1003; 1963, 85, 7536.
- 52) Colonge, J.; Grenet, J. *Academie Des Sciences Chimie Organique*, 1952, 1181.
- 53) Bachman, G. B.; Goebel, C. G. *J. Am. Chem. Soc.* 1942, 64, 787. Kerdesky, F. A. J.; Ardecky, R. J.; Lakshmikantham, M. V.; Cava, M. P. *J. Am. Chem. Soc.* 1981, 103, 1992.
- 54) Murahashi, S.; Okumura, K.; Naoto, T.; Nagase, S. *J. Am. Chem. Soc.* 1982, 104, 2466.
- 55) Fantazier, R. M.; Poutsma, M. L. *J. Am. Chem. Soc.* 1968, 90, 5490.
- 56) Kornprobst, J. M.; Doucet, J. P. *J. De Chimie Physique* 1974, 71, 1129.
- 57) Simmons, H. E.; Smith, R. D. *J. Am. Chem. Soc.* 1959, 81, 4256. Casey, C. P.; Miles, W. H.; Tukada, H. *J. Am. Chem. Soc.* 1985, 107, 2924.
- 58) Braude, E. A.; Evans, E. A. *J. Chem. Soc.* 1955, 3324.
- 59) Hamon, D. P. G. *Aust. J. Chem.* 1975, 28, 2641.
- 60) Thummel, R. P.; Rickborn, B. *J. Org. Chem.* 1972, 37, 4250.
- 61) Many of the problems discussed below have been dealt with in much greater detail in the following texts (see references 29 and 62 as well) as well as other basic NMR books not listed. Kalinowski, H. K.; Berger, S.; Braun, S. *Carbon-13 NMR Spectroscopy*; John Wiley and Sons 1988.
- 62) Atta-ur-Rahman *Nuclear Magnetic Resonance*; Springer-Verlag, 1986.

- 63) The T_1 may be shortened by adding a relaxation agent, $\text{Cr}(\text{Acac})_3$, to the sample. See ref 39.
- 64) Bain, A. D.; Fahie, B. J.; Kosluk, T.; Leigh, W. J. *Magnetic Resonance in Chemistry*. Submitted for Publication.
- 65) Note that since carbons 5 and 6 have the same chemical shift the formula for determining the enrichment at these position becomes:
- $$\text{Enrichment at Carbon X} = \text{Slope (for Carbon X)} - 2[\text{Slope (for Carbon 4)}]$$